ABSTRACT

Title of Dissertation: Dual Quorum Quenching Capsules: Disrupting two bacterial communication pathways that lead to virulence

Melissa K Rhoads, Doctor of Philosophy, 2016

Dissertation directed by: Professor William E. Bentley
Fischell Department of Bioengineering

Healthcare Associated Infections (HAIs) in the United States, are estimated to cost nearly $10 billion[1] annually. And, while device-related infections have decreased, the 60% attributed to pneumonia, gastrointestinal pathogens and surgical site infections (SSIs) remain prevalent[2,3]. Furthermore, these are often complicated by antibacterial resistance that ultimately cause 2 million illnesses and 23,000 deaths in the US annually[4].

Antibacterial resistance is an issue increasing in severity as existing antibiotics are losing effectiveness, and fewer new antibiotics are being developed. As a result, new methods of combating bacterial virulence are required[5,6]. Modulating communications of bacteria can alter phenotype, such as biofilm formation and toxin production. Disrupting these communications provides a means of

controlling virulence[7,8] without directly interacting with the bacteria of interest, a strategy contrary to traditional antibiotics.

Inter- and intra-species bacterial communication is commonly called quorum sensing because the communication molecules have been linked to phenotypic changes based on bacterial population dynamics. By disrupting the communication, a method called ‘quorum quenching’, bacterial phenotype can be altered. Virulence of bacteria is both population and species dependent; each species will secrete different toxic molecules, and total population will affect bacterial phenotype[9]. Here, the kinase LsrK and lactonase *Sso*Pox were combined to simultaneously disrupt two different communication pathways with direct ties to virulence leading to SSIs, gastrointestinal infection and pneumonia.

To deliver these enzymes for site-specific virulence prevention, two naturally occurring polymers were used, chitosan and alginate. Chitosan, from crustacean shells, and alginate, from seaweed, are frequently studied due to their biocompatibility, availability, self-assembly and biodegrading properties[10-12] and have already been verified *in vivo* for wound-dressing[13 14]. In this work, a novel functionalized capsule of quorum quenching enzymes and biocompatible polymers was constructed and demonstrated to have dual-quenching capability. This combination of immobilized enzymes has the potential for preventing biofilm formation and reducing bacterial toxicity in a wide variety of medical and non-medical applications.

Dual Quorum Quenching Capsules: Disrupting two bacterial communication pathways that lead to virulence

by

Melissa K Rhoads

Dissertation submitted to the Faculty of the Graduate School of the
University of Maryland, College Park in partial fulfillment
of the requirements for the degree of
Doctorate of Philosophy
2016

Committee Members:
Professor William E Bentley, Chair
Professor Philip DeShong
Assistant Professor Steven M Jay
Professor Gregory F Payne
Associate Professor Ian White

DEDICATION

This work is dedicated to:

My grandparents, some of the greatest of the greatest generation.

My parents, Deborah and Hank, for whom there are not words that adequately acknowledge everything they have provided over the past three years, and previous three decades.

And to my family and friends, who have proven to be a support-system unmatched in their ability to provide levity, love, and empathy when each was needed most.

ACKNOWLEDGEMENTS

I would like to thank my advisor, Dr. William E. Bentley for the support, guidance, and latitude he has provided over the last few years. He was willing to accept someone from industry, an engineer, with an unheard of time-line and mold me into a scientist.

The Bentley Lab members have been an outstanding team to be a part of and will always hold a special place in my memory of this experience. They have become great friends and provided a strong support system to make what can be a difficult process, far more enjoyable. A most special thank you to Dr. Pricila Hauk and Dr. Jessica Terrell, whose guidance, experience, expertise, patience and understanding made this process one that I will look upon more fondly because they were part of it.

I would like to acknowledge my dissertation committee members Dr. Gregory F. Payne, Dr. Steven M Jay, Dr. Ian White and Dr. Philip DeShong as well as those that served for my proposal exam Dr. Srinivasa Raghavan and Dr. Herman O. Sintim for their time and advice. I also acknowledge the facilities provided by the Institute of Biotechnology and Bioengineering Research, the Fischell Department of Bioengineering at the University of Maryland, and Lockheed Martin, which sponsored this research and, without which, this research would not have been possible.

TABLE OF CONTENTS

TABLE OF FIGURES

TABLE OF TABLES

ABBREVIATIONS

AHL – Acyl-homoserine lactone

AI-1 – Autoinducer-1

AI-2 – Autoinducer-1

ATP – Adenosine tri-phosphate

CAUTI – Catheter-associated urinary tract infection

CLABSI – Central line-associated bloodstream infection

HAI – Healthcare Associated Infections

OdDHL/3-oxo-C12HSL/OdDHL – N-(3-oxododecanoyl)-l-homoserine lactone

OP – Organophosphate

OPH – Organophosphatase

PTE – Phosphotriesterases

SSI – Surgical site infections

VAP – ventilator-associated pneumonia

WHO – World Health Organization

WHOPES – World Health Organization Pesticide Evaluation Scheme

CHAPTER 1 INTRODUCTION

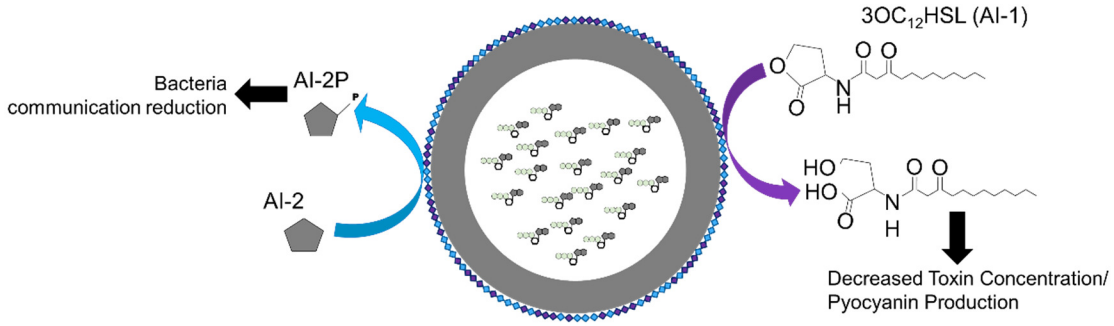

Figure 1: Functionalized capsule for dual quorum quenching
The multifunctional quorum quenching capsule developed in this work will be the first to modulate two classes of bacterial communication molecules, autoinducer-2 (AI-2) and autoinducer-1 (AI-1).

Resistance to antibiotics is an issue increasing in severity as existing antibiotics are losing effectiveness, and fewer new antibiotics are being developed. As a result, new methods of combating bacteria are required to prevent illness and infection. Disrupting bacterial communications provides a means of preventing the harmful effects of bacteria without directly interacting with the bacteria, a strategy contrary to traditional antibiotics.

Bacterial communication is commonly called quorum sensing because it provides a way for a population of bacteria, or quorum, to change behavior of individual bacteria. The small chemicals used for communication typically vary between types of bacteria, however, one type is recognized by bacteria, plants and animals, allowing cross-species communication. By intercepting or modifying these small chemicals, a method called ‘quorum quenching’, the individual bacterial changes can be prevented, and thereby preventing virulence or infection.

Here, two proteins, or enzymes, are used that modify two different communication molecules. One chemical was mentioned earlier and provides inter- and intra-species communication, the other is specific to a handful of bacteria which are particularly troublesome. These enzymes, by modifying the small chemicals, demonstrate the capability to alter bacterial behavior, which in-turn could reduce effects of bacterial infection when the enzymes are present.

To deliver these enzymes to a specific site, two naturally-occurring polymers are used, chitosan and alginate. Chitosan, from crustacean shells, and alginate, from seaweed, are already used for drug delivery and wound-dressing, so have been demonstrated safe to use in humans. Using chitosan and alginate to construct a capsule with both enzymes, the capsule was demonstrated to modify two both communication chemicals and subsequent behavior of bacteria. This combination of enzymes has the potential for preventing infection and reducing the harmful impacts of bacterial in a wide variety of applications.

1.1 Background

Healthcare Associated Infections (HAIs) in the United States were estimated to cost nearly $10 billion annually[1] for nearly one million infections[3]. There are commonly four classifications of infection central line-associated bloodstream infections (CLABSI), ventilator-associated pneumonia (VAP), surgical site infections (SSIs) and catheter-associated urinary tract infection (CAUTI). , However, a fifth has been increasingly common in recent years, the gastrointestinal pathogen, *C. difficile*,[1-3] and has proven more costly than

CAUTIs[1]. Each of these infections is also associated with antibacterial resistant infections that cause 2 million illnesses and 23,000 deaths in the US annually[4].

These infections have toxic consequences inside the body, which result in extended hospital stays and readmission. In addition, infections increase healthcare costs and require the use of broad-spectrum antibiotics, which, if not successful, can lead to death [4,15-18]. Device-related infections, when bacteria form biofilms in medical equipment such as catheters, diagnostics or ventilators, can escalate the spread of infection[3,19]. Broad spectrum antibiotics and prophylactic use has precipitated the emergence of antibacterial resistant strains (see Figure 2) now prevalent in hospitals and clinical settings that have reached alarming proportions[4-6].

Figure 2: Emergence of Antibiotic Resistance
The illustration above explains how antibiotic resistance develops as bacteria mutate and then the resistant forms proliferate in the prescence of antibiotics. These mutated bacteria can even transfer resistance to other bacteria. (*courtesy CDC*)

Less antibiotic discovery and development efforts by pharmaceutical companies' [20-22], concern for maintaining healthy bacteria populations[23] and increased antibiotic resistance has further encumbered treatment options for combating biofilm and bacterial pathogen toxicity. As a result, new, and perhaps game-changing technologies for combating biofilms – from prevention to removal – are increasingly being explored.

1.2 Bacterial Communication – An Alternative to Antibiotics

Inter- and intra-cellular communication between bacteria via small molecule-induced signaling, also known as quorum sensing, has been shown to control bacterial phenotypes, including biofilm formation and virulence [7-9,24-28]. As a result, these small molecules, known as autoinducers, are increasingly a focus of research in bacterial metabolism. Specifically, the focus has been on interrupting the small molecule signaling pathways between bacteria, a method called "quorum quenching", which has shown to reduce the strength or persistence of biofilms [29] and their formation [30-32 33].That is, quorum quenching – achieved by intercepting, altering, or 'confusing' the QS systems that effect molecular communication and biofilm formation/development – has emerged as a potential mediator of cell pathogenicity that might avoid entirely the use of traditional antibiotics [34]. An illustration of how quorum sensing and quenching affects the bacterial life-cycle is found in Figure 3.

Biofilms are specifically identified in association with infection and toxicity because cells in this state pose greater challenges for treatment and increase risk of chronic infection[35]. When cells form a biofilm they go through a transition

from free (planktonic) cells to operating in a colony of cells that function almost as a multicellular organism. To begin forming this colony or film, they use the autoinducers to determine the concentration of cells and make phenotypic changes. These phenotypes, which include increased motility and surface attachment, ultimately contribute to film construction. In biofilm formation the cells produce and excrete polysaccharides around the colony, which can be composed of multiple species. This protective layer formed by the exopolysaccharide matrix and the 3-D structure of the film makes it hard to treat or remove, even with antibiotics, as the polysaccharide acts as a protective layer which the antibiotics often cannot penetrate[36]. In addition, cells are released back into the surrounding environment so infection can spread beyond the film[27,37].

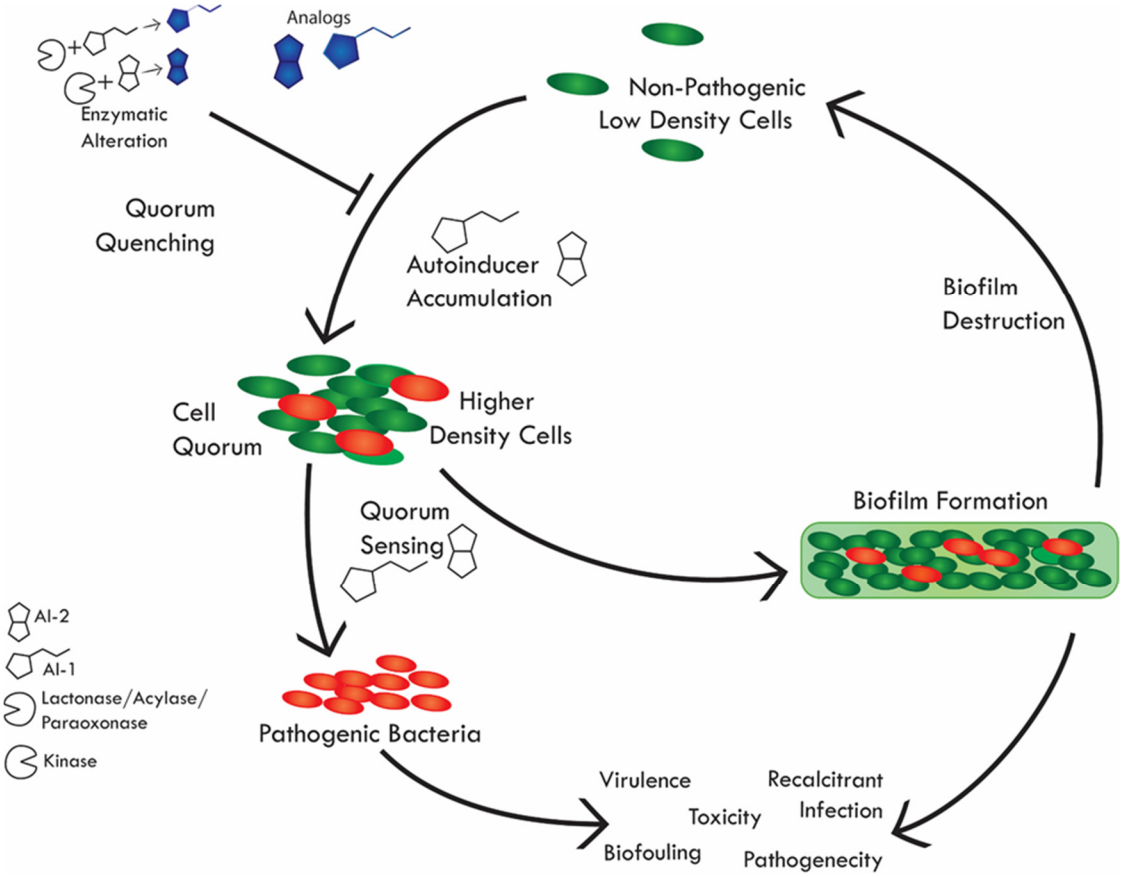

Figure 3: Illustration of quorum sensing and quorum quenching
This illustrates how autoinducers, here AI-1 and AI-2, contribute to pathogenicity and biofilm formation. In addition it illustrates how quorum quenching can reduce growth, pathogenicity and biofilm formation by interrupting the autoinducer signaling.

1.3 Classes of Quorum Sensing Molecules

There are several QS system modalities, distinguished primarily by the class of their cognate communication or signal molecules. In this work, the focus is on two: autoinducer-1 and autoinducer-2.

Acylhomoserine lactones (AHLs or AI-1) are primarily associated with inter- and intra-species bacterial communication in Proteobacteria which includes Gram-negative bacteria, or those that have both inner and outer membrane layers[38]. However more recently, AHLs have also been associated with the plague[39]. AI-1 signal molecules are composed of a homoserine lactone ring attached to a fatty

or nonfatty acyl group and are detected by LuxI/R. This acyl group can vary greatly in size, from a 4-carbon to 18-carbon chain with a single species using more than one, and varying from species to species [7,9,38,40].

A second class of communication molecules, autoinducer-2 (AI-2), is often referred to as the 'universal' molecule as it is produced by scores of bacteria, including both Gram-negative and Gram-positive species, and is also recognized by eukaryotic organisms [8,41,42]. AI-2 molecules consist of varying forms[43-45], and include a boronated ring structure in transduction systems that utilize cell surface receptors [46-48]. AI-2 is produced as part of the activated methyl cycle in bacteria, a by-product of the conversion of s-ribosylhomocysteine (SRH) to homocysteine (HCY) by LuxS [48].

1.4 'Quenching' Bacterial Communication

As mentioned, there are several methods of quorum quenching: intercepting, altering, or 'confusing' the QS systems. Intercepting or altering the molecules is straight-forward – elimination or modification to the molecule of interest. To confuse the system, molecular analogs interrupt communication by inserting into the native molecular 'network' a natural or chemically-synthesized, highly similar molecule that functions to supplant the natural molecules and affect downstream behavior. This method of quorum quenching by 'confusing' the system has become increasingly prevalent as evidenced by the issue of several analog patents [49-53]. While analogs have been shown effective in providing an alternative to antibiotics in lab environments, many are 'one time use' and therefore not self-

sustaining, and only a handful have provided a delivery mechanism of their quenching capabilities. Engineered bacteria have been demonstrated as a way of providing self-sustained treatment[29 54 55 56,57], and there are recent examples of bacteria that provide quorum quenching while contained in capsules and films [29,58].

1.4.1 AI-1 Quenching

It has previously been shown that lactonases are capable of quenching AHL quorum sensing by hydrolyzing the AHL. This prevents the molecule from binding to the receptor in the cell[59]. Lactonases hydrolyze AHLs at the C3 ketone as illustrated in Figure 4, and can also reduce the acyl chain of AHLs to make them branched or unsaturated. The action of lactonases to mediate quorum sensing has been successful in reducing biofilm development and in the reduction of pre-formed biofilms. However, 'neutralizing' this class of molecules enzymatically is challenging as they are quite diverse. As a result, any specific lactonase may be effective in neutralizing some AHLs but not others [60]. This specificity in targeting could be either a benefit or a limitation, depending on the application. Kyeong et al. used docking analysis to design lactonases that were specifically targeting short acyl chain AHLs [61]. In contrast, Hiblot et al. has worked with several lactonases from extremophiles, including *Sso*Pox, from the hyperthermophilic *Sulfolobus solfataricus*[62], which has been

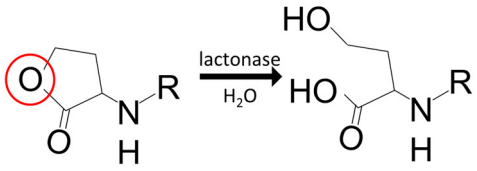

Figure 4. Hydrolysis of C3 Ketone This provides a simplified illustration of the hydrolysis of the C3 ketone on an AHL. Here, the R represents the remainder of the acyl chain.

shown to hydrolyze a variety of acyl chain lengths, making it effective in quorum quenching against a wide variety of Gram-negative bacteria [63,64].

1.4.2 AI-2 Quenching

AI-2 was chosen for interception for several reasons: it is used in signaling in both Gram-positive and Gram-negative bacteria[8], it is not produced by eukaryotic cells[48], the mechanism of AI-2 phosphorylation is understood[65], and its production is based on positive-feedback[8]. AI-2 is also associated with biofilm formation in *Klebsiella, E. coli, Salmonella, Enterobacter* and *Yersinia* [66,67]. Analogs are a common means of targeting activities of the 'universal' quorum sensing molecule autoinducer-2 (AI-2). From interfering with production [68], to forms of AI-2 precursors [69], to insertion of inert analogs which prevent downstream processing [52,70], quorum sensing inhibitors (QSIs) have been identified which interfere with nearly every step of the AI-2 life-cycle.

Use of enzymes to alter or destroy the molecule is less common. Though, Varnika Roy of the Bentley Lab showed that the *E. coli* AI-2 kinase, LsrK, can phosphorylate AI-2 *in vitro*, and that this extracellular phosphorylation of AI-2, prevents its uptake, obviating its natural activity[71]. She went on to show this reduced the native quorum sensing response in *E. coli*, *Salmonella typhimurium* and *Vibrio harveyi* [71]. The mechanism of AI-2 phosphorylation by LsrK with ATP was further elaborated by Zhu, et al [65]. Building on Varnika's work by expanding the possible mechanisms for use of LsrK in quorum quenching is a critical element of this work.

1.5 Biomaterials

Beads, films and capsules composed of naturally occurring polymers are increasingly being studied for use in a wide variety of pharmaceutical and anti-bacterial applications[10-12,29,72,73]. Many are using chitosan and alginate due to their biocompatibility, availability and biodegrading properties, as well as ease of construction due to formation of polyelectrolyte complexes (PECs), a result of the opposite charges of chitosan and alginate[74-78]. In the Bentley Lab these two biopolymers were used to construct a simple capsule which contained an enzyme-complex produced in the lab[10]. These capsules formed the starting point for development of the robust chitosan-alginate capsules formed here. These two molecules not only self-assemble, but are already used as wound-dressing[13 14] and for enzymatic and antibiotic drug delivery [77 79].

1.6 Research Motivation

Recent estimates of the number of annual HAIs is lower than in previous years 700,000 vs 1.7M, however the majority are still attributed to non-device related pneumonia, surgical site infections and gastrointestinal infections[3]. These types of infections have not received the same focus as device-related infections[3]. As a result, it is important that focus continue to be placed on preventing these infections in the patient.

The most common pathogens found in infection are: *C. difficile, S. aureus,* Enterobacteriaceae – including *Klebsiella, E. coli,* and *Enterobacter* – and *P. aeruginosa* [3], and, each of these has exhibited antibiotic resistance, or been associated with antibiotic resistance[80]. Methicillin-resistant *Staphylococcus*

aureus, MRSA, has received a significant amount of press, and as a result of surveillance and improved practices has decreased in the UK and US, however it has seen a rise in India and non-hospital related infections[80] .

The family of bacteria Enterobacteriaceae includes *Salmonella*, *E. coli*, *Yersinia* (plague), *Klebsiella* (pneumonia) and *Shigella* (diarrheal), which are Gram-negative bacteria and commonly known pathogens. Of these, *Klebsiella, E. coli, Salmonella, Enterobacter* and *Yersinia* have been found to have both the LuxS, AI-2 producing, and Lsr/Lsr-like, AI-2 recognition systems [66,67]. Addition of the recognition system to *Shigella* proved to provide a growth advantage[81] indicating that the presence of the recognition system is indicative of AI-2 affecting bacterial growth. Furthermore, AI-2 has been specifically linked to biofilm formation in *Salmonella* and *E.coli* [82].

In addition to the family Enterocateriaceae, biofilm formation in *S. pneumoniae* has also been found to be positively regulated by the LuxS system in cultures both with and without human cells[26]. It has also been shown that a quorum sensing peptide, or AIP, contributes to biofilm formation under certain *in vivo* conditions[83]. Similarly, though the exact mechanisms are still under debate it is accepted that the AI-2 system, production and receipt, has a role in *S. aureus* virulence and biofilm formation[84,85].

P. aeruginosa is known to use at least three quorum sensing signals including AI-2, and two AHLs: BHL/C4-HSL and OdDHL/3-oxo-C12HSL/OdDHL which are directly tied to virulence. Specifically, OdDHL binding to LasR activates *rhlR* and

production of the second AHL. Inhibiting OdDHL binding and activation of *rhlR* has been demonstrated to reduced pyocyanin production and biofilm formation *in vitro* and *in vivo* [86,87] In addition, quenching this molecule, which has adverse impacts to mammalian cells and inhibits biofilm formation in Gram-negative bacteria provides a broader impact than just neutralizing a *P. aeruginosa* toxin[88]. Providing a dual quenching capability is important specifically in *P. aeruginosa* because concentrations of AI-2 below 10nM have been found to lead to increased virulence and biofilm formation[89]. As a result, reducing both AI-2 and the critical AHL concentration provide improved solutions for preventing toxicity in in *P. aeruginosa*.

While a complete understanding of the role AI-2 plays in *C. difficile* biofilm formation and virulence has not been determined, the absence of the LuxS system in this pathogen does prevent biofilm formation [33]. AI-2 production during growth mirrors that of many Enterobacteriaceae[90] and toxins are only produced in the stationary phase[91]. If reduction of AI-2 limits biofilm formation or an Lsr-like recognition system is found, the reduction in AI-2 in the environment could also reduce *C. difficile* toxicity, which is currently attributed to a third class of quorum sensing molecules[91].

Delivery of enzymes in lieu of bacteria provides distinct advantages: limiting new bacteria introduction and a less-variable, more controlled system[9]. And while there is evidence of delivering quenching enzymes in capsules and on membranes [92,93] none have targeted AI-2 or used a combination of enzymes to modulate the two types of bacterial communication molecules. By taking this

combinatorial approach the functionalized capsule will have a broader range of impact – for example, it will not only reduce the concentration of OdDHL which is harmful to mammalian and other bacterial cells[94], but also reduce the concentration of AI-2, a universal signaling molecule which leads to biofilm production in several species of bacteria – particularly those exhibiting antibiotic resistance.

1.7 Global Objective and Specific Aims

This work will engineer and purify proteins for attachment to designed biopolymer capsules for the purpose of quenching two different types of quorum sensing molecules, AI-1 and AI-2. This dual quenching capability will provide further control of phenotypes across several species of bacteria and within species, as many use multiple molecules in inter- and intra-species communication.

1.7.1 Aim 1: Functionalized Capsule for AI-2 Quorum Quenching

Self-contained capsules constructed of biocompatible biopolymers to modify the molecular dynamics of the AI-2 communication pathway are developed. Newly modified forms of the naturally occurring AI-2 kinase, LsrK, which has previously been shown to 'quench' bacterial communication[71] are purified and activity is verified during covalent binding. In addition, capsules are constructed to deliver the primary substrate, adenosine tri-phosphate (ATP), to provide kinase quenching in an *in vitro* environment. These capsules have the potential to reduce biofilm formation of several species of bacteria, and specifically the family *Enterobacteriaceae* which has developed antibiotic resistance.

1.7.2 Aim 2: Functionalized AHL lactonase Quorum Quenching Capsule

Using the same capsule developed for delivery of LsrK, the second aim focuses on quenching of another prevalent communication molecule of Gram-negative bacteria, AHL or AI-1, specifically OdDHL. Reduction of this molecule in the presence of *P. aeruginosa* reduced production of pyocyanin[86] which has been shown to be responsible for 90-95% of *P. aeruginosa*'s strains ability to resist attack from other bacteria[95], capable of altering immune response including evasion[96] and killing mammalian cells[86]. To modulate the AHL communication pathway, an AHL lactonase, *Sso*Pox, is modified with a hexahistidine-tag for purification and a separate tag providing the ability to be covalently bound to a surface. For the first time, activity of engineered *Sso*Pox is demonstrated when covalently bound to a surface. In addition, *Sso*Pox incorporated into a biomaterial-based capsule provides new means of delivery of lactonase and, possibly, organophosphate hydrolysis activity.

1.7.3 Aim 3: Multi-functional System for Bacterial Quorum Quenching

The third aim will focus on tying the first two elements together to construct a multifunctional system of biocompatible materials to intercept two classes of bacterial communication molecules. Combining two types of quorum quenching enzymes is a new and novel concept. As a result, it must first be demonstrated that the two enzymes are active in the same environment, and able to simultaneously quench both AI-2 and AI-1 quorum sensing molecules. These two enzymes will then be bound to the same capsule used previously to demonstrate a novel means of delivering dual quorum quenching capabilities on a

biocompatible functionalized device. This combination of quenching enzymes has the potential to be far more effective as an alternate to antibiotics as it could address virulence of several types of bacteria simultaneously.

2 OVERVIEW OF QUORUM SENSING INHIBITION

2.1 Abstract

Antibiotics combat virulence by their bactericidal or bacteriostatic activities; unfortunately, these medicines are losing effectiveness, marked by the seemingly incessant emergence of resistant strains. Moreover, such activities are diminished when treating cells in biofilms as opposed to those in a planktonic state. Concomitantly, cell-cell communication or quorum sensing (QS) systems have emerged as targets for antimicrobials as they represent an orthogonal approach to the traditional drugs. Instead of directly inhibiting cellular activity, QS 'quenching' molecules or processes silence virulence by interrupting communication; the notion being avoiding 'cidal' or 'static' activities that represent drivers of evolutionary escape. Researchers from microbiology, bioengineering, food science, agriculture, soil science, human health, and others, have been exploring natural and synthetic molecules to 'quench' quorum sensing, combat biofilm formation, or promote their removal. In this review, which builds on years of study, we focus on results of the last few years. Both compounds and their methods of application that effect biofilm-born bacteria by targeting QS are highlighted.

2.2 Introduction

Biofilms affect a wide variety of processes or conditions in many fields. Biofilm formation in mechanical and process systems (biofouling) afflicts HVAC units, waste-water treatment and many other filtration systems [97]. Preventing and combating biofilms on food and food packaging is a significant health problem, as

precious food supplies are destroyed due to preventable contamination [98]. Also, the persistent emergence of drug resistant bacteria within hospitals and clinical settings has reached alarming proportions [5,6]. For example, bacteria are at times 'living' in biofilms on and in medical equipment that is deployed in diagnostics (colonoscopy) or other therapies, exacerbating the fundamental problems [19].

Confounding these issues of biofilm formation and removal is the fact that many pharmaceutical companies have dropped discovery and development efforts to meet present and future demands [20-22], and there is interest to maintain healthy bacteria while simultaneously eliminating harmful bacteria [23]. As a result, new and perhaps game-changing technologies for removing biofilms, preventing their formation, and reducing their effects are increasingly being explored, particularly in academic settings.

2.3 Targeting QS Communication via Molecular Intervention

One method increasingly used for effecting bacterial growth and biofilm formation is through targeted modulation of bacterial communication. Inter- and intra-cellular communication between bacteria via small molecule-induced signaling, also known as quorum sensing, has been shown to control bacterial phenotypes, including biofilm formation and virulence [7-9,24-28]. Interrupting the small molecule signaling pathways between bacteria, a method called "quorum quenching", has been shown to reduce the strength or persistence of biofilms [29] and their formation [30-32]. That is, quorum quenching – achieved by intercepting, altering, or 'confusing' QS systems by the use of signal analogs that effect molecular communication and biofilm formation and development – has emerged as a

potential mediator of cell pathogenicity that might avoid entirely the use of traditional antibiotics [34].

There are several QS system modalities, distinguished primarily by the class of their cognate communication or signal molecules. The first identified, autoinducer 1 (AI-1) is comprised of acylhomoserine lactones (AHLs) and is employed primarily by Gram-negative bacteria. AI-1 signal molecules can vary greatly in size – stemming from a 4-carbon to 18-carbon acyl chain, they vary from species to species and a single species may recognize more than one AI-1 molecule [7,38,40]. A second, autoinducer-2 (AI-2), has been referred to as the 'universal' molecule as it produced by scores of bacteria, including both Gram-negative and Gram-positive species. It is also recognized by eukaryotic organisms [8,41,42]. AI-2 molecules consist of either a linear form, which is phosphorylated into an active species [43-45], and a boronated ring structure in transduction systems that utilize cell surface receptors [46-48]. Autoinducer-3 (AI-3), believed to be an aromatic compound, is recognized by the same receptors as those that recognize epinephrine/norepinephrine and has associated with inter-species signaling including that between gut flora and intestinal cells [99]. Similarly, autoinducing peptides (AIPs) that bind to transmembrane receptors are used by Gram-positive bacteria [27,100,101]. In addition to these autoinducers, indole-based QS signaling has been associated with *E. coli, P. aeruginosa, V. cholera* and others [102-105] and species-specific α-hydroxyketones (AHKs) are used by *V. cholera* and *L. pneumophila* to regulate virulence and biofilm formation [106-109]. Cyclic dimeric GMP (cyclic di-GMP or c-di-GMP) is a secondary signaling molecule that

regulates both virulence and biofilm formation among other cellular functions [110], including increased exopolysaccharide cellulose production [111] and motility [112]. And recently, peptide signaling in the presence of stress have been increasing studied including integration of the QS network and stress network (IQS) in *P. aeruginosa* [113] and peptide signaling in *E. coli* and *S. mutans* under stress conditions [114-116].

In the sections that follow, QS and mediators of molecular communication are considered as targets for modulating biofilms. We survey the most recent results that intersect QS communication with biofilm formation or attenuation.

2.4 Communication Molecule Analogs

Signal molecule analogs interrupt communication by inserting into the native molecular 'network' a natural or chemically-synthesized highly similar molecule that functions to supplant the natural molecules and effect downstream behavior. This method of quorum quenching by 'confusing' the system has become increasingly prevalent; several analog patents have been issued [49-53]. Brackman and Coenye provide a nice comprehensive review with significant chemical detail on quorum sensing molecules and their inhibitors [27]. We briefly summarize here, highlighting features relative to chemical structure.

2.4.1 AI-2

Several synthetic analogs have been reported targeting activities of the 'universal' quorum sensing molecule autoinducer-2 (AI-2). Kadirvel developed a fluoro-analog of the linear form of AI-2, 1,3 dipentandione (DPD); a 4-fluoro-5-

hydroxypentane-2,3-dione that inhibited bioluminescence and growth of *Vibrio harveyi* [69]. Li reported three compounds similar to S-ribosylhomocysteine were effective in inhibiting LuxS – the terminal synthase which produces AI-2 as a part of the activated methyl cycle. These compounds were shown to inhibit growth of swine pathogens *A. pleuropneumoniae*, *H. parasuis* and *S. suis* [68]. Roy et al developed C-1 alkyl analogs of AI-2 that modify the QS responses of *E. coli*, *S. typhimurium*, and *V. harveyi*. These analogs are phosphorylated by the native kinase, LsrK, and interfere with the native transcriptional activator, LsrR, and therefore modulate AI-2 specific gene transcription (Roy, 2010). Jang and coworkers demonstrated that two quorum sensing inhibitors (QSIs) – (5Z)-4-bromo-5-(bromomethylene)-2(5H)-furanone and D-ribose were effective against formation of biofilms by periodontopathogens *F. nucleatum*, *P. gingivalis*, *T. denticola* and *T. forsythia* [117]. Brackman et al. showed two molecules mimicking the ringed form of autoinducer-2 (AI-2) reduced QS signalling activity among reporter strains. That is, thiazolidinediones, which are used to treat diabetes, and dioxazaborocanes, which have a boronated ring, interfered with AI-2 quorum sensing, reducing signaling by more than 99% (*V. harveyi* BB170) and 90% (*V. harveyi* MM32). It was also found that the alkylidene chain length in the thiazolidinedione derivatives elicited varied effects on quorum quenching [70]. Gamby also developed analogs affecting *E. coli*, *S. typhimurium,* and *P. aeruginosa* [53]. The diversity of these analogs and their varying ability to inhibit AI-2 binding suggest ‘tunable’ quorum quenching.

We further note an example of exploiting a combination of AI-2 quorum quenching compounds and antibiotics. Roy demonstrated that isobutyl-DPD, a C1-alkyl AI-2 analog, inhibited *E. coli* biofilm maturation with a microfluidic device that readily provided biofilm density. They also showed biofilm degradation and clearance when used in combination with gentamicin [118].

2.4.2 AHL

AI-1 analogues have also been developed which have greater specificity for the target bacteria due to species-specific variations in acyl chain length of the native forms. This molecular variability is exploited to target specific bacteria, or specific signaling pathways in bacteria. For example, *Pseudomonas aeruginosa* uses at least two AHL signaling molecules, 3-oxo-C_{12}-HSL and C_4-HSL and exhibits several modes of toxicity including production of pyocyanin and pseudolysin (LasB) [86,119-121]. O'Loughlin analyzed several synthetic molecules that effected the *P. aeruginosa* quorum-sensing receptors, LasR and RhlR, finding that meta-bromo-thiolactone (mBTL) and chlorolactone (CL) prevented QS-mediated production of pyocyanin and biofilm formation [86]. Park also demonstrated that an alkaloid from the venom of fire ants disrupted quorum sensing and likely targeted the *rhl* system exploiting C_4-HSL [120]. Stacy was successful in demonstrating that AHL analogues prevented the formation of *A. baumannii* biofilms. In these studies they monitored the degree to which various compounds inhibited the activity of AbaR – homolog of LuxR - and measured growth and inhibition of the films on plates [122].

Interestingly, it has also been shown that a degradation product of the *P. aeruginosa* quorum sensing molecule 3-oxo-C_{12}-homoserine lactone, the tetramic acid 3-(1-hydroxydecylidene)-5-(2-hydroxyethyl)pyrrolidine-2,4-dione (C(12)-TA), is a potent antibacterial agent [123,124]. Lowery determined that the mechanism for the antibiotic activity of these molecules was the ability to modify the pH gradient and membrane potential of Gram-positive bacteria, proving effective against *B. anthracis* (anthrax), *S. aureus* (using a methicillin resistant strain) and *M. tuberculosis* (tuberculosis) [123].

Similar to the work of Roy, Estrela noted that antibiotics and quorum quenching provide a more effective means of reducing or eliminating biofilms, specifically furanones, increasing *P. aeruginosa* sensitivity to tobramycin [125]. Brackman also showed that known quorum sensing inhibitors, baicalin hydrate (BH) or cinnamaldehyde (CA), when combined with tobramycin, led to significantly greater cell death in *P. aeruginosa*, *B. cenocepacia* and *B. multivorans* biofilms than if only tobramycin was used [126].

2.4.3 Polyamines & Peptides

Polyamines – including norspermidine and spermidine – are a well-studied class of linear organic cations that have been shown to exhibit both anti- and pro-bacterial qualities, perhaps specific to the polyamine and bacteria [127]. As such, they represent a promising addition to the antimicrobial arsenal. Karatan proved that norspermidine, produced by prokaryotes and eukaryotes, is responsible for *V. cholerae* surface accumulation [128]. Kolodkin-Gal found that norspermidine acts with the D-amino acids of *B. subtilis* polysaccharide matrix for biofilm

disassembly [129]. Lee identified an alternative polyamine biosynthetic pathway using aspartate β-semialdehyde instead of decarboxylated S-adenosylmethionine as the aminopropyl group donor in formation of norspermidine and spermidine. They later demonstrated that removal of either the carboxynorspermidine dehydrogenase (CANSDH) or carboxynorspermidine decarboxylase (CANSDC) genes reduced growth rate and biofilm formation and noted that this alternate pathway is widespread (Lee, 2009). Nesse found that norspermidine and spermidine reduced biofilms of *E. coli,* but increased *S. enterica* biofilm formation [130]. Cockerell, using genomic analysis, determined that a variety of bacteria have NspS-like proteins – NspS is responsible for signal transduction of spermidine and norspermidine – and determined that polyamine signaling is processed by cyclic di-GMP networks [131]. We note that spermidine has a variety of effects on eukaryotic cells from memory and stress in *D. melanogaster* to reduced translation and growth of mammalian cells [132-134]. To date, however, much of spermidine research has focused on modifying intracellular concentrations of the polyamine: increasing concentrations in *S. cerevisiae* for toxin resistance through mutation [135], or reducing concentration with the ornithine decarboxylase inhibitor difluoromethylornithine to treat type I diabetes in a mouse model [136]. The identification of IQS, which enables LasB production even in the absence of C_4-HSL [113], may explain why some compounds were found to have both antagonist and agonist qualities as well as variability across strains [86,126]. To combat this process, Zhu found that targeting

LasB with mercaptoacetamides was effective in reducing toxicity of *P. aeruginosa in vivo* in *C. elegans* [121].

Peptides have been shown to have rolls in inter-, intra-bacterial species signaling as well as between bacterial cells and eukaryotic cells [137]. *S. aureus* uses at least four classes of auto-inducing peptides (AIPs) with specific transmembrane receptors for quorum sensing, recently Tal-Gan et al. determined the structural characteristics required to modulate these quorum sensing signals through analogs [138]. Several other studies exist in which natural and known drug agonists were identified to disrupt AIP systems and attenuate toxicity [139,140]. Guo et al. found that their synthetic peptide was effective at reducing the target *S. mutans* population without adversely affecting beneficial bacterial in an oral biome environment [141]. In some cases, such as Extracellular Death Factor (EDF) peptides released by *P. aeruginosa* and *B. subtilis*, species have demonstrated the capability to trigger cell-death in other species, in this case *E. coli* [116]. Recent research has also found links between bacterial peptide signaling and initiation of colon cancer cell proliferation [142], demonstrating a possible correlation between a person's microbiome and cancer susceptibility.

2.4.4 Other Small Molecules

Indole signaling has also been associated with reduced biofilm formation by inducing SdiA-mediated transcription [104]. Notably, indole marginalized EHEC and *P. aeruginosa* infections [143,144] indirect correlations between *E. coli* biofilm formation and indole concentration [145]. Bunders demonstrated that desformylflustrabromine (dFBr) and derivatives were similarly effective in

inhibiting biofilm formation in *E. coli* and *S. aureus* through interactions with the transcriptional regulator SdiA [105].

To combat virulence of *L. pneumophila,* Harrison focused on inhibiting its replication in the host cells, specifically intracellular replication in 'Legionella-containing vacuoles' (LCVs) as these bacteria are typically 'protected' from antibiotics. Harrison demonstrated successful reduction of intracellular replication using a synthetic compound and showed that *A. castellanii* provides a viable way to screen for effective inhibitors [146].

2.5 Naturally-Occurring Quorum Sensing Modulation

On several occasions naturally occurring molecules have proven effective in altering quorum sensing and preventing or dislodging biofilms. Naturally occurring furocoumarins – bergmottin and dihydroxybergamottin (DHB) – found in grapefruit juice have been shown to quench both AI-1 and AI-2 QS transduction pathways in *E. coli*, *S. typhimurium* and *P. aeruginosa,* as measured using the *V. harveyi* BB170 assay. In addition, furocoumarins, or furanocoumarins, were shown to impact biofilm growth of both *E. coli* and *S. typhimurium* [147]. Owing to their structural similarity to both AHL and AI-2, Bergamottin and DHB are possibly functioning as communication molecule analogues. Another naturally-occurring molecule, curcumin, from the spice, turmeric (*Curcuma longa*) inhibited biofilm formation and disturbed existing biofilms of *E. coli*, *P. aeruginosa* PAO1, *P. mirabilis* and *S. marcescens*. Curcumin was found to significantly reduce exopolysaccharide production in studied organisms and alginate production in PAO1, both of which enable biofilm

formation. Curcumin was also demonstrated to effect quorum sensing-associated behaviors such as swimming and swarming, and was found to enhance efficacy of conventional antibiotics when co-administered, though the specific mechanisms were not elucidated [148]. Additionally, vanillin, the main component of vanilla extract, was shown to have quorum quenching properties against the Gram-negative *C. violaceum* [149] and prevent biofilm formation of *A. hydrophila*, a known biofouling Gram-negative bacterium [97]. Choo noted there was no structural similarity between vanillin and autoinducers, however. It is interesting that in a recent follow-on vanillin reduced growth of *E. coli* in a food medium [150]. Additionally, Perez-Montano found that *O. sativa* (rice) and *P. vulgaris* (beans) produced molecules that despite not having the ring of AHLs were able to modify quorum sensing of *S. fredii* and *P ananatis* which affect plants [151].

Inorganic modulators of biofilms have also attenuated QS activity. In addition to organic compounds, small concentrations (<1mM) of nickel and cadmium have been shown to inhibit *B. multivorans* biofilm formation without affecting growth. Both nickel and cadmium were shown to down-regulate genes associated with quorum sensing including *bmuIR*, the activator gene for C8-HSL production in *B. multivorans* [152]. Garcia-Lara et al. used ZnO nanoparticles to demonstrated quorum quenching and reduced virulence on clinical strains of *P. aeruginosa* [153].

2.6 Enzymatic Effectors of QS Signaling and Biofilm Formation

Lactonases hydrolyze AHLs at the C3 ketone; they also can reduce the acyl chain of AHLs to make them branched or unsaturated. The action of lactonases to mediate quorum sensing has been proven successful in reducing biofilm

development and in the reduction of pre-formed biofilms. However, 'neutralizing' this class of molecules enzymatically is challenging as they are quite diverse. As a result, any specific lactonase may be effective in neutralizing some AHLs but not others [60]. This specificity in targeting could be both beneficial or a limitation, depending on the application. For example, Hiblot has worked with several lactonases from extremophiles that have been shown to hydrolyze a variety of acyl chain lengths, making them effective quorum quenching molecules against a wide variety of Gram-negatives [63,64]. In contrast, Kyeong used docking analysis to design lactonases that were specifically targeting short acyl chain AHLs [61]. Meanwhile, Vinoj tested for specificity, identifying an AHL lactonase produced by native gut bacteria of white shrimp (*Fenneropenaeus indicus*) that reduced growth of *Vibrio parahaemolyticus* as well as its biofilm development [154]. Similarly Chow engineered a lactonase from *Geobacillus kaustophilus*, a robust bacterium capable of surviving pH 2-10 and 5-78 ºC [155], and demonstrated reduction of *A. baumannii* biofilm mass [156].

There are other AHL hydrolases, including paraoxonases and acylases. Paraoxonase (PON), specifically human paraoxonases, hPON1, hPON2, hPON3 have been shown to be effective lactonases of the *P. aureginosa* AHL $3OC_{12}$-HSL, capable of quenching the AI-1 signal and reducing biofilm growth [157,158]. Acylases, which include both amidases and aminoacylases, hydrolyze amide bonds within AHLs; they also have biofilm inhibiting activities [159]. Independently, acylases have also been shown to inhibit accumulation of quorum sensing

molecules, and in turn, regulate virulence [160]. Further enzyme engineering of this same acylase quenched QS activity of several *Burkholderia* species [161].

Enzymes have also been exploited that modulate QS activity based on altering the QS signal transduction process, as opposed to degrading the signal molecules themselves. Roy showed that the *E. coli* AI-2 kinase, LsrK, can phosphorylate AI-2 *in vitro*, and demonstrated that AI-2 that was extracellularly phosphorylated, prevents its uptake obviating its natural activity. The LsrK activity reduced the native quorum sensing response in *E. coli*, *Salmonella typhimurium* and *Vibrio harveyi*[71]. The mechanism of LsrK phosphorylation of AI-2 was shown in more detail later [65]. Exploitation of kinases, when used in this manner, may prove an effective way of modifying other sensing circuits, such as LAI-1 in *L. pneumophila*, where Lqs1 regulates pathogen-host interactions and competence [109,162].

2.7 Non-QS mediators of biofilm formation

Other methods associated with QS-linked phenotypes, but not specifically attributed to altered QS activity, also reduce biofilm formation and strength. We briefly mention these as they represent interesting pathways for further study. For example, quorum sensing is shown to rely on the ability of bacterial cells to swim either towards or away from various signal molecules, including QS autoinducers as demonstrated by Bansal and Hegde with AI-2 [163,164]. Should the bacteria be non-motile, the effects of these molecules is reduced as cells are less able to co-locate with either themselves or others to form a biofilm. It has been shown, for

example, that expression of surface proteins such as curli, flagella, and pili influence biofilm production through chemotaxis-independent means [165-168].

For example, Pilicides are compounds that prevent pili formation, which in turn provide motility. Chorell and coworkers and, independently, Greene and coworkers, synthesized pilicides of varying strengths in an effort to reduce the ability for *E. coli* to form a quorum and ultimately a biofilm [169,170]. Chabane demonstrated that virstatin, known to reduce virulence in *V. cholorae*, effected biogenesis of *A. baumannii* pili and subsequently reduced biofilm formation and strength [171].

2.8 Delivery Systems for QQ and QS-associated Biofilm Reduction

There is a great deal of evidence demonstrating the ability of non-traditional antibiotics, such as QQ molecules, signaling antagonists, effector enzymes, and their application for reducing bacterial pathogenicity and/or reduce biofilms. However, effective delivery and targeting of these treatments remains a significant technical hurdle and it is becoming increasingly important that recognition of the coupling between transport and function can guide future advances. For example, beyond the QS inhibition molecules noted above and the many we have omitted here but that have been recently reviewed, they have limited activity until they are delivered to the cells or within the cells. Further, we note that studies, including our own[118], show promise to reduce biofilms, but are as yet incapable of completely eliminating bacteria from within biofilms. Accordingly, we also highlight technological approaches that have emerged to elucidate the interactions between QS-inhibiting or biofilm-inhibiting molecules

and the bacteria they target. Perhaps these combinatorial methods, also proposed by Allen et al [172], will prove more efficacious, in both fundamental study and in developing treatment paradigms, as new and more potent molecules are discovered.

That is, in delivering quorum quenching capabilities it may be important that the supplied compound remains sequestered from non-target environments, or is otherwise released at such a rate that it does not cause harm greater than the film it is intended to effect. While not typically described in reviews of quorum sensing, the delivery of molecular modulators can be as important as the molecule's function as it ensures effective use or otherwise, complete inability to function as a modifying agent. In addition to many materials-based surface modification approaches [173-175] there are a few delivery mechanisms have been reported recently that work to enhance QS-based molecular effectors. For example, by adsorbing acylase onto mesoporus silica spheres, Lee et al. demonstrated the attenuation of *P. aeruginosa* PAO1 biofilm formation on filtration membranes used in water treatment systems; importantly, without releasing the enzyme into the water [176]. Xiong et al provided a review of using polymer particles to deliver antibiotics that includes additional examples of this method [177]. The site-specific assembly of QS-active enzymes was also demonstrated by Pei who encoded lactonase synthesis in bacteriophages to deliver to biofilm-localized *P. aeruginosa* and *E. coli*. In this 'one-two' punch system, the lactonase quenched AI-1 signaling at the same time as promoting lysis of the resident bacteria[178].

There are also examples of delivering quorum quenching capabilities on substances/molecules that have other beneficial qualities. Quorum quenching capabilities have also been delivered on reconstituted High Density Lipoproteins (reHDL) for distribution in the blood stream. Deakin engineered a chimeric protein of PON2 (an intracellular paraoxonase) with PON1 (an extracellular paraoxonase) for attachment to reHDL [179]. Attaching this chimera provided quorum quenching activity on the surface of reHDL, a reconstituted version of 'good cholesterol' in human arteries [180]. In addition, Stroescu used vanillin as the cross-linking agent for chitosan, which has previously been shown to have anti-microbial properties [73,181,182], to combine the properties of both compounds [182].

In recent years, microfluidics have been increasingly used to provide insight into microbial growth and behavior [183,184] and test new methods of reducing or preventing biofilms [185,186]. Previously, microfluidics were used to test a combination of quorum quenching techniques and antibiotics [118] and test biofilm dispersion [54]. And as suggested by Hol and Dekker, nanoparticles have also been used to deliver an autoinducer that reduces toxicity in *V. cholerae* capabilities [187] and quorum sensing inhibitors to effect *P. aeruginosa* [188].

We also note that for many applications, such 'single-shot' treatments for prevention or clean-up is insufficient. The techniques described above have also served to underpin self-sustaining capabilities that have longer-lasting effects. For example, engineered cells can be introduced into various settings that, in turn, can provide for sustained treatment., Hong demonstrated a system in which an engineered bacterial species was inserted into a biofilm first supplanting the

initial cell population and subsequently dispersing the film when prompted by chemical induced switch [54]. Also, Zargar demonstrated a bacteria that 'controlled' the common quorum sensing molecule AI-2, providing a constant withdrawal of AI-2 from the extracellular milieu that inhibited biofilm formation [55]. Gupta and Hwang also engineered cells that sensed and destroyed specific species and dissipated extant biofilms, respectively [56,57]. Additionally, there are recent examples of bacteria that provide similar functionality while contained in capsules and films so that new bacteria are precluded from entry Oh [58] and Kim [29].

Finally, several recent studies and reviews have focused on the evolution of resistance [189-191] which will also provide insight into how best to combat the growing antibiotic resistance problem.

2.9 Conclusions

As traditional antibiotics lose efficacy, new ways of fighting bacteria virulence are continually being developed, however fewer involve discovery of new antibiotics. Using natural and synthetic compounds as well as innovative delivery mechanisms new methodologies are emerging that serve to reduce cell growth and pathogenicity without killing bacteria. While it is thought this slows the evolution of resistant bacteria, there are equally interesting results on the evolutionary and modulation of growth and molecular production/release capabilities that quorum sensing/quenching molecules may provide. Methodologies that target the human microbiome (e.g., the GI tract) are likely to be well-received as the impact of overuse of antibiotics is becoming more tractable. Additionally, the use of quorum quenching strategies, antibiotic

counter-inhibitors, development of new antibiotics and more judicious use of existing drugs each offer capabilities to reduce infection and biofouling and have been powerful when used in combination.

3 CHAPTER 3: FUNCTIONALIZED CAPSULE FOR AI-2 QUORUM QUENCHING

3.1 Introduction

Bacterial formation of biofilms becomes toxic to humans and degrades system functionality[192]. These bacterial constructs have been shown to delay wound-healing[193], are problematic in the oral cavity, especially on permanent fixtures[194] or in older patients[195] and can form on medical devices[196]. Detection and removal of these destructive films can be difficult and the widespread use of antibiotics to prevent toxicity has precipitated the development of antibacterial resistant strains which require alternate methods of combating biofilm formation[5,6].

Intercellular communication between bacteria via small molecule-induced signaling, also known as quorum sensing, has been shown to control bacterial phenotypes, including virulence[7,8,24]. As a result, these small molecules, known as autoinducers, are increasingly a focus of research as a means of controlling virulence[197]. Specifically, the focus has been on interrupting these small molecule signaling pathways between bacteria, a method called “quorum quenching”, which has been demonstrated to reduce the strength and formation biofilms[29,89,198].

In this work, the focus is on intercepting signal reception of a specific autoinducer, autoinducer-2 (AI-2), using a natural enzyme delivered with its primary reactant in the form of a self-contained capsule. This enzyme, the kinase LsrK, derived from *E. coli*, phosphorylates AI-2 to phospho-AI-2, AI-2P, which prevents its cellular uptake as shown previously[71]. AI-2 was chosen for

interception for several reasons: it is used in signaling in both Gram-positive and Gram-negative bacteria[8], it is not produced in eukaryotic cells[48], the mechanism of AI-2 phosphorylation is understood[65], and its production is based on positive-feedback[8]. AI-2 is constitutively expressed in *E. coli*, and production is increased in the presence of AI-2, which leads to the positive feedback effect, and as a result, amplification of the AI-2 signal modulation.

This first enzymatic 'quorum quenching' capsule is composed of oppositely charged chitosan and alginate contains adenosine 5'-triphosphate (ATP). ATP is a common energy carrier in biological systems, and the primary substrate for LsrK, in the phosphorylation of ATP. By modifying the powerful AI-2 quenching enzyme, LsrK such that it can be bound to both chitosan films and capsules there is now a means for local AI-2 quorum quenching capability.

3.2 Materials & Methods

3.2.1 Plasmid construction and bacterial strains

3.2.1.1 LsrK-Tyr and LsrK-Gln

The plasmid pETLsrK-Tyr was used to express the AI-2 kinase, LsrK, fused with a spacer and tyrosine tag, herein referred to as LsrK-Tyr. To construct the plasmid, *E. coli lsrK* (*ydeV*) was amplified with primers as indicated in Table 1 from *E. coli* W3110 genomic DNA using Vent DNA polymerase (New England Biolabs; NEB). After purifying the PCR product via the QIAquick gel extraction kit (Qiagen), the blunt-ended fragment was inserted into pET200/D-TOPO (Invitrogen), which has a hexa-histidine tag at the N-terminus for purification after

the protein expression. The sequence of pETLsrK-Tyr was confirmed by sequencing facility (DNA Core Facility of the Institute for Bioscience and Biotechnology Research, University of Maryland). After transforming the plasmid into the BL21 (DE3) host strain, the LsrK-Tyr enzyme (MW: 62.9 kDa) was expressed and purified.

The plasmid pETLsrK-Gln was used to express the AI-2 kinase, LsrK-Gln, fused with spacer and glutamine tag, herein referred to as LsrK-Gln. To construct the plasmid, the gene LsrK-Tyr was cut from the pET200 backbone with NheI and SacI and amplified with Taq polymerase (New England Biolabs; NEB) using LsrK-Gln_Fwd and LsrK-Gln_Rev primers obtained from IDT (Coralville, IA, USA). After purifying the PCR product via the QIAquick gel extraction kit (Qiagen), the gene was digested, and ligated with the previously digested pET200 backbone. The sequence of pETLsrK-Gln was confirmed by Genewiz (Frederick, MD). After transforming the plasmid into the BL21(DE3) PLysS host strain, the LsrK-Gln enzyme (MW: 62.310 kDa) was expressed and purified.

Blue- LsrK; Green - Restriction Enzyme; Orange- Tyrosine tag; Teal – Glutamine tag

Short Name	Description	Sequence
LsrKTyrFrwd	Forward Primer with pET200 Histidine tag pET200His-LsrK-	5'- C ACC ATG GCT CGA CTC TTT ACC CTT TC -3'
LsrKTyr5R1	Reverse Primer with tyrosine tag LsrK-linker-Tyr-Stop -pET200end	5'- CTA ATA ATA ATA ATA ATA GAA TTC CTT TAA CCC AGG CGC TTT CCA TAA C -3'
LsrK-Gln_Fwd	Forward Primer with pET200 Histidine tag pET200His-NheI-LsrK	5'- GCT AGC ATG ACT GGT GGA CAG CAA AT -3'
LsrK-Gln_Rev	Reverse Primer with glutamine tag LsrK-linker-Tyr-Stop -pET200end	5'- GAG CTC CTA TTG CTG TTG CTG CTT TAA CCC AGG CGC TTT -3'

Table 1. Primers for LsrK-X plasmid construction

3.2.1.2 Reporting Cells

A modified strain of the AI-2 sensing *E. coli,* CT104, used by Tsao et al, 2010 and Gupta et al, 2013 was used to measure and prove quenching. This CT104 (pCT6-amp^r+pET-dsRed-kan^r) synthesizes the red fluorescent protein dsRed in lieu of AI-2 due to a LuxS mutation [10,199]. The BB170 *V. harveyi* strain was also used here to determine AI-2 concentration[200].

3.2.2 Overexpression and Purification of LsrK-Tyr

After growth at 37 ℃ at 250 rpm, expression of LsrK-Tyr and LsrK-Gln was induced by isopropylthio-β-galactoside (IPTG, 1mM final concentration) when cell concentrations reached OD_{600} of 0.4. The cells were swirled in an ice-water slush during induction and for several minutes after, which is believed to ultimately de-repress the heat-shock proteins which aids solubility of foreign proteins[201,202]. The induced culture was incubated at 30 ℃, 250 rpm for approximately 16 hours, and the cells were collected by centrifugation, discarding the supernatant. The cell pellet was re-suspended in phosphate buffered saline (PBS, pH 7.4 0.01M) with 10mM imidazole and sonicated using a Fisher Scientific 550 Sonic Membrator at power 3 for 15 minutes 0.5 seconds on/off to disrupt the membrane and release the protein. After sonication, the solution was centrifuged and the supernatant was retained for immediate purification.

Protein purification was achieved using a Ni^{2+}-loaded GE Healthcare Life Sciences HiTrap™ Chelating HP Column, using the hexahistidine-tag on the LsrK-Tyr/Gln protein. After loading, the column was ‘rinsed’ with concentrations of 10mM and 50mM imidazole, and the enzyme was eluted with 300mM

imidazole in IMAC Buffer (50 mM $NaPO_4$, 1.25M NaCl, pH 7.4). The eluted enzyme underwent a series dialysis in PBS at 4℃ to ensure a less than 100 nM concentration of imidazole. The dialyzed enzyme concentration was measured using a nanodrop and appropriate MW/Extinction coefficients (LsrK-Tyr: 102.5k, LsrK-Gln: 95k) and stored in 40% sterile glycerol in 50-100 µL aliquots at -20℃.

3.2.3 Production of AI-2 *in vitro*

AI-2 produced *in vitro* was used unless otherwise stated, to best isolate the LsrK-Tyr activity. The AI-2 was produced using a variation of the nanofactories as described in Fernandes et al [203]. In this study HLPT was used in lieu of HGLPT as the IgG-binding domain was not required.

3.2.4 Binding of LsrK-Tyr to Chitosan

As was previously stated, LsrK-Tyr, was constructed with a pentatyrosine tag on the C-terminus for the binding of the protein to a surface. Specifically this was chosen based on success in maintaining activity in other proteins after attachment to chitosan [204]. Methods similar to Wu et al.[204] were used in forming chitosan films on 96-well plates, except the films remained in the wells. Chitosan (Medium MW, Sigma, St. Louis, MO) was dried either overnight in a 30 ℃ incubator or by vacuum incubation at 30 ℃, then neutralized with 1M NaOH. The films were rinsed with HEPES, pH 7 (Sigma, St. Louis, MO). LsrK-Tyr was added in varying concentrations with 350u of tyrosinase (Sigma, St. Louis, MO) to a final volume of 125 µL. After allowing the tyrosinase and LsrK-Tyr to incubate for 1 hour at 37 ℃ with shaking, the well was rinsed with 1M NaCl or 50mM HEPES, pH 7.0, three times.

Verification of LsrK-Tyr binding to chitosan films and capsules was completed using LsrK-Tyr labeled with DyLight™ Sulfhydryl-Reactive Dye.

3.2.5 Construction of Capsules

Alginate solution 2.5% (w/v) was made by dissolving medium viscosity alginate from brown algae (Sigma, St. Louis, MO) in deionized water. The solution was dissolved by heating, without boiling, and magnetic stirring, then filtered with a 0.22µm Millex®-GP syringe filter (Merck KGaA, Darmstadt, Germany) to remove undissolved substances and impurities. Medium molecular weight chitosan (MMC) from crab shells, 85% deacylated, (Sigma, St. Louis, MO) was dissolved in deionized water (0.8L) containing 2% glacial acetic acid with stirring. The chitosan solution was then twice-filtered to remove undissolved substances and impurities. This yielded a 2% (w/v), pH 5 solution of chitosan as determined by pH test strips 0.0-14.0 (Sigma, St. Louis, MO). A 1% (w/v) calcium chloride solution was prepared by dissolving calcium chloride dihydrate, $CaCl_2$, (JT Baker, Phillipsburg, NJ) in distilled water, and again the solution was filtered using the same Millex® filter to remove impurities. ATP, 100mM, was obtained (Thermo Scientific Inc., Rockford, IL) and diluted to 10mM concentration with autoclaved MilliQ water (Millipore, Darmstadt, Germany).

3.2.5.1 Capsules

Initially a robust, tri-lamellar capsule was used to test LsrK-Tyr binding to a capsule as a proof of concept. The base of the capsule was an alginate bead formed by adding 1% alginate drop-wise via syringe into 1.5M $CaCl_2$. After approximately 5 minutes, the beads were removed from the $CaCl_2$ and rinsed in

350 µL of 0.15M NaCl. The bead was then transferred to a 0.5% chitosan solution, rinsed in 0.15M NaCl, transferred to a 0.5% alginate solution, again rinsed in 0.15NaCl, transferred to 0.5% chitosan solution to add the final layer, and finally rinsed with 0.15M NaCl.

Construction of the functionalized uni-lamellar capsules is based on the charged polymers chitosan and alginate for self-assembly as has been used in previous works[10,205] and has been referred to as a one-stage procedure[206]. ATP (10mM) was mixed with alginate (2.5%) for final concentration of 222µM ATP, vortexed, and added drop-wise by syringe needle (27G) to a magnetically-stirring solution of 1.1% (w/v) chitosan and 0.27% (w/v) $CaCl_2$. The alginate-chitosan capsules were left in the solution for 10 minutes before being removed and rinsed in 0.02% (w/v) $CaCl_2$. These capsules were then transferred for individual attachment of the enzyme. Capsule construction and rinsing was done at room temperature. This process is illustrated in Figure 5.

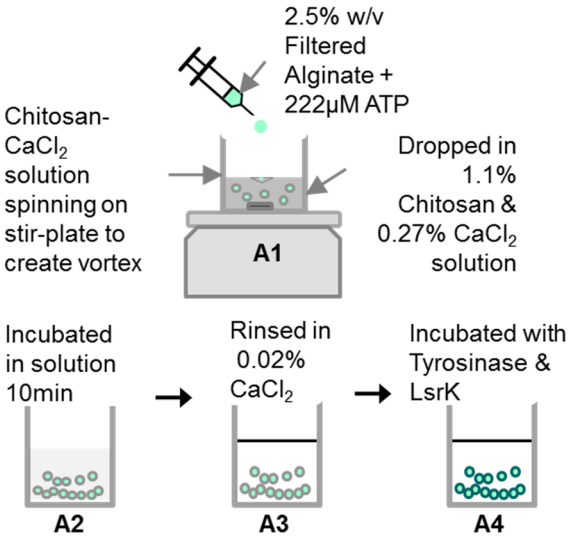

Figure 5. Capsule construction
As illustrated in this figure, capsules were constructed by dropping a mixture of 2.5% w/v filtered alginate and 222µM ATP via 27G needle into stirring Chitosan-$CaCl_2$ to form capsules (A1) which were then incubated 10 min (A2). The capsules were removed from the incubation media and rinsed in 0.02% w/v $CaCl_2$ (A3) before enzyme binding (A4) and subsequent quenching.

3.2.5.2 Calculating Amount of bound LsrK-Tyr

Binding of enzymes to chitosan films and capsules was verified by labeling LsrK-Tyr with DyLight™ sulfhydryl-reactive dye. The amount of chitosan in the bottom of the 96-well plate and surface area of the well was used to calculate amount of LsrK-Tyr per surface area of chitosan. The radius of the capsule (1.375 mm) and shell thickness of capsules (0.2 mm) were measured immediately after rinsing using an MVX10 MacroView fluorescence stereomicroscope (Olympus, Center Valley, PA) as shown in Figure 16-B4. This information was used to calculate the average surface area of the capsule (.24 cm^2) and subsequent amount of bound LsrK-Tyr based on the surface area of a well of a 96-well plate (0.32 cm^2). The Zeiss LSM-310 laser-scanning microscope using the RFP filters was used to construct z-stack confocal images seen in Figure 16.

The chitosan film in the bottom of a 96-well plate was used initially to verify binding and estimate binding density. Labeled LsrK-Tyr was incubated with the dried chitosan in a 96-well plate (surface area of 0.32 cm^2) and a plate reader was used to take fluorescent readings during incubation and after rinsing. Using these post-rinse fluorescent readings and a standard curve the amount bound was calculated as shown in Figure 6.

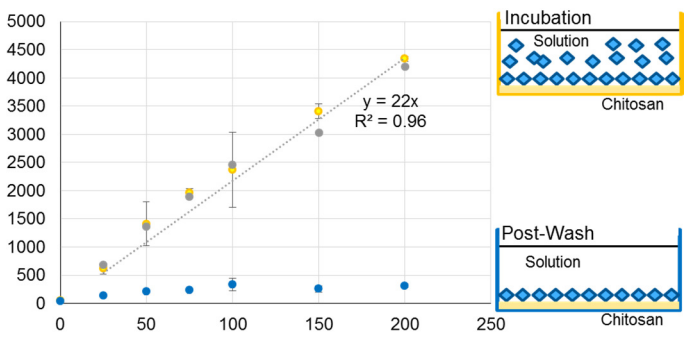

Figure 6. LsrK Binding Measurements in the chart were completed in 96-well plate, illustrated to the right of the graph and are the average of 3 samples of each quantity, taken at the completion of incubation (orange) and after washing. Error bars represent standard deviation. The grey line is a standard curve of labeled enzyme, and the corresponding linear best-fit line and R^2 are for this standard.

In addition, the maximum amount of enzyme per surface area was calculated using the molecular weight of LsrK-Tyr (62.9kDa) for each well. It is assumed LsrK-Tyr is a soluble, globular protein, so the partial specific volume is 0.74 cm^3/g[207]. Multiplying this by the molecular weight and dividing by molecules per mole yields a cubic centimeter estimate of volume per molecule and subsequent radius of $2.64x10^{-7}$ cm. Assuming a spherical molecule, the surface area this sphere would cover can be determined, $2.19x10^{-13}$ cm^2, and this becomes a circle packing problem onto the bottom of a 96-well plate with an area of 0.32 cm^2. While formulas for efficient packing of up to 20 circles have been found[208], packing additional circles becomes a complex coding optimization problem. As a result, for purposes of this work, the square packing hexagon model, also shown as 7 circles within a circle as seen in Figure 7, is used to estimate ratio of surface area covered. Here the inner circles are the enzyme radius, $2.64x10^{-7}$ cm, and the radius of the outer circle is $3*(2.64x10^{-7}$ cm). As the area of a circle is πr^2, this means approximately 7/9 or 78% of the surface area is covered. This is the same percentage that was found using an online calculator[1] and extrapolating, where $1.15x10^{12}$ molecules, or 1.9 picomoles of LsrK, covering an area of 0.25 cm^2 were found to fit on the bottom surface of a 96-well plate. This translates to an area covered by enzyme of .25 cm^2, or LsrK-Tyr coverage of 78% of the total area, or 5.94 picomoles enzyme per cm^2 chitosan. This calculation of coverage only considers the estimated size of the enzyme, and does not consider

[1] http://www.engineeringtoolbox.com/smaller-circles-in-larger-circle-d_1849.html

additional distance that may occur between enzymes due to repulsion of the similarly charged molecules.

Assuming a single layer of enzyme, this layer is 5.28×10^{-7} cm thick, while the chitosan layer in the well is approximately 0.05 mm thick, meaning the enzyme layer is less than 0.1% the size of the chitosan layer.

3.2.5.3 Verifying Activity of LsrK-Tyr/Gln

To verify that the modified enzyme was active both in solution and attached several means were chosen. An ATP assay, Kinase-Glo® Plus (Kinase-Glo Luminescent Kinase Assay Platform, Promega, Madison, WI) was used in addition to the commonly-used BB170 assay[200] [55] and a previously developed reporter cell, CT104[199]. AI-2 produced by nanofactories *in vitro* [203] was used to

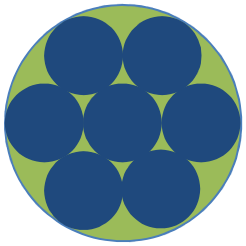

Figure 7. Circle Packing
Here the blue circles represent the enzyme and the green the area to be covered.

provide a controlled and measurable means of verifying AI-2 quorum sensing inhibition. The use of reporter cells to indicate inhibition of quorum sensing is an increasingly common means of verifying quorum sensing inhibition [209,210] and use of known quantities of AI-2, whether synthetic or *in vitro* have also been used as a measure of quorum sensing [199]. The final step in verification of the system was using conditioned media from the AI-2 producing *E. coli*, BL21, incubated with the CT104 reporter cells to further demonstrate the quorum quenching capabilities using naturally-produced AI-2.

3.3 Results

3.3.1 LsrK-Tyr and LsrK-Gln Purification, Yield and Activity

Both forms of LsrK were purified as described and summarized in Figure 8A. Here is presented a comparison of other examples of LsrK purification (A) as well as examples of SDS-PAGE gels (B, E) and Western blots (D, F) to verify the purity of the enzyme. In addition, an SDS-PAGE of the cell lysate of an empty plasmid in the same cell line under the same growth conditions is included in C to

A

Cell	Gene (Organism)	Protein Modification	Purification Method	Yield (mg/L)	Source
E. coli	LsrK (*E. coli*)	N-Terminus His-Tag C-Terminus Tyr-Tag	His-Tag with Ni^{2+} Column & dialysis	20	This study
E. coli	LsrK (*E. coli*)	N-Terminus His-Tag C-Terminus Gln-Tag	His-Tag with Ni^{2+} Column & dialysis	9	This study
E. coli	LsrK (*E. coli*)	N-Terminus His-Tag	Ni 2^{+} Resin	None Reported	Roy, 2009
E. coli	LsrK (*S. typhimurium*)	N-Terminus His-Tag	QIAexpression kit	None Reported	Tsuchikama, 2012

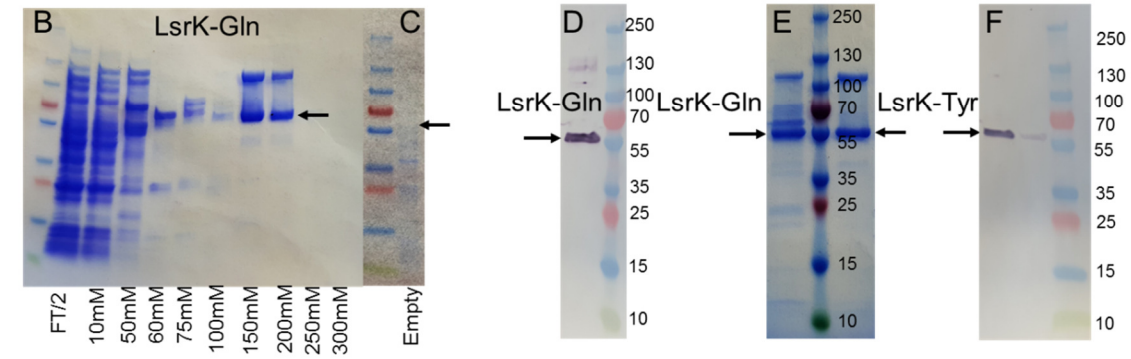

Figure 8. LsrK modification, expression and purification
Native *E. coli* LsrK was modified with two tags and purified used Ni^{2+} column and dialysis. No protein yields have previously been reported as shown in A. Modified LsrK is found on the SDS-PAGE gel (B, E) and Western blot (D, F) just above the 55kDa ladder band. The second line at approximately 120kDa (twice the size of LsrK) (B, E) was found reduced with 'old' samples (those stored at 4 ℃ in PBS without glycerol). In B, the lanes represent the enzyme flow-through of column diluted by half, then increasing concentrations of imidazole until elution as seen with 150 and 200mM concentrations. In C the gel demonstrates that no enzyme is present in the empty plasmid. In D, the lane of the Western to the left of the ladder is the His-tagged LsrK-Gln. In E, the lane to the left of the ladder is LsrK-Gln and the right is LsrK-Tyr. In F, the first lane is the His-tagged LsrK-Tyr and the second lane is an older LsrK-Tyr sample (stored at 4 ℃ in PBS without glycerol). The gel (E) and Western blots (D, F) are representative of what was found during purification of at least 5 different instances of growth, expression and purification.

demonstrate that there is not a band present representing LsrK-Tyr/Gln. It is noted that in the SDS-PAGE and Western that a second band, approximately twice the weight of LsrK-Tyr/Gln is present on fresh samples but was not as visible on samples stored at 4 ℃ in PBS without glycerol.

With the next step to verify LsrK-Tyr and LsrK-Gln the linear range of the luminescent reporter, BB170 was determined by using a standard of AI-2 produced *in vitro* in LB as shown in Figure 9. Here, the values are normalized to a negative control of LB and are the result of the average of three samples with error bars shown, though only visible for the 40µM sample.

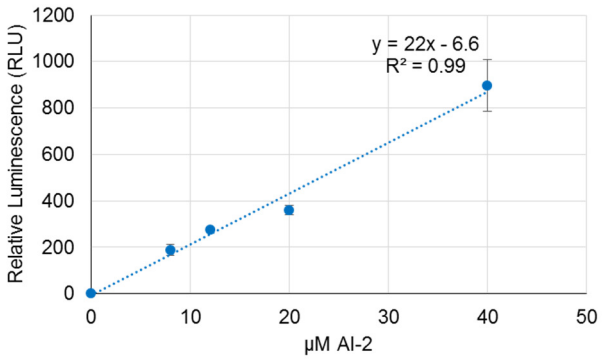

Figure 9. Linear range of BB170 reporter.
Here the linear range of the BB170 bioassay AI-2 luminescent reporter is shown. Values shown are the result of three sample averaged, with standard deviation displayed, but only visible in the 40µM concentration. The linear best-fit formula is shown with the R^2 value.

Both LsrK-Tyr and LsrK-Gln were tested for activity in a final solution of 200µL with 20 uM AI-2 and 30 uM ATP incubated at 37 ℃ with shaking for up to 2 hours. Varying picomoles of LsrK, from 0 to 200, were added as indicated by the second row of the chart in Figure 10. Both charts A and B are broken into three sets of data for the three time-points, 0.5 hours, 1 hour and 2 hours. For each of these time-points triplicate samples from a control of 0 picomoles of enzyme and

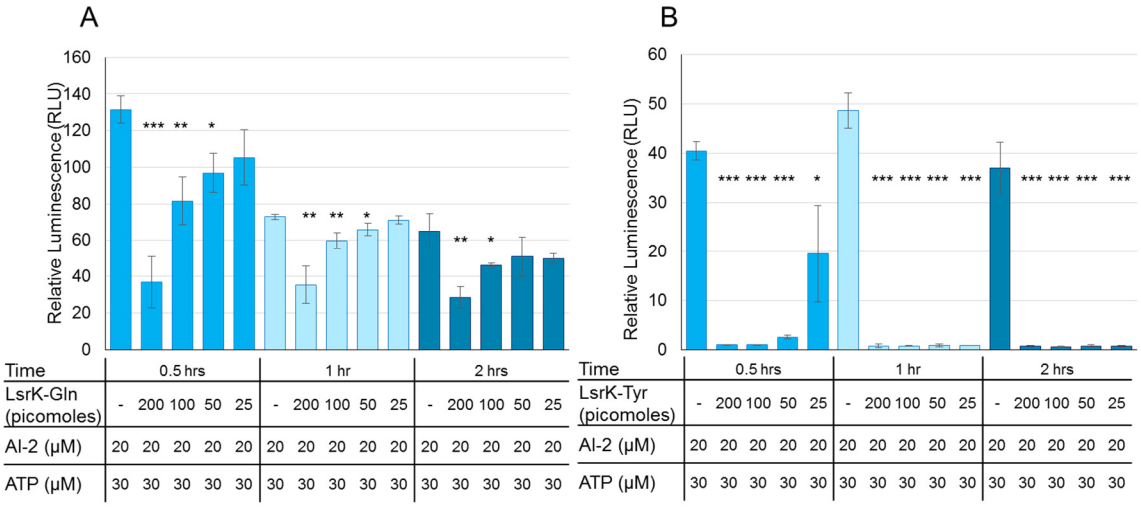

Figure 10. Modified LsrK activity.
Activity of both forms of LsrK was demonstrated over time with varying amounts of enzyme. Chart A is LsrK-Gln, and chart B is LsrK-Tyr. Aliquots of three biological samples of each enzyme amount were taken at the stated times, and were subsequently measured for AI-2 Activity using the BB170 assay. Each bar is the result of the average of the three samples with standard deviation shown by error bars. P-values are calculated using a Student's T-Test, two-tailed, type 2; * < 0.05, ** < 0.008, *** < 0.0008

200, 100, 50 and 25 picomoles of enzyme were taken. In A, the first five columns/bars show the AI-2 activity after the samples were incubated for half an hour with LsrK-Gln, here it can be seen that with 200 picomoles present there is a significant decrease in AI-2 activity as indicated by a Student's T-test p-value less than 0.0008. In addition, both 100 and 50 picomoles also demonstrated a statistically significant decrease in AI-2 activity. 25 picomoles of LsrK-Gln did not produce a statistically significant drop in AI-2 activity for any time point. As shown in Figure 10B, LsrK-Tyr demonstrated a significant decrease after just half an

hour for all samples (200, 100, 50 and 25 picomoles). Unfortunately the structure of LsrK has not yet been published so the specific reason for the disparity in activity of the two forms is difficult to determine. It is suggested that the glutamine tag disrupts folding, which could be due to use of a shorter linker as was necessary to overcome cloning challenges, or the potentially protonated amino group of the glutamine. Ultimately, as a result of the better performance in reducing AI-2 activity, it was decided to proceed with additional experiments with LsrK-Tyr only.

3.3.2 LsrK-Tyr Binding to Chitosan & Activity

Bound LsrK-Tyr activity was determined initially by binding the enzyme to a chitosan film. The pentatyrosine tag on the C-terminus of the LsrK-Tyr was specifically added for binding of the protein to an amine-rich surface, in this case, chitosan. The tyrosine residues are converted to reactive *o*-quinone residues by tyrosinase which can then bind to the amine groups of chitosan as illustrated in Figure 11A. This method was chosen based on success in maintaining activity in other proteins after attachment to chitosan by Wu et al[204].

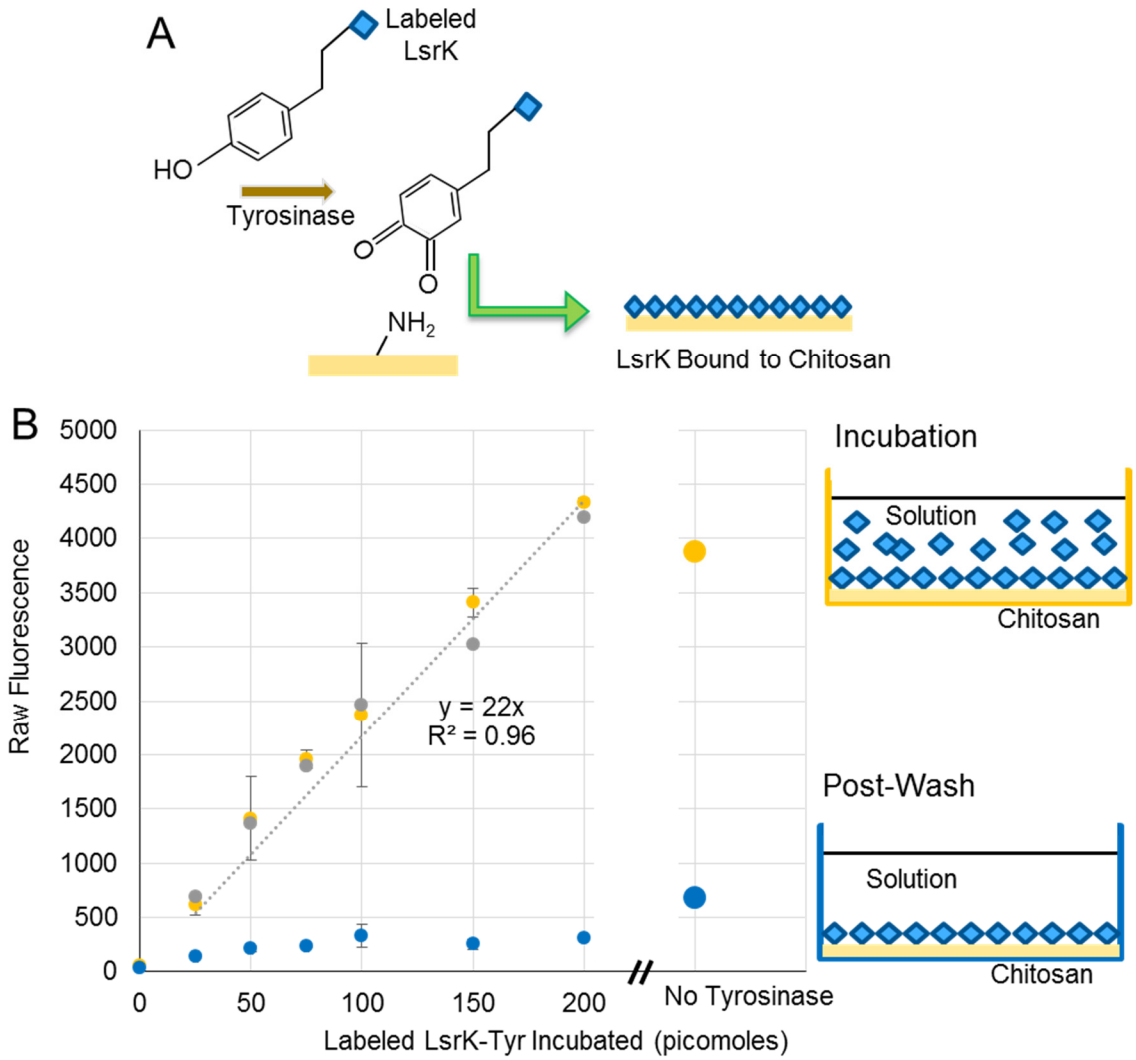

Figure 11: LsrKTyr bound to chitosan film
As illustrated in A, fluorescently-labeled LsrK-Tyr was incubated with tyrosinase so that the tyrosine residue was converted to *o*-quinone for binding to the amine group on chitosan. This was completed in a 96-well plate as illustrated to the right of the graph in B. The graph is the result of fluorescent readings, 3 samples of each quantity, taken at the completion of incubation (orange) and again after two washes (blue), the points are the result of the average with provided standard deviation. The grey line is a standard curve of labeled enzyme, and the corresponding linear best-fit line and R^2 are for this standard.

Figure 11B includes a chart of the fluorescence as measured by a plate reader and illustrations of the conditions being measured. Initially known quantities of fluorescently labeled LsrK-Tyr were incubated with tyrosinase in wells of a 96-well plate that had a chitosan film in the bottom as illustrated in the yellow well.

During incubation, a fluorescence measurement was taken as represented by the yellow dots on the chart for each amount of labeled LsrK-Tyr, where the dots are the average of three samples with error bars representing the standard deviation of these samples. After incubation the wells were washed and another reading was taken of the same wells as represented by the Post-Wash illustration and represented by the blue dots on the chart. Again these dots are the average of three samples with error bars reflecting the standard deviation. At the same time as the washed samples were measured, the fluorescence of samples with known quantities of labeled LsrK-Tyr were measured to create a standard curve represented by the grey dots and linear best fit indicated on the chart in Figure 11B. The average of three samples (100, 150, 200 picomoles initially) was calculated to be 300 raw fluorescence units, plugging this into the standard curve the experimental amount bound was determined to be 13.66 picomoles. The experimental result is nearly an order of magnitude larger than the amount of LsrK-Tyr calculated to be bound based on enzyme size, 1.9 picomoles. This discrepancy may indicate that an area larger than the surface of the well was available. It is possible that labeled LsrK-Tyr could bind in the matrix of chitosan, rather than just the flat surface. Adding approximately seven-times more LsrK molecules to the chitosan matrix to match experimental results, would mean that the enzyme would only penetrate a maximum 0.1% the thickness of the chitosan, based on previous calculations and assuming layers without packing.

In addition to the samples with tyrosinase there were three samples that were incubated without tyrosinase, and then washed in the same manner as the other

samples. The fluorescence from these samples is seen on the right side of the chart in Figure 11B and represented by the larger dots labeled “No Tyrosinase”. It does appear that more enzyme is bound non-covalently/nonspecifically as indicated by this “No Tyrosinase” sample. With a pI of 5.45, and the enzyme incubated in HEPES pH 7 this would make the enzyme relatively negatively charged. Even though the chitosan is neutralized as a film the amine groups may still bind to this negatively charged enzyme.

Having verified successful binding, kinase activity was verified two ways, both by measuring the resultant amount of ATP and the resultant AI-2 activity. Figure 12 illustrates the kinase activity of LsrK-Tyr in phosphorylation of AI-2 to AI-2P by bound LsrK-Tyr and ATP, and shows the results of the ATP and BB170 luminescence assays. All samples contain 20 µM AI-2 and 30 µM ATP in LB. In Figure 12A the ATP Assay is used to verify LsrK-Tyr activity when bound and unbound. The reaction which produces luminescence is found above the chart. All conditions in the chart have dried and neutralized chitosan and are the result of the average of three samples of each condition with the standard deviation provided as error bars. From left to right there is first the sample without LsrK-Tyr, then one with tyrosinase which was incubated and washed. The next four bars are the experimental conditions which all demonstrated a statistically significant decrease in ATP concentration compared to the tyrosinase or no tyrosinase controls as appropriate. Here it is evident that the covalently bound LsrK-Tyr (fourth bar from left), and non-covalent/non-specific binding of LsrK-Tyr

(third bar from left) are both active and demonstrate a statistically significant decrease in ATP concentration compared with controls.

In Figure 12 the same samples were evaluated using the BB170 bioassay which determines relative AI-2 activity. The samples have been laid out in the same order and here it can be seen that the non-covalent/non-specifically bound LsrK-Tyr, when compared with the tyrosinase-free sample also demonstrates a statistically significant decrease in AI-2 activity. The presence of tyrosinase even

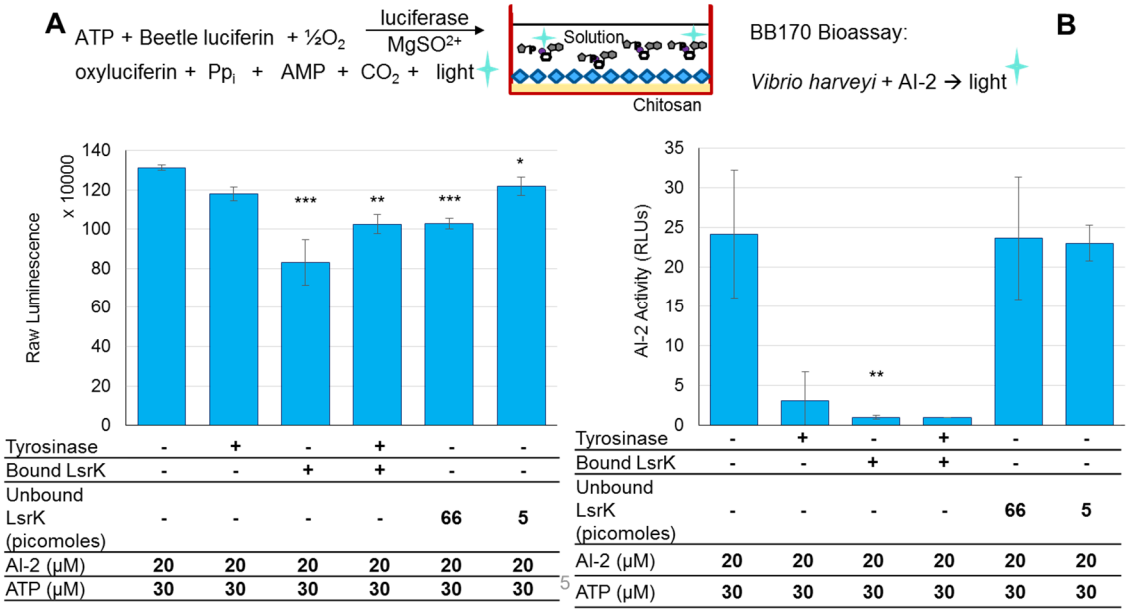

Figure 12: Activity of bound LsrK-Tyr
Here the activity of bound LsrK-Tyr was verified using two methods. In A the amount of remaining ATP is measured, where luminescence is produced as illustrated by the figure above the chart. In B, the BB170 bioassay is used to provide information on relative AI-2 activity, again using the production of luminescence as illustrated above the chart. In both, the values are the average of three samples and dried and neutralized chitosan is present in all samples. P-values are calculated using a Student's T-Test, two-tailed, type 2; * < 0.03, ** < 0.008, *** < 0.0008.

after washing, likely also non-specifically bound to chitosan also seems to reduce AI-2 activity or have an effect on the BB170 assay. It is noted that tyrosinase only seems to have this effect when incubated in LB, as a similar effect was not seen when incubated in PBS (data not provided).

3.3.3 LsrK-Tyr Quorum Quenching Capsules

Next, the reporter cells were used to verity the activity of bound LsrK-Tyr. In Figure 13A is an illustration of the cellular logic used to produce fluorescence with this system and Figure 13B demonstrates the direct relationship between an increase in AI-2 concentration and percent reporter cells fluorescing.

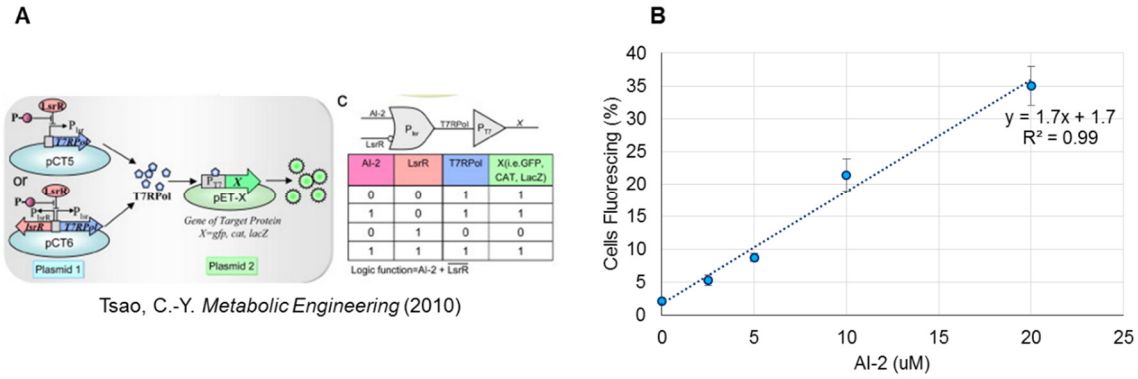

Figure 13: Linear range of fluorescent AI-2 reporter
The reporter cell developed by Tsao et al is used, which works as illustrated in panel A. In panel B, the average percent fluorescing cells of three sample (out of 50,000 as counted by flow cytometry) is presented vs the concentration of AI-2 to which the cells were exposed.

At this point a robust multi-lamellar capsule with an alginate core and alternating layers of chitosan-alginate-chitosan was fabricated as a proof of concept for binding LsrK-Tyr to a chitosan-coated capsule. The capsule, with LsrK-Tyr bound with tyrosinase, was placed in a well and a solution of media containing *E. coli* CT104 OD_{600} 0.4 with ATP and varying concentrations of AI-2 in LB media was added to demonstrate LsrK5'-1 phosphorylation of AI-2, as illustrated in Figure 14A. Results as measured by flow cytometry (FACS) are in Figure 14B. Here it is

clear that the wells with capsules have less fluoresce with a statistically significant margin. It has previously been shown that increasing concentrations of

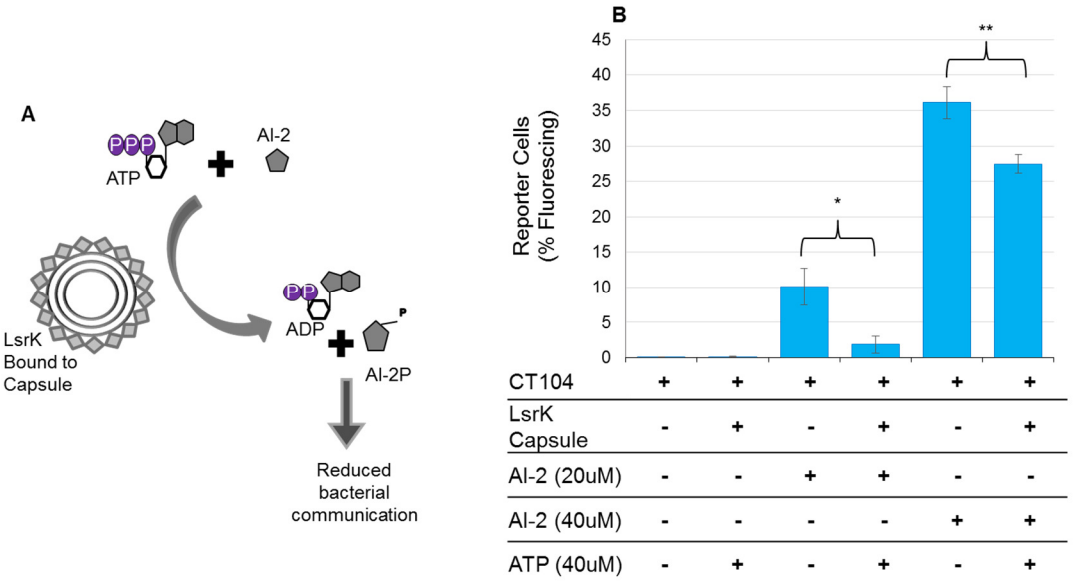

Figure 14: Quorum quenching with capsules
The concept capsule composed of an alginate core with alternating layers of chitosan and alginate was used to verify that LsrK could be bound to a surface layer of chitosan on a capsule and remain active according to the reaction in A. In B, the percent of CT104 reporter cells fluorescing 10 hours after the introduction of AI-2 and ATP was determined using FACS. Chart values are based on three samples of 50,000 cells and p-values were found using a Student's T-test one-tailed distribution and two-sample unequal variance: * < 0.03, ** < 0.008.

AI-2 results in increasing amounts of biofilm formation across several E. coli strains, with significant increases in biofilm formation occurs bewteen 3.2 and 11 µM AI-2[32]. As the linear relationship between AI-2 concentration and percent cells fluorescing was previously shown, and the sample initially at 20 µM was reduced by over 80%, it is logical to assume that the AI-2 concentration has been reduced to less than 5 µM. This concentration of less than 5 µM AI-2 was demonstrated to have lead to less biofilm formation than higher concentrations (11 µM) and therefore would this reduction in AI-2 concentratioin by LsrK-Tyr bound to a capsule would lead to less biofilm formation[32].

The next step was to implement a capsule capable of delivering the primary substrate, ATP. These capsules were specifically designed for ease of construction, requiring only a syringe, needle and stir-plate, and to be robust to withstand bacterial growth conditions in addition to being able to deliver ATP. A uni-lamellar capsule was constructed capable of maintaining integrity during bacterial growth conditions (10+ hours, 37 ℃, 250 rpm, LB media) as described in the methods section.

Labeled LsrK-Tyr was again used to verify binding to the capsule as can be seen in Figure 16. When confocal imagery showed binding to the outer layer (B3) capsules were measured to determine surface area and, ultimately, calculate the amount of bound LsrK-Tyr to the outer surface. Using the average measured diameter of a capsule, 2.75 mm, the surface area of a capsule is 0.24 cm^2, and the amount of bound LsrK-Tyr, 1.4 picomoles, assuming 78% coverage as with the chitosan film. Fluorescence measurements of capsules in the plate reader revealed that capsule fluorescence was not statistically different than the well, as seen in Figure 15. This was anticipated, as efforts were made to employ similar amounts of protein in the wells as in the capsules, based on similar surface areas. This may indicate higher amount of LsrK-Tyr binds per surface area of the capsule (57 picomoles/cm^2) vs the well (43 picomoles/cm^2). Even when

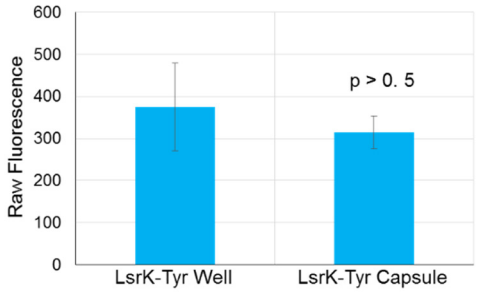

Figure 15: LsrK-Tyr binding: Well vs Capsule. Here the raw fluorescence as produced by LsrK-Tyr bound to the bottom of a well of a 96-well plate and to a capsule after washing is shown. The bars are representative of the average of three samples with the error bars representing the standard deviation. Here it is clear that the amount bound is similar in both conditions as measured by fluorescence.

considering this slightly higher binding density, the LsrK-Tyr layer size, compared with the capsule shell is similar that of the chitosan in the well, less than 0.1% the depth of the chitosan layer.

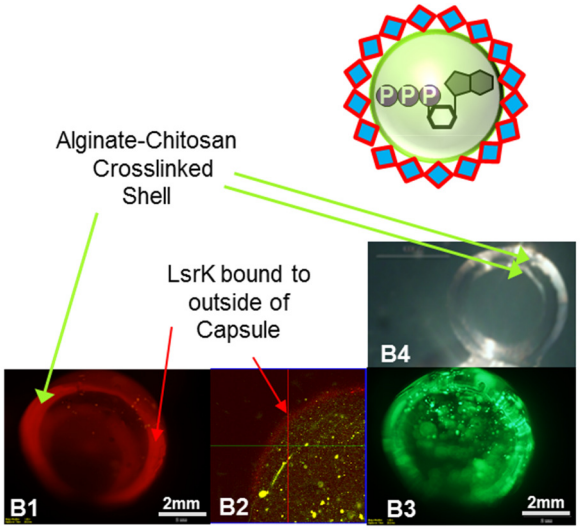

Figure 16: LsrK binding to quenching capsules
The images of the capsules as taken by a stereo microscope (B1, B3, B4) are shown in Figure B. Here red fluorescently-labeled LsrK is bound to a capsule with green fluorophores mixed in the alginate. A confocal microscope was used to produce the image which shows the labeled LsrK on the outermost edge of the capsule (B2).

Initially, uni-lamellar capsules without ATP were verified for quenching capability. These capsules were placed in the wells of a 24-well plate and media containing *E. coli* CT104 OD_{600} 0.4 was added with varying concentrations of AI-2 in LB media and incubated at 37 ℃ for 8 hours with shaking. After incubation, the capsules were observed to still be intact, demonstrating ability to maintain structure in bacterial growth environment.

Aliquots of each sample were taken and FACS was again used to obtain a count of per-cell fluorescence for the uni-lamellar capsules. Figure 17 contains the results of averaging FACS results from three samples of each condition. The statistical significance seen between the positive controls of AI-2 and CT104 cells in solution with capsules without LsrK-Tyr and those with capsules with LsrK-Tyr bound demonstrates that AI-2 concentration is decreased by over 98% by LsrK-

Tyr bound on the capsule in common bacterial growth conditions. This data indicates that the LsrK-Tyr functionalized capsule is capable of reducing the AI-2 communication signal for a population of *E. coli* cells such that on average no cells were fluorescing, indicating sub-micromicromolar concentrations and therefore leading to less biofilm formation[32].

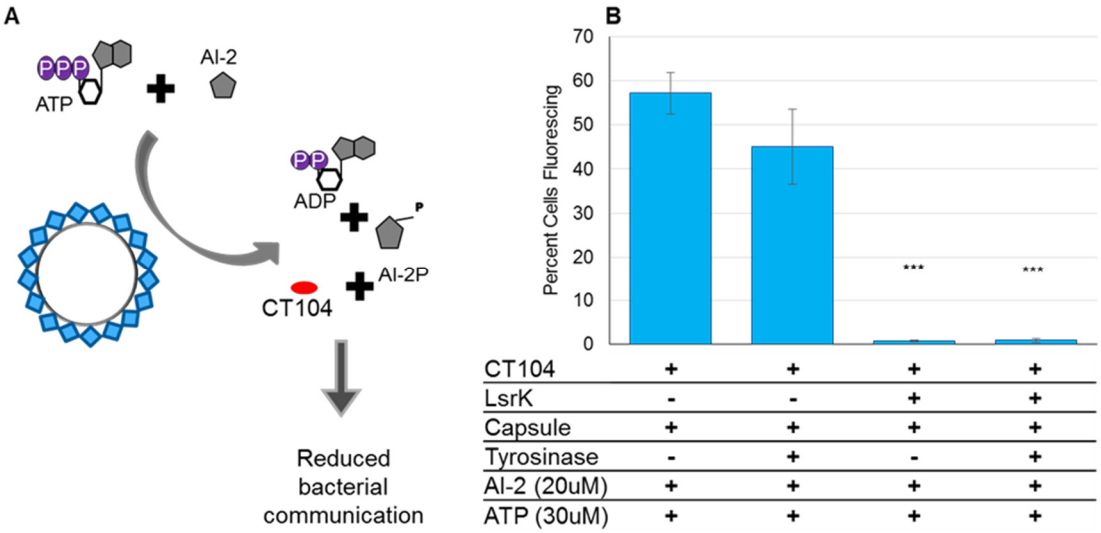

Figure 17: Uni-laminar capsules with *in vitro* produced AI-2
Panel A of the figure illustrates the reaction which is taking place. Here a capsule as described previously, without ATP in the core, is introduced to a solution containing ATP and AI-2. The LsrK-Tyr bound to the outside of the capsule phosphorylates the AI-2 to AI-2P, so that the reporting cells, CT104**,** no longer recognize the communication signal. A quantitative measure of this quenching is provided in the chart, where each bar is the average of three 50,000 cell samples. These show the percent of fluorescing CT104 reporter cells as counted by flow cytometry. P-values are calculated using a Student's T-Test, two-tailed, type 2; *** < 0.0008**.**

Capsules with 222 µM ATP mixed with alginate during formation were analyzed to verify that the ATP was diffusing out of the capsule. Twenty-four single-layer

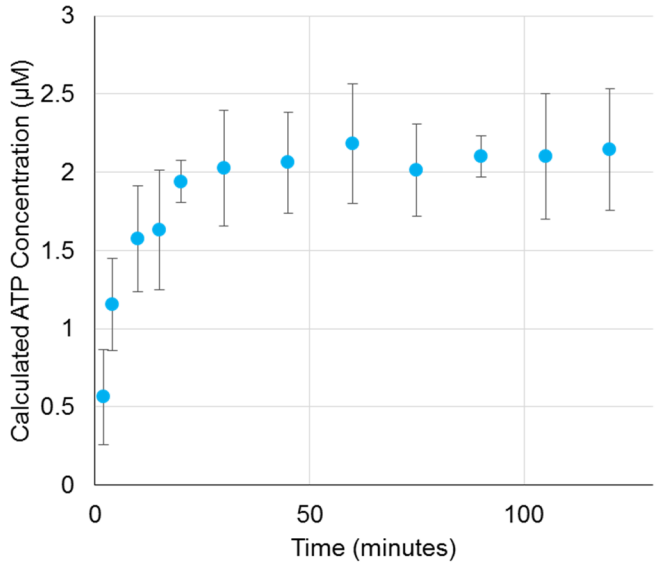

Figure 18: ATP diffusion out of capsules
Here is provided the diffusion of ATP out of capsules over time. 8 capsules were placed in 2mL of LB and incubated at 37 ℃ with shaking. Aliquots were removed at indicated times and measured for ATP activity using Kinase-Glo® Plus.,ATP concentration was calculated using a standard curve.

ATP/alginate-chitosan capsules were divided across three wells of a 6-well plate so that eight capsules were in each well and 5 mL of LB was added to the capsules. The capsules were then shaken on a rotating shaker at 37 ℃ and aliquots of the LB were removed at various time intervals until 120 minutes had elapsed. At the completion of a 120 minutes the ATP assay was used, with a standard curve, to determine the resultant concentration of ATP in solution at each time point. A graph of the data is found in Figure 18, demonstrating that the ATP does diffuse out of the capsule and equilibrium was reached within 50 minutes of the start of shaking. (Additional information and calculations on ATP diffusion are found in Appendix A.)

To this point, AI-2 produced *in vitro* was used in known quantities to reduce variability of production by cellular populations. To more fully prove the functionality of the capsules, media from a culture of BL-21, an AI-2 producing *E.*

coli, and the reporting *E. coli,* CT104, was used. The AI-2 producing cells were grown to OD_{600} of 1.0 in LB media, and the cells were removed by syringe filtering the solution with a 0.22µm filter. This solution was then diluted with LB (2:1) and incubated with the capsules for 10 minutes at 37 ℃. After incubation an equal amount of reporting *E. coli* was added to the solution and capsules and incubated for 8 hours with shaking at 37 ℃. After 8 hours aliquots were taken and diluted with PBS for flow cytometry. Figure 19A is an illustration of this experiment and Figure 19B are the flow cytometry (FACS) results of the average percent of fluorescing cells of three separate samples. All samples have a capsule, however, the second, fourth and sixth columns from the left have a capsule with covalently bound LsrK-Tyr. The first two columns reflect reporter cells fluorescence and decrease in fluorescence when using a known quantity of AI-2 and ATP in addition to that found in the capsule. The last four columns represent the reporter cell fluorescence as a result of the conditioned media from the AI-2-producing cells and subsequent decrease in percent cells fluorescing

when a capsule with LsrK-Tyr is present as represented by columns four and six. In columns three and four, a known quantity of ATP was added exogenously, in

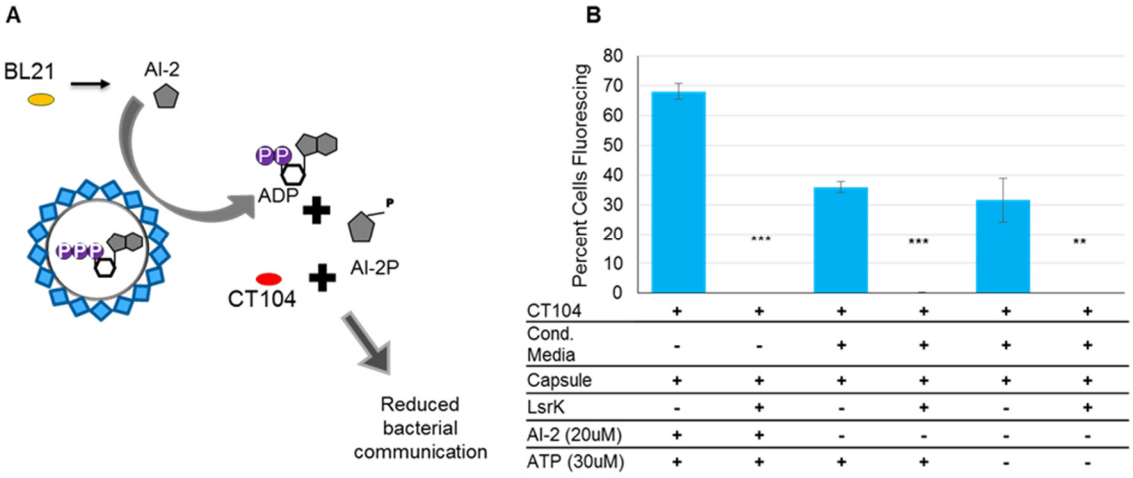

Figure 19: Functionalized quenching capsules
In A the capsule with ATP inside and LsrK-Tyr on the outside is illustrated phosphorylating AI-2 which has been produced by the BL21 cell-line of *E. coli*. This phosphorylated AI-2 is not recognized by the CT104 reporter strain, preventing it from fluorescing red. The decreased red fluorescence as counted by flow cytometry is shown in B, each bar the average of three samples. Here it is shown that very few cells fluoresce in the presence of the functionalized capsule. P-values are calculated using a Student's T-Test, two-tailed, type 2; ** < 0.008, *** < 0.0008.

addition to that contained within the capsule. From the results shown in Figure 19 it is clear the capsule composed of ATP/alginate and chitosan with covalently bound LsrK-Tyr is capable of reducing the concentration of AI-2 as measured by the AI-2 reporter cells, CT104. These results specifically indicate a nearly complete elimination of AI-2 in solution.

3.4 Conclusion & Discussion

It has been demonstrated in this work that both modified forms of LsrK are active in solution. The tyrosine-tagged LsrK was successfully attached to both a chitosan film and a capsule, demonstrating quenching in both cases. Immobilization of this enzyme, capable of quenching the 'universal' quorum sensing molecule, on a surface using free amine groups is a significant

advancement. There are already several examples of surfaces being amine-modified[211,212] so the enzyme as it exists could be added to this materials to provide AI-2 quorum quenching capabilities to a wide variety of environments.

The immobilization of the kinase LsrK-Tyr on both a flat surface and capsule demonstrate a new delivery mechanism for this powerful kinase. In addition, while kinases are notoriously unstable it appears that binding the enzyme to a surface provides some stability. Specifically, while the enzyme, even in high concentrations of glycerol loses effectivity after a single freeze-thaw-freeze cycle (not shown), the bound enzyme was found here to maintain activity after incubation for one hour at 37 ℃ with shaking as seen in Figure 17 Figure 19). Should binding, both covalently and non-covalently, increase stability of LsrK-Tyr it would broaden the 'real-world' applicability of using LsrK-Tyr for quenching AI-2. As a result, it would be prudent to study the stability of the bound enzyme.

The amount of ATP in the capsule used herein is limited and diffuses rapidly. Other nanoparticles, composed of chitosan, have previously been shown to have a slower release of ATP over 24 hours[213]. These nanoparticles are also significantly smaller, which provides more surface area in the same volume for additional delivery of LsrK-Tyr in addition to the more controlled release of ATP. The more controlled release of ATP would allow more of this primary substrate be added to the capsules initially, and when combined with the capability to both deliver more of the LsrK-Tyr enzyme could result in additional reduction of AI-2 concentration over a longer period of time.

While the amount of ATP delivered in the capsule is limited, and for surface-bound LsrK, no ATP is provide with the enzyme, however this may not be a significant issue. Extracellular ATP is found in supernatant of cultures of *E. coli, Salmonella, Klebsiella, Acinetobacter, Pseudomonas*, and *Staphylococcus* in concentrations of 20 – 600 nM, indicating both delivery mechanisms may have some effectivity in environments with bacteria [214,215]. In addition, it was found that *E. coli* and *Salmonella* had increased survival in the presence of ATP-supplemented culture[216]. As a result, this immobilized enzyme may not only reduce biofilm formation and toxicity by quenching AI-2, but also by consuming ATP in the process.

As both chitosan and alginate are already used in wound dressing[13 14], functionalizing these substances with LsrK provides an active barrier in the prevention of biofilm formation. Capsules could be placed in wounds to prevent biofilm formation and infection, and surfaces could be coated with the enzyme for oral applications. And because the materials used, chitosan and alginate, are already used in healthcare, there are procedures for sterilization that also maintain material properties[217,218].

4 CHAPTER 4: MODIFICATION AND BIOPOLYMER ATTACHMENT OF A VERSATILE LACTONASE FOR

4.1 Introduction

The World Health Organization has identified antibiotic resistance as "… one of the biggest threats to global health today. It can affect anyone, of any age, in any country."[219] Despite this large global health concern, few new antibiotics are being developed, and current antibiotics are losing effectivity. As a result, new methods of combating harmful bacterial effects are being explored, including affecting bacterial communication pathways as a means of effecting bacterial biofilm formation and toxicity. There are several classes of bacterial communication molecules that can be targeted, including homoserine lactones, N-Acyl homoserine lactones (AHLs), or AI-1, which are used by Gram-negative bacteria including *Pseudomonas aeruginosa*. Enzymes that hydrolyze the ester bond of lactones, lactonases, have been shown to render the communication molecule unrecognizable to cells, disrupting the communication pathway. Cell population phenotypes can be modified by interfering with bacterial communication, providing a non-invasive way of altering bacterial behavior including reducing toxicity [27]. Quenching AHL communication is complicated by the fact that many different molecules, used by different bacteria are contained within the class of AHL, unlike AI-2 which is more universal. As a result, it is desirable to choose a lactonase that is more promiscuous, meaning that a single enzyme is capable of hydrolyzing several different AHLs.

The WHO has also identified chemicals of major public health concern. This list of ten chemicals includes hazardous pesticides, which are so pervasive the WHO established their Pesticide Evaluation Scheme (WHOPES) to monitor pesticide safety[220]. Organophosphates (OP), discovered during the development of nerve gas, are commonly used in pesticides and have known neurologic effects. OPs inhibit acetyl cholinesterase activity, which leads to decreased nerve function[221] and have been shown to cause long-term developmental and behavioral neurological effects [222,223]. OPs have also been shown to affect liver, respiratory and cardiac function [223]. As a result, phosphotriesterases (PTEs), which neutralize organophosphates by hydrolysis of organophosphate esters [224], are of particular interest for treatment both prophylactically and after exposure[225,226]. Because hydrolysis is required in 'neutralizing' both molecules, an increasing number of studies have been conducted on enzymes which have both lactonase and PTE activity[225,227].

Based on these requirements the enzyme *Sso*Pox, named such based on organism of origin (*Sulfolobus solfactircus, Sso*) and its initial identification as a paraoxonase (Pox) was chosen as the lactonase for incorporation into a functionalized system. *Sso*Pox, from hyperthermophilic *Sulfolobus solfataricus*[62], has previously been shown to exhibit promiscuous lactonase activity with a preference toward AHLs with 8 - 10 carbon aliphatic chains and oxo-lactones with shorter chains[63]. It has been produced in *E. coli* and has as structure where the active site is opposite the N- and C- termini, as seen in Figure 20, indicating that modifications to these may not affect activity *Sso*Pox has also been studied

for its ability to hydrolyze organophosphates[228,229] and homoserine lactones[63]. The structure of *Sso*Pox is of particular interest as it enables high thermostability

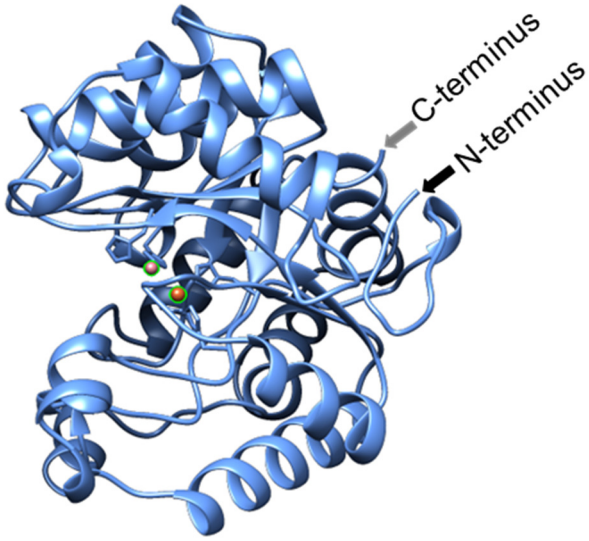

Figure 20: Cartoon of *Sso*Pox
This cartoon, generated using the expasy swiss-model and then visualized using Chimera from UCSF, illustrates the orientation of the N- and C-terminus as well as highlights the colbalt ions at the location of the active site.

[62], relatively non-specific hydrolysis[230] and the location of the N-and C- termini – opposite the dimer binding site and loop 8 active site [63] – providing the potential to modify the enzyme for purification and attachment.

In this work, three tags have been added to two modified *Sso*Pox proteins, a hexa-histidine tag has been added to the N-terminus in both and a penta-tyrosine tag or quaternary glutamine tag added to the C-terminus. The hexa-histidine tag provides a simpler method of purification – previously heating, H/F-PLC, NaCl gradient and dialysis has been used in *Sso*Pox purification [228,231]. In addition to the hexa-histidine tag, tyrosine and glutamine tags have been added to the C-terminus to facilitate covalent binding to the biopolymer chitosan[204,232]. These were specifically chosen based on success in maintaining activity in other proteins after attachment to chitosan[204] and more wide-spread use of free-amine binding for functionalizing surfaces[212].

Attaching *Sso*Pox to the biopolymer chitosan, which is commonly used for drug delivery and wound healing applications[233], will provide new ways of delivering lactonase and potentially, organophosphate hydrolysis activity. Here lactonase activity is verified for the AI-1, OdDHL/3-oxo-C12HSL/OdDHL, which stimulates inflammation in mammalian cells and promotes production of the toxin pycyonin in *P. aeruginosa*[94].

4.2 Materials & Methods

4.2.1 *Sso*Pox Expression Plasmids

The *Sso*Pox genetic sequence was optimized for *E. coli* using the IDT codon optimization tool and the gBlock and primers for insertion into pET200 plasmid were ordered from IDT (Coralville, IA, USA). The primer sequences are in Table 2 and the gBlock sequence is found in Appendix 2.

To construct the tyrosine-tagged *Sso*Pox, the gBlock was amplified using F-*Sso*Pox and *Sso*PoxR-Tyr. The purified PCR product was digested with SacI and NheI for sticky-end ligation into the pET200 backbone to create pH*Sso*PoxTyr. To add the glutamine tag the pH*Sso*PoxTyr plasmid was digested with NheI and SacI. The *Sso*Pox gene was amplified with Q5 (NEB, Ipswich, MA) with the same forward primer as used previously and the new reverse primer, *Sso*PoxR-Gln was used to add the glutamine tag. This PCR product was digested and ligated into the backbone previously digested. The sequence of the resultant plasmids (pH*Sso*PoxT and p*Sso*PoxG) were verified by Genewiz (Frederick, MD). After transformation into *E. coli* BL21(DE3) pLysS cells the enzymes SsoPox-Tyr (MW: 39.694 kDa) and SsoPox-Gln (MW:38.719 kDa) were expressed and purified.

Purple – *Sso*Pox; Green - Restriction Enzyme; Orange- Tyrosine tag; Teal – Glutamine tag		
Short Name	Description	Sequence
F-*Sso*Pox	Forward Primer with pET200 Histidine tag pETHisNhel-HisSpacer2*Sso*Pox-F	5'-ACT GAA GCT AGC GAT CGT GAA GAT CGT AAG GAA GAT CGT ATC CCG CTG GTA GGG AAG-3'
*Sso*PoxR-Tyr	Reverse Primer with tyrosine tag *Sso*PoxSpacer3Tyr-SacIStop - pET200end	5'- TAT GCA GAG CTC TTA ATA ATA ATA ATA ATA CTT ACG ATC TTC ACG ATC CGA GAA GAA TTT -3'
*Sso*PoxR-Gln	Reverse Primer with tyrosine tag *Sso*PoxSpacer3Tyr-SacIStop - pET200end	5' – GAG CTC CTA TTG CTG TTG CTG CTT TAA CCC AGG CGC TTT-3'

Table 2. Primers for *Sso*Pox-X plasmid construction

4.2.2 Overexpression and Purification of Modified *Sso*Pox

Cells were inoculated from frozen stock and grown overnight in Luria Burtania, LB (Fisher, Pittsburgh, PA), and 50µM kanamycin at 37 ºC, 250 rpm. These cells were re-inoculated to OD_{600} 0.05 in 200mL ZYP-5052 media without metals mix [234]. Cells were initially grown at 37 ºC with shaking (250 rpm) until the culture reached OD_{600} 1.0 (3.5 – 4 hrs). The culture was then subjected to cold-shock – swirled in ice-water for approximately 5 minutes – during which 0.2 mM $CoCl_2$ was added as was done previously [229]. Cell growth continued at room temperature (~24 ºC) for 20 hours with shaking (250 rpm). Cells were then pelleted (10000g, 4 ºC, 10 min), and re-suspended in a lysis buffer similar to that used by Hiblot et al (50 mM HEPES pH 8, 150 mM NaCl, 0.2 mM $CoCl_2$, 0.1 mM PMSF and 20 mM $MgSO_4$)[229] and frozen at -80 ℃. A Fisher Scientific 550 Sonic Membrator at power 3.5 for 10 minutes 0.5 on/0.5off was used to disrupt the membrane and cell debris was removed by centrifugation (10000 g, 4 ºC, 10 min).

Protein purification was achieved using a GE Healthcare Life Sciences HiTrap™ Chelating HP Column, and the hexa-histidine-tag on the *Sso*Pox-X protein. Two columns were used in this work: one loaded with Ni^{2+}, and the other loaded with Co^{2+}. First, IMAC Buffer (50mM $NaPO_4$, 1.25M NaCl, pH 7.4) was used for both columns, then the Activity Buffer described by Hiblot et al[229] was used, both with increasing concentrations of imidazole after protein loading to determine optimal purification conditions. The most pure sample of *Sso*Pox-Tyr/Gln underwent dialysis in Activity Buffer with gentle stirring at 4 ºC until final imidazole concentration was less than 100nM. The dialyzed enzyme concentration was measured using a nanodrop and appropriate MW/Extinction coefficients (*Sso*Pox-Tyr: 39.7kDa/37.4k, *Sso*Pox-Gln: 38.7kDa/30k) and stored in 10% sterilized glycerol at -20 ℃.

4.2.3 AI-1 Reporter Construction

Construction of an AI-1 reporter was completed using constructs from Lindsay et al[235], 'standard parts', a constitutive promoter developed in-lab and the pET21a backbone. This reporter, using genes and proteins from *P. aeruginosa*, produces green fluorescent protein in the presence of the AI-1, OdDHL. All primers were obtained from IDT (Coralville, Iowa). Plasmid maps of the reporters are found in Appendix B.

The first plasmid constructed, pAHL-Reporter_Red-Green, constitutively expresses dsRedExpress2 and *P. aeruginosa* LasR. LasR binds to OdDHL to form the OdDHL-LasR complex, which binds to the *P. aeruginosa* DNA binding site also incorporated into this plasmid. This DNA binding site is a positive

transcriptional regulator that is activated upon binding of the OdDHL-LasR complex to the DNA, which activates transcription of sfGFP to signal the presence of OdDHL. This plasmid was transformed into the *E. coli* strain W3110 LuxS- which does not produce AI-2. Subsequently, modifications were made to the plasmid using the restriction enzyme BstEII to cut 200bps from the center of dsRedExpress2 from pAHL-Reporter_Red-Green, rendering the quaternary protein inactive, but maintaining LasR production, and forming a new plasmid: pAHL-Reporter_Green. The new plasmid was transformed into Top10 cells. Both reporter cells were stored as frozen stock and inoculated from frozen stock the day before use.

4.2.4 Determining Lactonase Activity of Modified *Sso*Pox

The modified *Sso*Pox enzyme activity was verified by two methods that used reporter cells to indicate the presence of AHL N-dodecanoyl-L-homoserine lactone (OdDHL), obtained from Cayman Chemical (Ann Arbor, MI). 225µM and 20µM concentrations of OdDHL were used in experiments, with samples diluted as required by the biological reporter cells. The first reporter cell, a luminescent reporter, developed and provided by the Ahmer Lab [235] provides a quantitative indication of OdDHL activity in the nanomolar range (10^{-9}-10^{-7}), requiring samples to be diluted. The second, developed here, uses the same *P. aeruginosa* LasR and DNA binding site, but includes fluorescent reporter that provided a new method of measuring the response.

Incubation was completed in a multi-well plate with positive controls and negative controls contained in the same plate as the experimental conditions. As a result,

all samples were incubated for the same times and temperatures and completed in triplicate. Sample aliquots were removed and diluted for both luminescent and fluorescent reporters.

The luminescent reporter was inoculated and grown overnight in LB with 50µM kanamycin and 5µM tetracycline at 37 ºC, 250 rpm. Cells from the overnight culture were diluted 1:2500uL in LB with 50µM kanamycin and 5µM Tetracycline and 180µL of diluted cells were added to 20µL of the diluted incubation sample in a 5 mL test tube or 90 µL of cells were added to 10µL of diluted sample in a 96-well white plate. The sample was incubated at 30 ºC, 250 rpm for several hours and luminescence was measured using a GloMax®-Multi Jr (Promega) or Synergy HT plate reader.

The fluorescent reporter cells were also inoculated and grown overnight in LB (100µM ampicillin/carbenicillin at 37 ºC, 250 rpm). These cells were re-inoculated and grown to OD_{600} 0.4 and again 180 µL of cell culture was added to 20 µL of the diluted incubation sample in a 5 mL test tube or 90 µL of cells were added to 10 µL of diluted sample in a 96-well white plate. This culture was incubated at 37 ºC, 250 rpm, for 3 hours and the percent of fluorescing cells was counted by flow cytometry.

4.2.5 Binding *Sso*Pox-Tyr to Chitosan

*Sso*Pox-Tyr was constructed with a penta-tyrosine tag on the C-terminus for the binding of the protein to a surface. Methods similar to Wu et al[204] were used, where 1.5% chitosan (Sigma, St. Louis, MO) was dried overnight by vacuum

incubation at 30 ℃ in a 96-well plate, then neutralized with 1M NaOH and rinsed with HEPES pH 7.0 (Sigma, St. Louis, MO). *Sso*Pox-Tyr was added in varying concentrations to 350u of tyrosinase (Sigma, St. Louis, MO) and HEPES pH 7.0 added to a final volume of 100 µL per well. After allowing the tyrosinase and *Sso*Pox-Tyr to incubate for 1 hour at 37 ℃ with shaking, each well was rinsed with HEPES pH 7.0 three times, as was done in previously. Binding to chitosan films and capsules was verified by labeling *Sso*Pox-Tyr with DyLight™ Sulfhydryl-Reactive Dye (ThermoFisher Scientific, Grand Island, NY). Bound His-*Sso*Pox-Tyr activity was verified by binding the protein as described, then repeating the methods described previously for protein activity.

4.2.6 Binding *Sso*Pox-Gln to Chitosan

*Sso*Pox-Gln was constructed with a quaternary-tyrosine tag on the C-terminus for the binding of the protein to a surface. Methods similar to Bhokisham et al[232,236] were used, where the chitosan film was prepared as previously described. Here a 60 µL 1 mM K-Y-K peptide (Sigma, St. Louis, MO) in pH 7.0 HEPES was combined with 350u of tyrosinase and HEPES pH 7.0 was added to a total final volume of 100 µL. After allowing the peptide and to incubate for 1 hour at 37 ℃ with shaking, each well was rinsed with HEPES pH 7.0 three times, as was done in previously.

Next, the *Sso*Pox-Gln enzyme was bound to the peptide using microbial transglutaminase (MTG) (Sigma, St. Louis, MO). Here MTG was prepared by making a 5% w/v solution in 10mL of pH 7.0 HEPES and filtering this solution with a 0.22µ filter. Final concentration of the MTG solution was measured using a

nanodrop. 60 µM of MTG was used to bind varying concentrations of *Sso*Pox-Gln to the peptide with HEPES pH 7.0 supplementing the solution to 100 µL; again incubation of binding occurred for 1 hour at 37 ℃ with shaking. Binding to chitosan films and capsules was again verified by labeling *Sso*Pox-Gln with DyLight™ Sulfhydryl-Reactive Dye. Bound *Sso*Pox-Gln activity was verified by binding the protein as described, then repeating the methods described previously for protein activity.

4.2.7 Calculating Bound *Sso*Pox

Binding of enzymes to chitosan films and capsules was verified by labeling *Sso*Pox with DyLight™ sulfhydryl-reactive dye. The amount of chitosan in the bottom of the 96-well plate and surface area of the well was used to calculate amount of LsrK-Tyr per surface area of chitosan. The outer diameter (1.375 mm) and shell thickness of capsules (0.2 mm) were measured immediately after rinsing using an MVX10 MacroView fluorescence stereomicroscope (Olympus, Center Valley, PA) as shown in Figure 31. This information was used to calculate the average surface area of the capsule (23.76 mm^2) and subsequent amount of bound *Sso*Pox based on the surface area of a well of a 96-well plate (0.32 cm^2).

The chitosan film in the bottom of a 96-well plate was used initially to verify binding and estimate binding density. Labeled *Sso*Pox was incubated with the dried chitosan in a 96-well plate (surface area of 0.32 cm^2) and a plate reader was used to take fluorescent readings during incubation and after rinsing. Using these post-rinse fluorescent readings and a standard curve the amount bound was calculated as shown in Figure 21

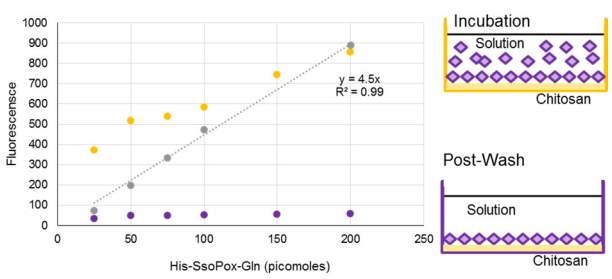

Figure 21. *Sso*Pox-Gln Binding Measurements in the chart were completed in 96-well plate, illustrated to the right of the graph and are the average of 3 samples of each quantity, taken at the completion of incubation (orange) and after washing (purple). Error bars represent standard deviation. The grey line is a standard curve of labeled enzyme, and the corresponding linear best-fit line and R^2 are for this standard.

In addition, the maximum amount of enzyme per surface area was calculated using the molecular weight of *Sso*Pox (38.7, 39.6kDa) for each well. For these calculations it is assumed *Sso*Pox is a soluble, globular protein, so the partial specific volume is 0.74 cm^3/g[207]. Multiplying this by the molecular weight and dividing by molecules per mole yields a cubic centimeter estimate of volume per molecule and subsequent radius of 2.25×10^{-7} cm for *Sso*Pox-Tyr and 2.24×10^{-7} cm for *Sso*Pox-Gln. Assuming a spherical molecule, the surface area this sphere would cover can be determined, 16×10^{-13} cm^2 for both enzymes and this becomes a circle packing problem onto the bottom of a 96-well plate with an area of 0.32 cm^2. While formulas for efficient packing of up to 20 circles have been found[208], packing additional circles becomes a complex coding optimization problem. As a result, for purposes of this work, the square packing hexagon model, also shown as 7 circles within a circle as seen in Figure 22, is used to estimate ratio of surface area covered. Here the inner circles are the same radius as that of the enzyme, r, 2.25×10^{-7} or 2.26×10^{-7} cm, and the radius of the outer is 3*r. As the area of a circle is πr^2, this means approximately 7/9 or 78% of the surface area is covered. This is the same percentage that was found using an

online calculator[2] and extrapolating, where $1.15x10^{12}$ molecules, or 1.9 picomoles of *Sso*Pox, covering an area of 0.25 cm^2 were found to fit on the bottom surface of a 96-well plate, 7.6 picomoles/ cm^2. This calculation of coverage only considers the estimated size of the enzyme, and does not consider additional distance that may occur between enzymes due to repulsion of the similarly charged molecules.

Assuming a single layer of enzyme, this layer is $4.5x10^{-7}$ cm thick, while the chitosan layer in the well is approximately 0.05 mm thick, meaning the enzyme layer is less than 0.1% the size of the chitosan layer.

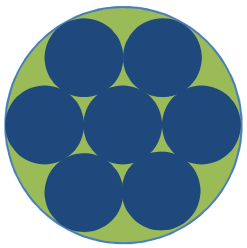

Figure 22. Circle Packing
Here the blue circles represent the enzyme and the green the area to be covered.

4.3 Results

4.3.1 Purification of Modified *Sso*Pox

Here, for the first time *Sso*Pox was successfully modified with a histidine tag, making it possible to purify the enzyme using this tag. The first modified *Sso*Pox, *Sso*Pox-Tyr, was initially purified a Ni^{2+} column with each of IMAC and the Activity buffer. While the IMAC elution yielded some enzyme, Figure 23B, the Activity Buffer did not due to ionic 'competition' between the Ni^{2+} column and the Co^{2+} in the buffer. Given this, and that *Sso*Pox is a metallo-enzyme with cobalt as

[2] http://www.engineeringtoolbox.com/smaller-circles-in-larger-circle-d_1849.html

the stabilizing metal ion a Co^{2+} column was used yielding a clean elution Figure 23C. The two Western blots for *Sso*Pox-Tyr purification with Ni^{2+} and Co^{2+}

A

Cell	Protein Modification	Purification Method	Yield (mg/L)	Source
E. coli	N-Terminus His-Tag C-Terminus Tyr-Tag	His-Tag with Co^{2+}Column & dialysis	24	This study
E. coli	N-Terminus His-Tag C-Terminus Gln-Tag	His-Tag with Co^{2+}Column & dialysis	10	This study
E. coli	None	Heat, Ammonium sulphate precipitation, Exclusion Size Chromatography	10	Hraiech, 2014
P. putida	None	Heat, Anion-exchange column, increasing NaCl gradient	9	Ng, 2011
E coli	None	Heat, FPLC with increasing NaCl gradient and decreasing $(NH_4)_2SO_4$	5	Merone, 2005

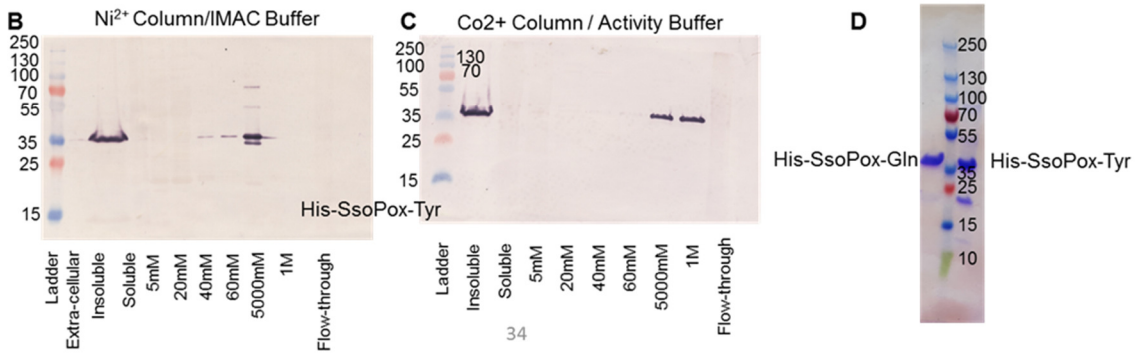

Figure 23: Purified *Sso*Pox-X
A summary of the construction, purification and yield of the enzymes developed in this work are compared to previous work in A. Figures B and C are the results of a Western blot comparing the purity of samples when a Nickel (B) vs Cobalt (C) column was used for purification. In both the lanes are first a ladder then extracellular sample for Ni2+ and the insoluble and soluble samples for each. This is followed by increasing concentrations of imidazole to determine best elution concentration and purity of samples. Finally in D the purification of each His-*Sso*Pox-Gln (left of ladder) and His-*Sso*Pox-Tyr (right of ladder) on an SDS-PAGE gel can be found.

columns are provided in Figure 23B, C. *Sso*Pox-Tyr was rinsed with 20mM and 60mM imidazole in Activity Buffer before being eluted with 1M imidazole. *Sso*Pox-Gln rinsed with 40mM and 100mM imidazole in Activity Buffer before being eluted with 300mM imidazole. The SDS-PAGE gel of the elution of each variant of the *Sso*Pox enzyme is also shown in Figure 23D with a summary of enzyme purification and yields Figure 23A.

4.3.2 AI-1 Reporter

All three reporters were verified for a direct response, luminescent or fluorescent, to increasing concentrations of the AI-1, OdDHL. In Figure 24 the direct relationship between AI-1 concentration and luminescence is shown. This standard was repeated for every measure of luminescence when using the Synergy HT plate reader.

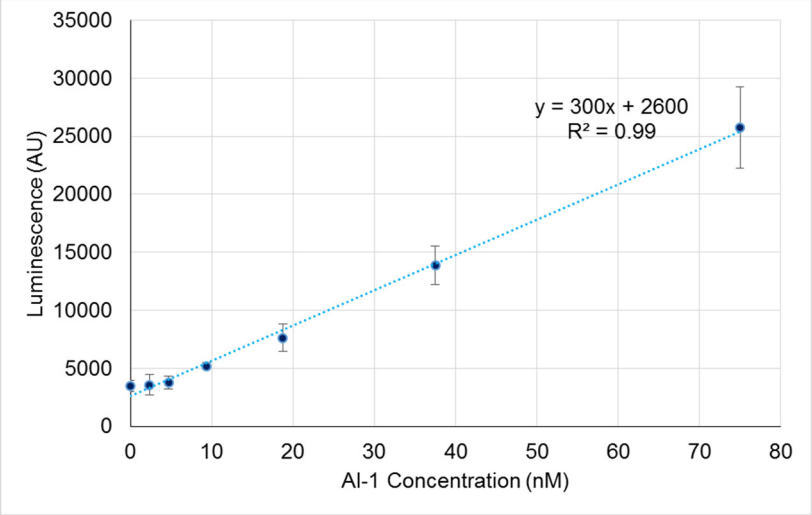

Figure 24: Linear range of luminescent AI-1 reporter.
The cells as developed by Lindsay et al were obtained and used as the primary means of determining reduction of AI-1 concentration. Here the linear range of this reporter is demonstrated. Luminescence was measured by plate reader. Each point is the average of three samples with standard deviation of results shown. The linear best fit line equation and R^2 value are shown.

Similarly, the AI-1 response of the two fluorescent reporters were also measured using flow cytometry and a 4-point standard was conducted when measurements were taken. In Figure 25 both the overall range and linear range of the reporters are shown. The Red-Green reporter did show better consistency between runs, as the overall range was comprised of two different days of tests, and this reporter provided a better linear best fit.

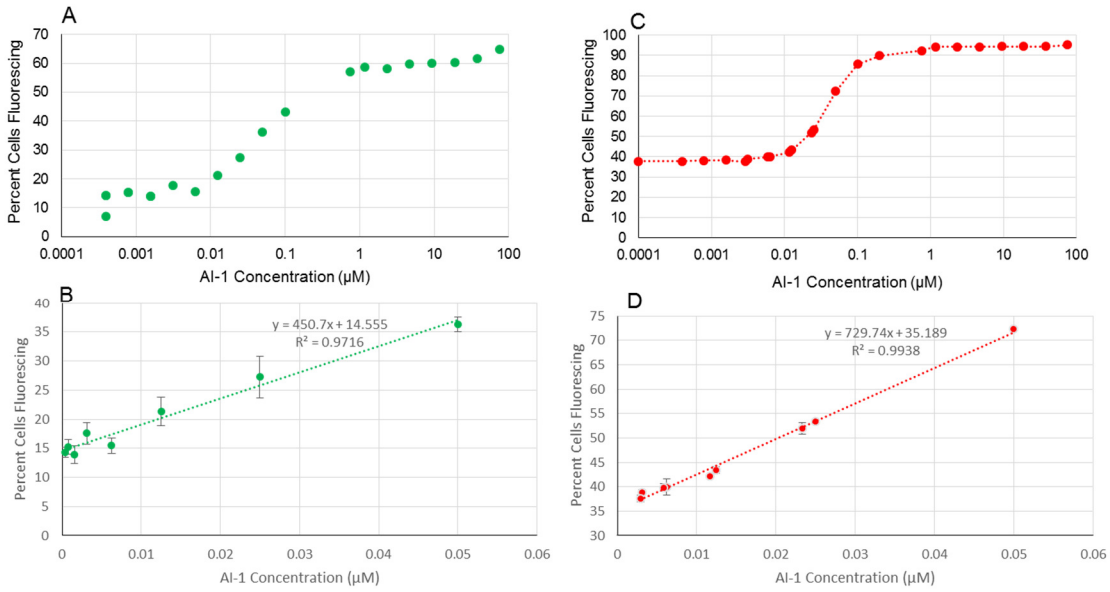

Figure 25: Linear range of fluorescent AI-1 reporter.
Here, two new reporter cells were used to measure the concentration of AI-1 in solution. They are both based on the same plasmid backbone, and placed in different cell-lines. Figures A and B are a reporter that only turns green in the presence of AI-1 in the Top10 cell-line. In C and D, the Red/Green reporter is constitutively expressing red and turns green in the presence of AI-1. This is in a cell line that does not produce AI-2 so could be used in AI-1 and AI-2 quenching environments. The data for all four charts are average percent of cells fluorescing of three cultures, with standard deviation, which is visible in the linear range in charts B and C. Each point is the result of 50,000 cells as counted/measured by flow cytometry.

4.3.3 *Sso*Pox-X Quorum Quenching

Using the luminescent reporter, the activity of the two modified forms of *Sso*Pox were verified in solution. Both *Sso*Pox-Gln and *Sso*Pox-Tyr were tested for activity in a final solution of 100µL with 225 uM OdDHL (AI-1) incubated at 37 ℃ with shaking for up to 4 hours. Varying picomoles of *Sso*Pox, from 0 to 200, were added as indicated by the second row of the chart in Figure 26. Both charts A and B are broken into three sets of data for the three time-points, 1 hour, 2 hours and 4 hours. For each of these time-points triplicate samples from a control of 0 picomoles of enzyme and 200, 100, 50 and 25 picomoles of enzyme were taken.

In Figure 26A, the first four columns/bars show the AI-1 activity after the samples were incubated for an hour with *Sso*Pox-Gln, here it can be seen that with 200, 100, 50 and 25 picomoles present there is a significant decrease in AI-1 activity as indicated by a Student's T-test p-value less than 0.0008. The same is true for the 2 hour time point, with all experimental samples exhibiting a statistically significant decrease in AI-1 activity. At hour four, statistical significance is maintained, but p-values are higher due to more variability in the control. As shown in Figure 26B, *Sso*Pox-Tyr demonstrated a significant decrease after just an hour for 200 and 100 picomole samples, but no statistically significant decrease was found when 25 picomoles were present, even after 4 hours.

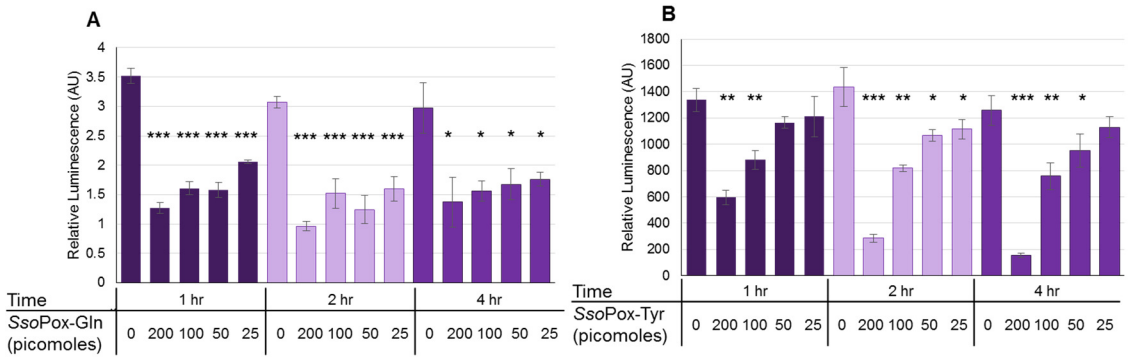

Figure 26: AI-1 Quenching with lactonase in solution.
In A, *Sso*Pox-Gln activity of known quantities was measured over several hours. In B, known quantities of *Sso*Pox-Tyr were monitored for activity over several hours. The average of triplicates of each sample are shown with standard deviations from samples in a 96-well plate. Aliquots of each sample were taken at 1, 2 and 4 hours as indicated.

The difference between the activity of the two forms of *Sso*Pox could be the result of differences in structure of the two attachment tags. As the N- and C-terminus are next to one another it is possible that the aromatic rings of the hexa-histidine tag and tyrosine tag are interfering with one another, and subsequently with folding in this area. It is also possible that the linker or aromatic ring of the tyrosine residues affect the α-helix which precedes both on the C-terminus.

With activity in solution of both variants of *Sso*Pox demonstrated, the next step was to verify the ability to bind the two variants to chitosan.

*Sso*Pox-Tyr binding to chitosan films and capsules was completed using *Sso*Pox-Tyr labeled with DyLight™ Sulfhydryl-Reactive Dye. The chitosan film in the bottom of a 96-well plate was used initially to verify binding and estimate binding density. Labeled *Sso*Pox-Tyr was incubated with the dried chitosan in a 96-well plate (surface area of .32 cm^2) and a plate reader was used to take fluorescent readings during incubation (yellow well and dots) and after rinsing (purple well and dots) as illustrated in Figure 27B. A fluorescence measurement was taken as represented by the dots on the chart for each amount of labeled *Sso*Pox-Tyr, where the dots are the average of three samples with error bars representing the standard deviation of these samples. After incubation the wells were washed and another reading was taken of the same wells as represented by the Post-Wash illustration and represented by the blue dots on the chart. Again these dots are the average of three samples with error bars reflecting the standard deviation. At the same time as the washed samples were measured, the fluorescence of samples with known quantities of labeled *Sso*Pox-Tyr were measured to create a standard curve represented by the grey dots and linear best fit indicated on the chart in Figure 27B.

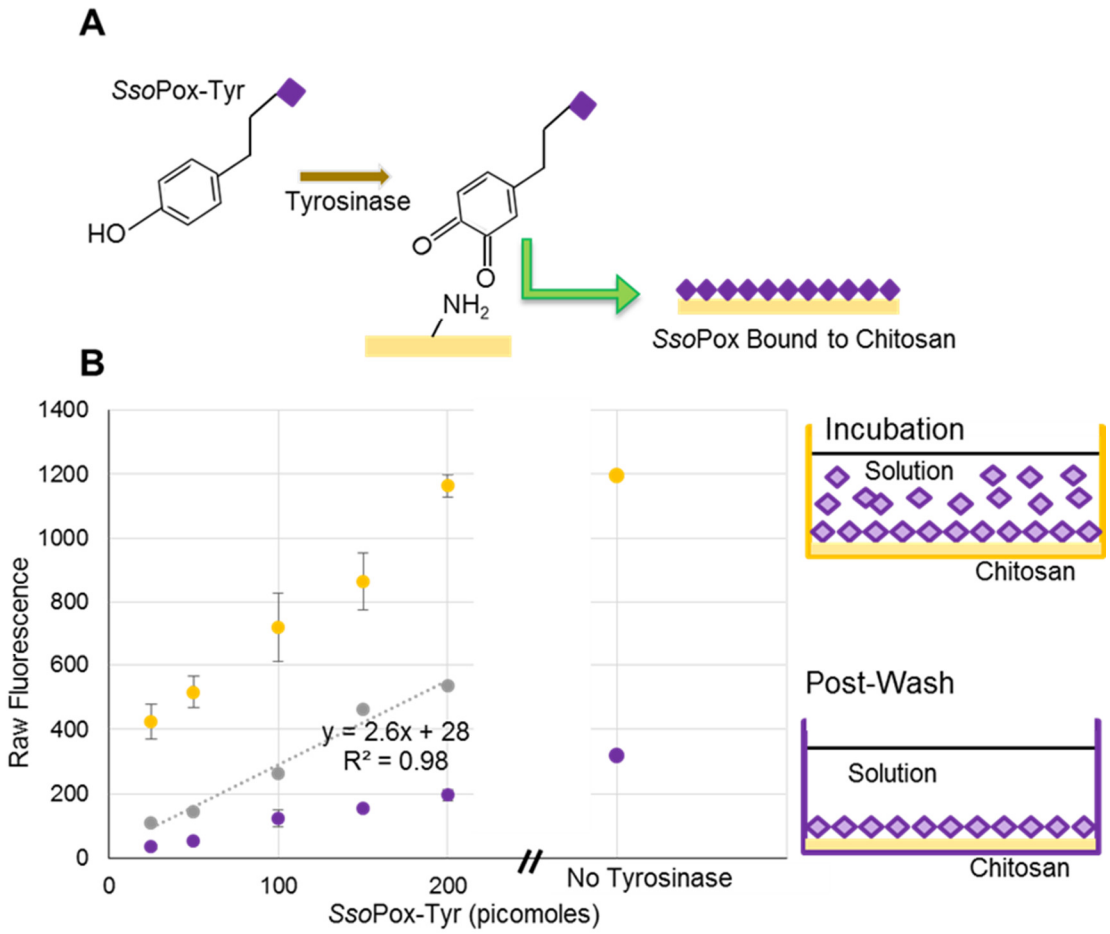

Figure 27: *Sso*Pox-Tyr binding to chitosan.
In A, the binding of *Sso*Pox-Tyr is illustrated using tyrosinase to form an *o*-quinone on the tyrosine residue which binds to the amine groups on chitosan. Figure B is the result of fluorescent readings taken at the completion of incubation (yellow) and again after washes (blue).Points are the result of the average of 3 samples with provided standard deviation. The grey line is a standard curve of labeled enzyme, and the corresponding linear best-fit line and R^2 are for this standard.

Using the average fluorescence of the samples with 150, and 200 picomoles initially, 175, and the standard curve the experimental amount bound was determined to be 57 picomoles, which is over an order of magnitude larger than that previously calculated based on enzyme size, 1.9 picomoles. This discrepancy may indicate that an area larger than the surface of the well was

available. It is possible that labeled *Sso*Pox-Tyr could bind in the matrix of chitosan, rather than just the flat surface or that the chitosan.

In addition to the samples with tyrosinase there were three samples that were incubated without tyrosinase, and then washed in the same manner as the other samples. The fluorescence from these samples is seen on the right side of the chart in Figure 27B and represented by the larger dots labeled “No Tyrosinase”. It does appear that more enzyme is bound non-covalently/nonspecifically as indicated by this “No Tyrosinase” sample. With a pI of 6.28, and the enzyme incubated in HEPES pH 7 this would make the enzyme slightly negatively charged. Even though the chitosan is neutralized as a film the amine groups may still bind to this negatively charged enzyme.

Similarly, binding of *Sso*Pox-Gln was tested with a fluorescently labeled protein. Figure 28A and B illustrate the two-step binding process. Figure 28C is the average of three samples as measured by the plate reader incubation of known quantities of labeled *Sso*Pox-Gln and then again after washing each well three times, with error bars representing the standard deviation of these standards. A standard curve was again created using known concentrations of labeled *Sso*Pox-Gln and this curve was used to calculate the amount of bound *Sso*Pox-Gln after washing (12.6 picomoles, using the average of the values measured for 150 and 200 picomoles). In addition to verifying binding via the two-step process for the *Sso*Pox-Gln, samples were incubated without tyrosinase and found to remain bound after washing. This is reflected in Figure 28C on the far right

labeled “NoTyrosinase” and using the standard curve represents 35 picomoles bound. Considering that *Sso*Pox-Gln has the same pI as *Sso*Pox-Tyr it is likely that the slightly negatively charged enzyme is binding to the neutralized chitosan.

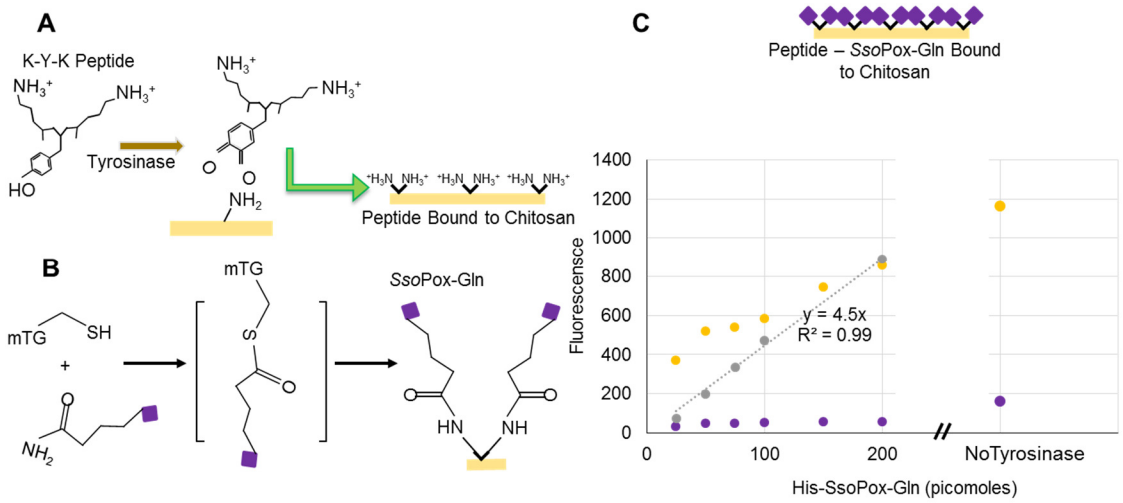

Figure 28: *Sso*Pox-Gln binding to chitosan.
In A, the binding of the K-Y-K peptide is illustrated using tyrosinase to form an *o*-quinone on the tyrosine residue which binds to the amine groups on chitosan. Figure B shows the multi-step process whereby MTG aids in binding the *Sso*Pox-Gln to the lysine groups of the peptide. Figure C is the result of fluorescent readings taken at the completion of incubation (yellow) and again after washes (blue). Points are the result of the average of 3 points with provided standard deviation. The grey line is a standard curve of labeled enzyme, and the corresponding linear best-fit line and R^2 are for this standard.

As outlined in the methods section the estimated amount bound of both *Sso*Pox-Tyr and *Sso*Pox-Gln was determined to be 7.6 picomoles/cm^2 for each given the small difference in radius between the two variations. This took into consideration circle packing for a coverage of 78%, and does not consider repulsion of the similarly charged molecules. While calculated or theoretical max is often more than experimental results, the opposite was found here and there are at least two explanations. First, it is likely that the chitosan is not dried perfectly flat, providing additional surface area, and secondly, there exists the possibility that enzyme is binding within the chitosan matrix, again, to a larger area than that of the bottom of the well. Should the case be that the enzyme is binding in the chitosan matrix,

adding between seven and thirty-times more *Sso*Pox molecules (to match experimental results) would mean that the enzyme would only penetrate 0.1-0.3% the thickness of the chitosan, based on a layer of enzyme 4.5 $x10^{-7}$ cm thick.

Both *Sso*Pox-Tyr and *Sso*Pox-Gln demonstrated successful binding to the chitosan surface, with experimental results indicating that the covalently and non-covalently bound *Sso*Pox-Tyr (57, 110 picomoles) bound in higher quantities when compared with *Sso*Pox-Gln (12.6, 35 picomoles). However, previously *Sso*Pox-Gln demonstrated more activity in solution so both variations were tested for bound enzyme activity. As described, chitosan was bound to the wells of a 96-well plate and both enzymes were bound within the same plate, with the first step of the two-step glutamine binding completed and then both enzymes binding at the same time with and tyrosinase. Positive controls of unbound enzyme were included to verify the enzymes were active. As can be seen in the first five columns of Figure 29A both unbound enzymes are active, with both demonstrating statistically significant decreases in AI-1 activity. However, only *Sso*Pox-Gln provided a statistically significant decrease in AI-1 concentration as seen the last two columns. In Figure 29B it is evident that there is a small difference between the two amounts of unbound *Sso*Pox-Gln (200 vs 50 picomoles) as is expected given previous results. And clearly less enzyme activity is seen in comparing between the 50 picomoles and that bound, though that bound is at least five times less than that which was added in solution.

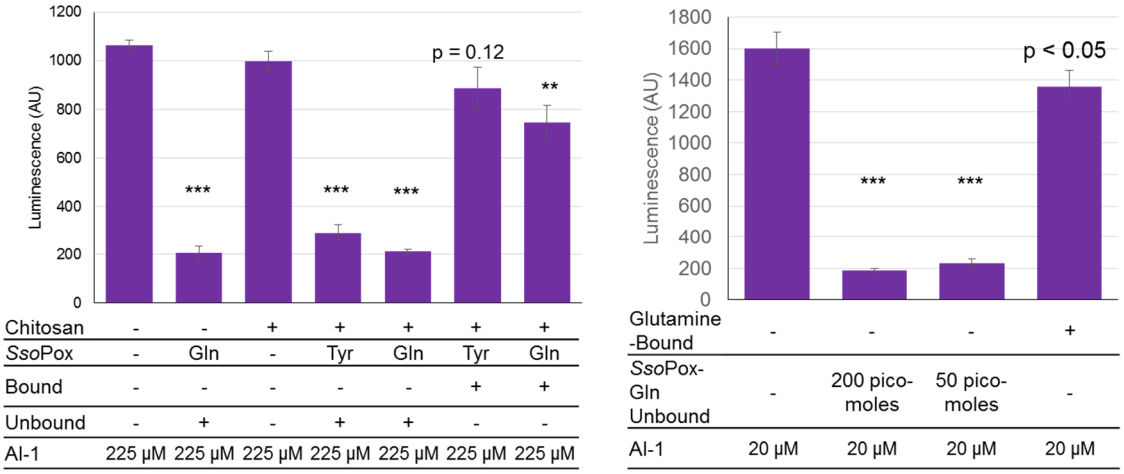

Figure 29: Activity of bound *Sso*Pox-X.
The above demonstrates the activity of bound and unbound SsoPox at two different Al-1 concentrations. In chart A, 200 picomoles of unbound *Sso*Pox were used and samples were incubated for 2 hours at 37 ℃. In chart B, only *Sso*Pox-Gln was tested and samples were incubated 1 hour, again at 37 ℃. In both charts the bars are the average of three samples with standard deviations provided. P-values are calculated by Student's T-Test, two tails, type 2; ** < 0.008, *** < 0.0008.

4.3.4 *Sso*Pox-Gln Capsules for Quorum Quenching

Construction of the functionalized uni-lamellar capsules is based on the charged polymers chitosan and alginate for self-assembly as has been used in previous works[10,205] and has been referred to as a one-stage procedure[206]. ATP (10mM) was mixed with alginate (2.5%) for final concentration of 222µM ATP, vortexed, and added drop-wise by syringe needle (27G) to a magnetically-stirring solution of 1.1% (w/v) chitosan and 0.27% (w/v) $CaCl_2$. The alginate-chitosan capsules were left in the solution for 10 minutes before being removed and rinsed in 0.02% (w/v) $CaCl_2$. These capsules were then transferred for individual attachment of the enzyme the outer diameter (1.375 mm) and shell thickness of capsules (0.2 mm) were measured immediately after rinsing using an MVX10 MacroView fluorescence stereomicroscope. Figure 31 illustrates the construction and shows stereomicroscope images of green-labeled *Sso*Pox-Gln bound to the outside of

the capsule. Note that here *Sso*Pox-Gln is being non-specifically/non-covalently bound as the incubation with microbial transglutaminase broke down the capsule in the second step of the two-step attachment process. To bind the *Sso*Pox-Gln non-specifically the capsules were incubated with the enzyme for 1 hour at 37 ℃ with shaking just as would be done for covalent binding. After incubation the capsules were rinsed three times with HEPES pH 7.0, again, just as is done after covalent binding. Fluorescence measurements of capsules in the plate reader revealed that capsule fluorescence was not statistically different than the well, as seen in Figure 30. This was anticipated, as efforts were made to employ similar amounts of protein in the wells as in the capsules, based on similar surface areas. This may indicate higher amount of *Sso*Pox-Gln binds per surface area of the capsule (146 picomoles/cm^2) vs the well (109 picomoles/cm^2) based on the slightly smaller average surface area of the capsules. Again even with this higher degree of binding per surface area, and likely due to binding within the matrix, the enzyme layer (4.5 x10^{-7} cm) is still less than 0.1% of the chitosan layer of the capsule (0.2mm).

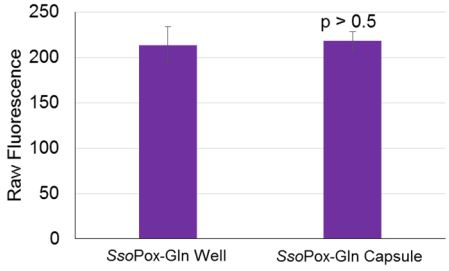

Figure 30: *Sso*Pox-Gln binding: Well vs Capsule. Here the raw fluorescence as produced by SsoPox-Gln bound to the bottom of the well of a 96-well plate and to a capsule after washing is shown. The bars are representative of the average of three samples with the error bars representing the standard deviation. Here it is clear that while there does appear more binds to a capsule the between that and well are not statistically significant.

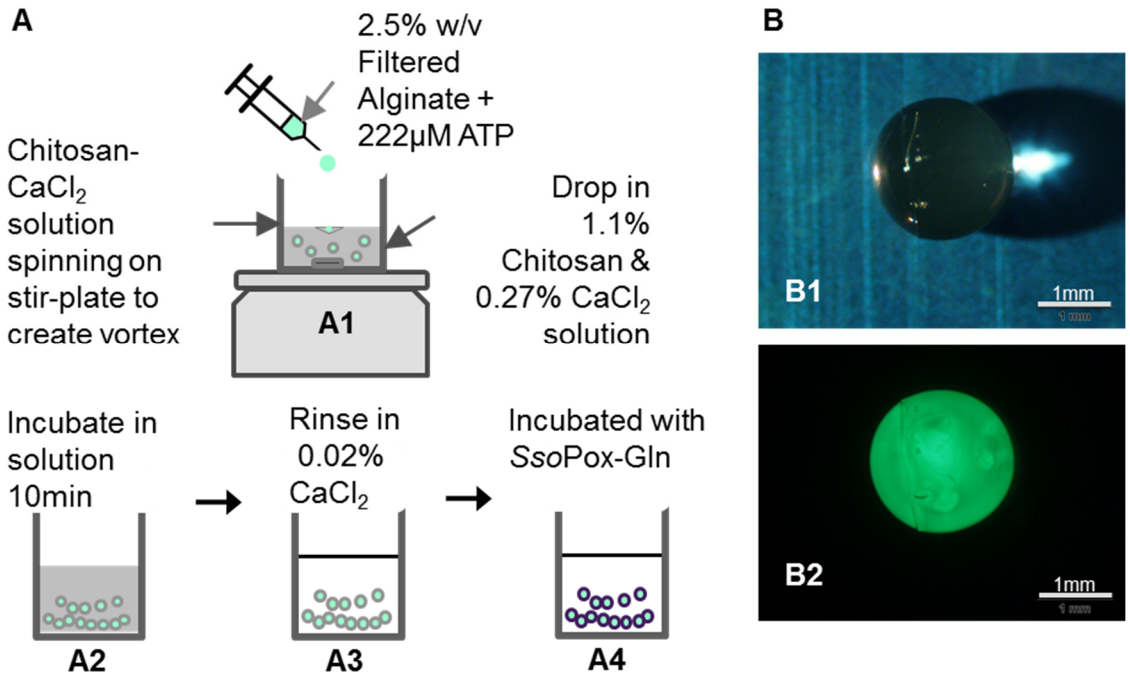

Figure 31: Capsule construction for AI-1 lactonase quenching.
As illustrated in Figure A, capsules were constructed by dropping either 2.5% w/v filtered alginate or a mixture of 2.5% w/v filtered alginate and 222µM ATP via 27G needle into stirring Chitosan-$CaCl_2$ to form capsules (A1) which were then incubated 10 min (A2). The capsules were removed from the incubation media and rinsed in 0.02% w/v $CaCl_2$ (A3) before binding (A4) and subsequent quenching. Images of the capsules as taken by a stereo-microscope (B1, B2) are shown in Figure B. Here green fluorescently-labeled *Sso*Pox-Gln is bound to a capsule.

Using this non-specific binding technique, where, in neutral pH the negatively charged *Sso*Pox-Gln, pI 6.28, is bound to the outside of a likely positively charged chitosan, the capsule was tested for its ability to quench the AI-1 communication signal. As shown in Figure 32, capsules were incubated in two different concentrations of AI-1 and aliquots of the solution were taken two hours after 2-hour incubation at 37 ℃. These same aliquots were measured with both the luminescent and the Red-Green fluorescent reporter. Here the non-specifically bound *Sso*Pox-Gln is shown to reduce AI-1 activity at both concentrations. In addition this data demonstrates that the two reporters produce comparable results. In Figure 32A a reduction of AI-1 activity by 44% in the case

of starting with 20 µM as indicated by the luminescent reporter, which could indicate a final concentration of approximately 11 µM AI-1. While relevant concentrations for *P. aeruginosa* are in the nanomolar range, reducing OdDHL (AI-1) concentration below 70 uM has been shown eliminate the antibody inhibition caused by higher concentrations of the molecule[237].

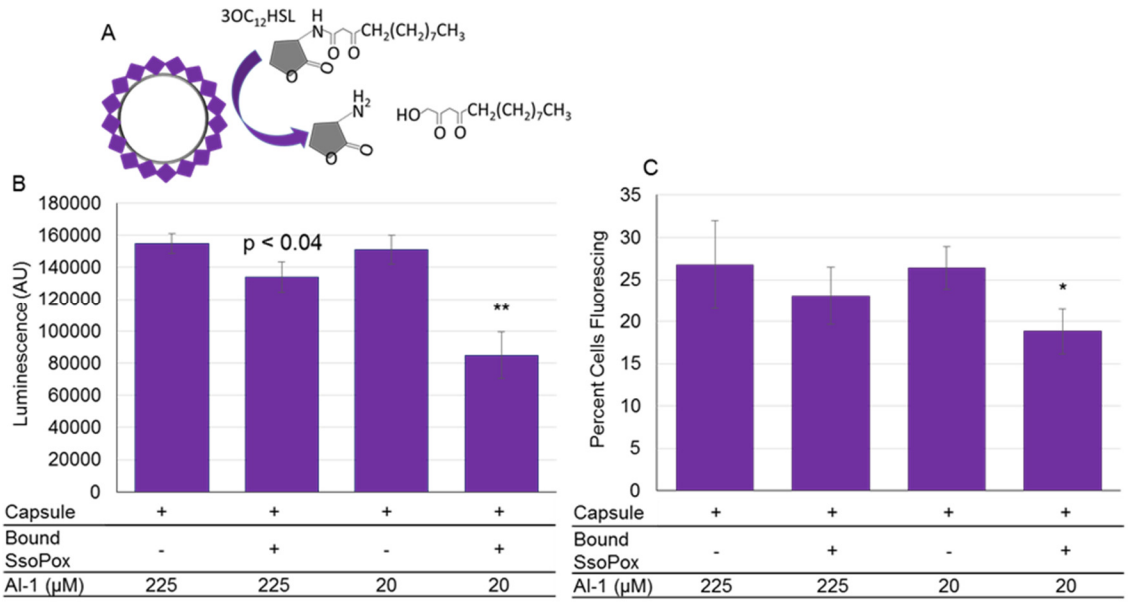

Figure 32: *Sso*Pox-Gln capsules for AI-1 quenching.
The above demonstrates the activity of *Sso*Pox-Gln bound to the outside of capsules using two different AI-1 reporters, and illustrates the reaction in A. In B the luminescent reporter is used to measure remaining AI-1 activity after samples were incubated for 2 hours at 37 ℃. In C, the same samples were measured with the red-green fluorescent reporter and the chart reflects the percent of cells fluorescing as counted from a total of 50,000 using flow-cytometry. In both charts the bars are the average of three samples with standard deviations provided. P-values are calculated by Student's T-Test, two tails, type 2; * < 0.03, ** < 0.008.

4.4 Discussion and Conclusions

The addition of tags to the N- and C-termini has provided new opportunities for purification and function/delivery of *Sso*Pox. Simpler purification could provide opportunities for yield improvement and attachment to surfaces means that this

powerful enzyme can be immobilized and delivered to specific areas for treatment.

Both modified *Sso*Pox enzymes proved to maintain lactonase activity in solution. In addition, *Sso*Pox-Gln demonstrated a statistically significant reduction of AI-1 activity and therefore lactonase activity when bound both covalently and non-covalently. Given previous success in quenching a wide variety of AHLs/AI-1 molecules, it would be prudent to verify that the promiscuous lactonase activity of SsoPox[63] was also maintained after modification. In addition, activity in the nanomolar range should also be verified as it is within this range, specifically between 5 and 20 nM, that *Pseudomonas aeruginosa* demonstrates transcriptional activation due to the OdDHL-LasR complex binding to the DNA binding site[238,239].

With the knowledge that these modifications for attachment and purification yielded viable enzymes improvements could be made. It would be possible to perform site-directed mutagenesis, as has been done previously, to improve the activity of the enzyme and stability in environments lacking cobalt[63,240]. Mutation for improved lactonase activity in the *Sso*Pox-Tyr variant would be particularly useful, as there was significant yield improvement and a simpler covalent binding mechanism.

Adding the hexa-histidine tag made *Sso*Pox purification by metal-affinity columns possible. In addition, this modification to the N-terminus may positively affect the activity of the modified *Sso*Pox. Previously, it was shown that adding a hexa-

histidine tag on the N-terminus of lactonases/PTEs, or organophosphotases (OPHs), increased OPH catalytic activity[241]. As organophosphate hydrolysis activity was not tested on the modified enzymes this would a logical next step in evaluating these new variants of *Sso*Pox. Should activity be maintained, or even improved, these new enzymes would have much broader applications beyond biofilm prevention. Organophosphates, while not as commonly used in fertilizers are increasing being used as fire-retardants[242,243].

Providing the capability to covalently bind a powerful lactonase/organophosphate hyrdolaze to surfaces using amine groups provides a new tool for functionalizing surfaces. Activated amine groups are commonly used to bind enzymes for surface functionalization and increasingly used for carbon-capture[212]. Using this readily available binding technique means that the enzymes modified here could be attached to a wide variety of surfaces from graphene to activated fabrics[244].

5 CHAPTER 5: TAKING A MULTIFACETED APPROACH TOWARD QUORUM QUENCHING

5.1 Introduction

A system capable of quenching both autoinducer-1 (AI-1/AHL) and autoinducer-2 (AI-2) bacterial communication molecules has been constructed. Enzymatic dual-quenching provides the capability to effect phenotypes of multiple types of bacteria. In addition, it could mitigate adverse effects of only quenching a single bacterial communication pathway. For example, OdDHL and *P. aeruginosa*'s production of pyocyanin has been shown to have antibiotic activities[96], however if pyocyanin production is reduced due to elimination of OdDHL, it would be advantageous to have another quenching capability to combat remaining bacteria. Additionally, the use of *Sso*Pox, a promiscuous lactonase[63], could provide quenching of other mid- to long-chain AI-1 molecules in addition to OdDHL affecting a broader range of bacteria. An illustration of this system is found in Figure 33, where two enzymes are bound to the outside of a biopolymer capsule containing ATP.

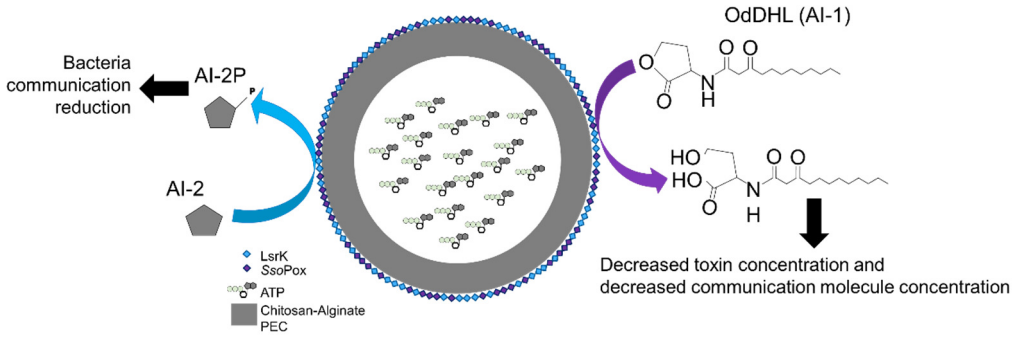

Figure 33: Dual quenching capsule.
The multifunctional quorum quenching capsule developed is the first to modulate two classes of bacterial communication molecules, autoinducer-2 (AI-2) and autoinducer-1 (AI-1) simultaneously using two different naturally produced enzymes.

5.2 Materials and Methods

5.2.1 LsrK-Tyr

The plasmid pETLsrK-Tyr was used to express the AI-2 kinase, LsrK, fused with a spacer and tyrosine tag, herein referred to as LsrK-Tyr. To construct the plasmid, *E. coli lsrK* (*ydeV*) was amplified with primers as indicated in Table 1 from *E. coli* W3110 genomic DNA using Vent DNA polymerase (New England Biolabs; NEB). After purifying the PCR product via the QIAquick gel extraction kit (Qiagen), the blunt-ended fragment was inserted into pET200/D-TOPO (Invitrogen), which has a hexa-histidine tag at the N-terminus for purification after the protein expression. The sequence of pETLsrK-Tyr was confirmed by sequencing facility (DNA Core Facility of the Institute for Bioscience and Biotechnology Research, University of Maryland). After transforming the plasmid into the BL21 (DE3) host strain, the LsrK-Tyr enzyme (MW: 62.9 kDa) was expressed and purified.

5.2.2 *Sso*Pox

The *Sso*Pox genetic sequence was optimized for *E. coli* using the IDT codon optimization tool and the gBlock and primers for insertion into pET200 plasmid were ordered from IDT (Coralville, IA, USA). The *Sso*Pox gene was amplified with Q5 (NEB, Ipswich, MA) and ordered primers for insertion into the pET200 plasmid and addition of the glutamine tag. The sequence of the resultant plasmid (p*Sso*PoxG) was verified by Genewiz (Frederick, MD). After transformation into *E. coli* BL21(DE3) pLysS cells the enzyme SsoPox-Gln (MW:38.719 kDa) was expressed and purified.

5.2.3 Capsule Construction

Construction of the functionalized uni-lamellar capsules is based on the charged polymers chitosan and alginate for self-assembly as has been used in previous works[10,205] and has been referred to as a one-stage procedure[206]. ATP (10mM) was mixed with alginate (2.5%) for final concentration of 222 µM ATP, vortexed, and added drop-wise by syringe needle (27G) to a magnetically-stirring solution of 1.1% (w/v) chitosan and 0.27% (w/v) $CaCl_2$. The alginate-chitosan capsules were left in the solution for 10 minutes before being removed and rinsed in 0.02% (w/v) $CaCl_2$. These capsules were then transferred for individual attachment of the enzyme. Figure 34 illustrates the construction of the capsule.

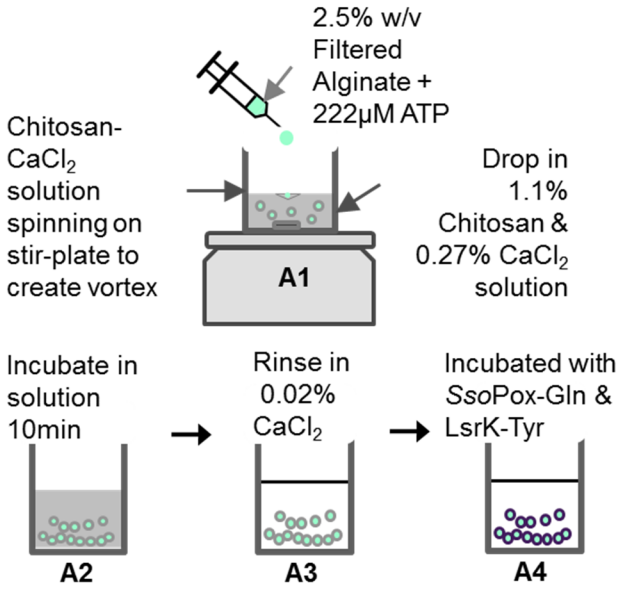

Figure 34: Capsule Construction. The multifunctional quorum quenching capsule developed is the first to modulate two classes of bacterial communication molecules, autoinducer-2 (AI-2) and autoinducer-1 (AI-1) simultaneously using two different naturally produced enzymes.

5.3 Results

The first step, as had been done previously with each enzyme individually, was to test activity of the two enzymes in solution. Each of LsrK-Tyr, 200 picomoles,

kinase activity *Sso*Pox-Gln lactonase activity was tested in AI-1 (OdDHL, 225 µM), AI-2 (15 µM, with 30 µM ATP) and a solution of both quorum sensing molecules (225 µM OdDHL, 15 µM AI-2 and 30 µM ATP) in a total volume of 100 µL, using HEPES pH 7 to complete the volume. In addition, LsrK-Tyr and *Sso*Pox-Gln were combined and tested under the same conditions as previously listed and corresponding kinase and lactonase activity was tested. In samples where LsrK-Tyr or *Sso*Pox-Gln were not present an equivalent volume of the appropriate enzyme storage buffer was added. Each condition was completed in triplicate and incubated in the same 96-well plate for 2 hours at 37 ℃ with shaking. The full volume of the samples were stored at -20 ℃ overnight. The next day these samples were thawed on ice and vortexed to ensure uniformity. From these, AI-2 samples were taken directly for the BB170 assay and an aliquot was diluted for detection with the AI-1 luminescent reporter. The results of these assays is found in Figure 35

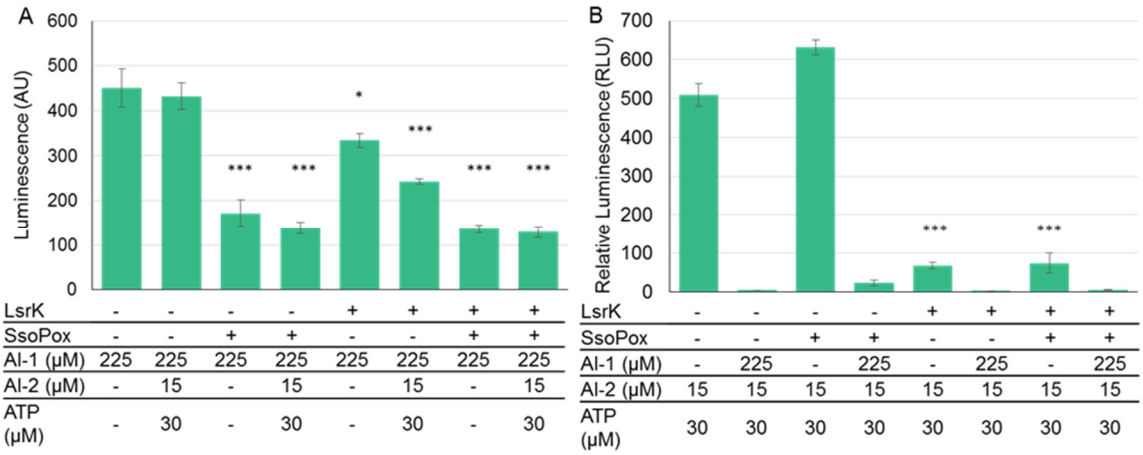

Figure 35: Enzyme activity in mixed environment.
A and B above have been generated from the average of three samples. When both AI-1 and AI-2 were present aliquots from the same samples were measured by both means. The samples were incubated in a 96-well plate for 2 hours at 37 ℃, and aliquots were taken for measurement of AI-1 and AI-2 concentration. Figure A shows the luminescent measurement of AI-1 activity using the cells from Lindsay et al. Figure B shows the relative luminescence of the BB170 assay. It is noted that the BB170 assay does not indicate AI-2 activity in the presence of the 225μM concentration of AI-1. However, AI-2 is detected when there is less AI-1 as in the fourth bar, where the SsoPox reduces the concentration of AI-1. P-values are calculated using a Student's T-Test, two-tailed, type 2; * < 0.03, *** < 0.0008.

In Figure 35A the AI-1 activity is measured across all samples containing AI-1. In the third and fourth column it is shown that there is a statistically significant decrease in AI-1 activity in the presence of *Sso*Pox-Gln, both with and without AI-2. In addition, in the seventh and eighth columns it is shown that there is a statistically significant decrease in AI-1 activity in the presence of both and LsrK-Tyr and *Sso*Pox-Gln, It is also interesting to note here that the presence of LsrK-Tyr did reduce AI-1 activity both with and without the presence of AI-2 and ATP. It is possible, though not verified, that LsrK-Tyr in the presence of ATP is acting as a homoserine kinase, which have been shown to phosphorylate L-homoserines[245]. While ATP concentration was not measured to confirm this, it is noted that ATP binds to LsrK first in the phosphorylation of AI-2 as shown by Zhu

et al. [65], and therefore would provide LsrK with the capability to phosphorylate another molecule.

In Figure 35B the AI-2 activity is measured across all samples containing AI-2. In columns five and seven it can be seen that LsrK-Tyr reduces AI-2 activity in the presence of *Sso*Pox-Gln. It is noted that there is a reduction in AI-2 activity in column eight, where both LsrK-Tyr and *Sso*Pox-Gln are present when compared to column four where *Sso*Pox-Gln is present, though this is not a statistically significant decrease. It is clear from the second column, the positive control containing both AI-1 and AI-2 that 225 µM of AI-1 results in an inability for the AI-2 assay to measure AI-2. However, given the increase in AI-2 activity in the fourth column, where AI-1 activity is reduced, there is indication that a lower AI-1 concentration may provide the capability to measure both AI-2 activity in the presence of AI-2.

With this information, it was determined prudent to move forward with testing simultaneous activity of immobilized enzymes on the outside of a capsule as illustrated in Figure 33. First, it needed to be determined if both enzymes could be non-specifically bound to the outside of a single capsule. Using the same DyLight™ Sulfhydryl-Reactive Dye as used previously, with *Sso*Pox labeled in green and LsrK labeled red, both labeled enzymes (100 picomoles of each) were incubated with a capsule for 1 hour at 37 ℃ with shaking. Upon completion of incubation the capsule was rinsed three times in HEPES pH 7.0. Several capsules were labeled in this manner. In addition, capsules were incubated without the enzymes and rinsed before being imaged with a stereo microscope

for Figure 36. Both enzymes were bound non-specifically as evidenced by the presence of both red (LsrK) and green (*Sso*Pox) fluorescence on the same capsule in Figure 36 (A2/A3 and B2/B3). That is, in neutral pH the enzymes are negatively charged *Sso*Pox (pI 6.28) and LsrK (pI 5.45) and bound to the outside of a positively charged chitosan layer on the outside of the capsule. During capsule formation the chitosan is never neutralized and while the capsule is placed in HEPES pH 7.0 allowing it to maintain some positive charge.

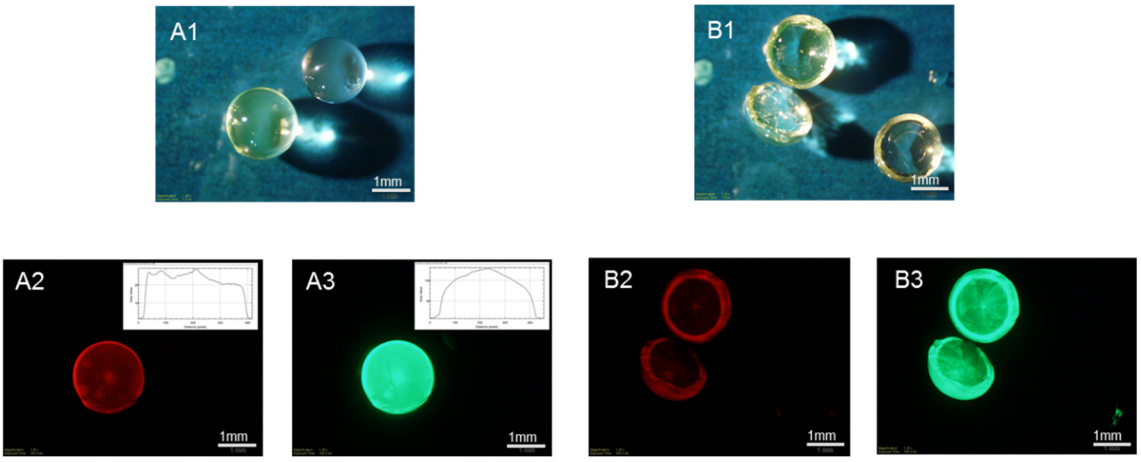

Figure 36: Combined capsules
In figure A, two capsules, one with labeled enzymes, the other without enzymes are shown as imaged on a stereomicroscope in bright-field (A1, B1), red fluorescently labeled LsrK-Tyr (A2, B2), and green fluorescently labeled *Sso*Pox-Gln (A3, B3). Figure B shows the same capsule cut to show the shell to which the enzymes are bound, again with half an unlabeled capsule.

Figure 36 demonstrates that both enzymes can be bound to the outside of the capsule as was done previously. Using ImageJ the intensity of the fluorescence was measured for the fluorescing capsules, the results of this analysis are found in the upper right corner of Figure 36A2 and A3. Here it is clear that there is uniformity of fluorescence across the capsule, indicating uniform binding of both enzymes on the capsule.

Having demonstrated dual binding the next step was to verify LsrK kinase and *Sso*Pox lactonase activity while both are bound to the same capsule. Capsules containing ATP were prepared with both enzymes as illustrated in Figure 34, rinsed and exposed to a solution of 20 µM AI-1 and 40 µM AI-2. This lower concentration of 20 µM AI-1 was used to avoid the issue seen earlier where 225 µM AI-1 interfered with the BB170 Assay. Capsules were incubated in these solutions for 2 hours at 37 ℃ with shaking. At the completion of incubation the entirety of the solution was removed and stored at -20 ℃ overnight. Again, aliquots from these samples were used directly for BB170 Assay, and diluted for AI-1 concentration testing. The results of these assays can be found in Figure 37. In Figure 37A the AI-1 activity is measured after incubation, and it is clear that in the presence of SsoPox the AI-1 activity is reduced by a statistically significant amount as seen in columns two and four. In Figure 37B the AI-2 activity is measured, here it is clear in columns three and four that the presence of LsrK reduces the AI-2 activity. It is also noted that the reduced initial concentration of AI-1 provided the capability for the BB170, AI-2 activity, assay to provide a reading of AI-2 activity in the presence of 20 µM AI-1. It is noted, however, that the addition of the *Sso*Pox capsule in column 2 did seem to increase overall luminescence in the BB170 Assay, though not in a statistically significant fashion, indicating there could still an adverse effect due to AI-1. Ultimately, there is statistically significant decreases in both quorum sensing molecules when both enzymes are present on the same capsule as seen in column four of both Figure 37A and B.

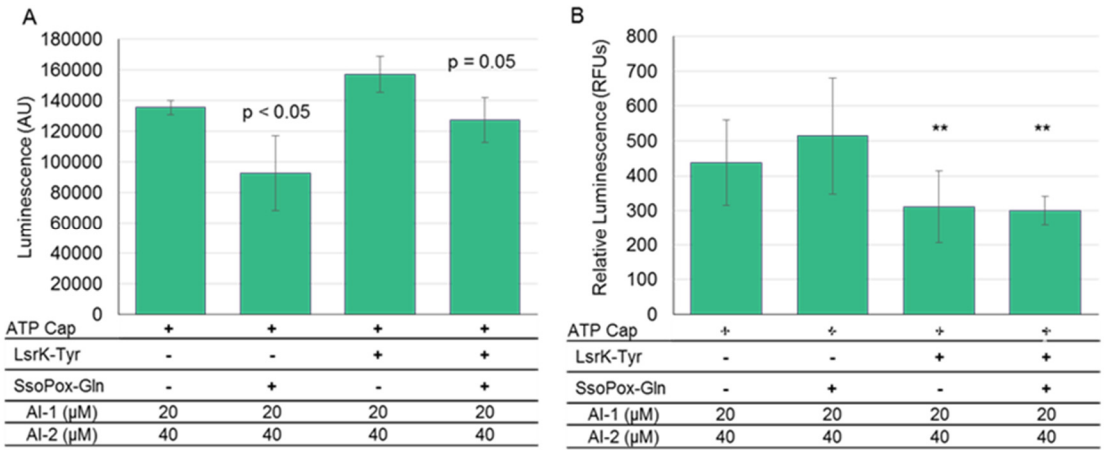

Figure 37: Dual-quenching delivered in a single functionalized capsule.
A and B above have been generated from the average of three samples. Aliquots from the same samples were measured by both means. Three samples of each condition were incubated in a 96-well plate for 2 hours at 37 ℃, and aliquots were taken for measurement of AI-1 and AI-2 concentration. Figure A shows the luminescent measurement of AI-1 activity using the cells from Lindsay et al. Figure B shows the relative luminescence of the BB170 assay indicating AI-2 Activity. P-values are calculated using a Student's T-Test, two-tailed, type 2; * < 0.03, ** < 0.008.

It had been noted previously that ATP is a limiting factor in LsrK-Tyr kinase activity in quenching AI-2. As a result, a second set of capsules were exposed to solutions containing the same concentration of AI-1 (20 µM) and AI-2 (40 µM), however, 60 µM ATP was added to the solution. It is evident in Figure 38 that the addition of ATP (6 nanomoles, final concentration 60 µM) does improve the overall performance of the system, providing more statistically significant decreases in both AI-1 and AI-2 concentrations. The added ATP, which is six times that found in a single capsule (see Appendix A), is one and one half times the amount of AI-2 present in solution. This additional ATP is also readily available for binding to LsrK and subsequent phosphorylation of AI-2, while that contained within the capsule is not only insufficient for one-to-one phosphorylation, but could be contributing to crosslinking of chitosan as was

seen previously[213]. Again a decrease in AI-1 concentration was noted in the presence of LsrK and ATP, but the result was not statistically significant.

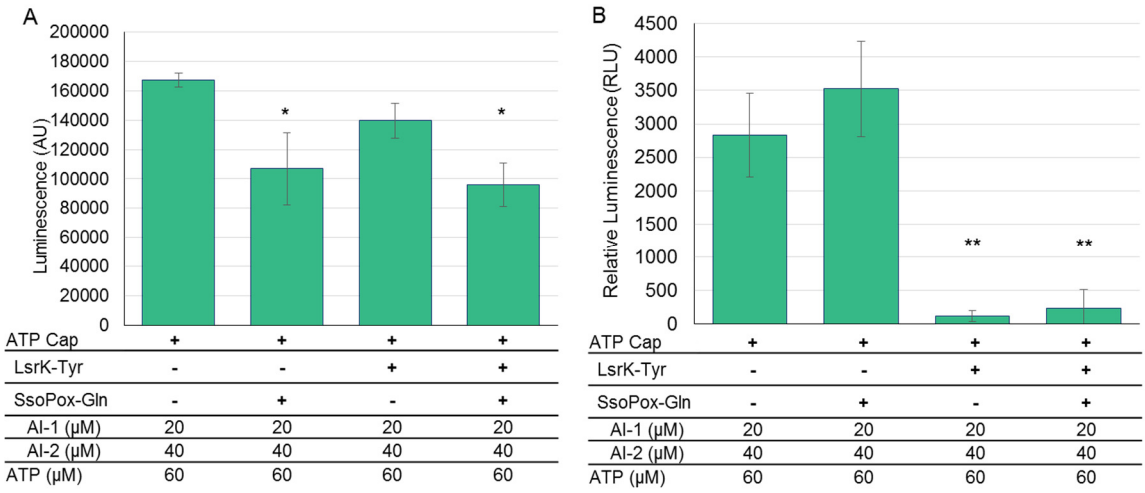

Figure 38: Adding ATP improves performance of dual-quenching capsules.
As in Figure 36, A and B above have been generated from the average of three samples.. Here ATP was added to the samples during incubation in a 96-well plate for 2 hours at 37 ℃, and aliquots were taken for measurement of AI-1 and AI-2 activity. A shows the luminescent measurement of AI-1 activity using the cells from Lindsay et al. B shows the relative luminescence of the BB170 assay indicating AI-2 Activity. P-values are calculated using a Student's T-Test, two-tailed, type 2; * < 0.03, ** < 0.008.

6 CHAPTER 5: CONCLUSIONS

6.1 Results Summary

In this work, for the first time, a functionalized capsule of modified quorum quenching enzymes and biocompatible polymers has been constructed and demonstrated to have dual quenching capability.

In chapter 2, an AI-2 quenching capsule was developed using biopolymers and a modified form of the natural kinase, LsrK, with its primary substrate, ATP. Two modified forms of LsrK were engineered with tags for immobilization, produced, purified and verified for activity both in solution and when bound. Both modifications of the kinase were successful in phosphorylating AI-2 *in vitro* and rendering the signal unrecognizable to *V. harveyi* reporter cells. With significantly more activity, the tyrosine-tagged LsrK-Tyr was used to demonstrate activity when covalently bound to both a chitosan film and the outer layer of a chitosan-alginate capsule. Furthermore a functionalized capsule composed of biocompatible biopolymers that delivers the modified LsrK with its primary substrate, ATP, was developed and demonstrated robustness in mixed culture environment.

In chapter 3, an AI-1 quenching capsule was developed using the same construction as in chapter 2, replacing the kinase with the promiscuous lactonase, *Sso*Pox. Here, *Sso*Pox was, for the first time, modified with tags at the N- and C-terminus, produced, purified and verified as active. A hexa-histidine-tag was added at the N-terminus for ease of purification, and two different tags were

added to the C-terminus for covalent binding to chitosan. Both forms of *Sso*Pox proved active in solution, that is, rendering the AI-1, OdDHL, unrecognizable. However, *Sso*Pox-Gln, performed better when covalently bound to a chitosan film. A new fluorescent cell reporter was also constructed in this work that provided a means of indicating AI-1 presence without affecting the amount of AI-2 in the environment. Using LasR and the DNA binding site from *P. aeruginosa*, these reporter cells produce green fluorescence in the presence of OdDHL. Ultimately a capsule with bound *Sso*Pox-Gln was produced that proved to quench the AI-1, OdDHL.

In chapter 4, the modified enzymes, LsrK-Tyr and *Sso*Pox-Gln, were first demonstrated to be simultaneously active in solution, quenching two different quorum sensing signals. This was the first time both AI-2 and AI-1 have been enzymatically quenched in the same *in vitro* environment. Finally, these two enzymes were bound to the developed capsule to provide a functionalized dual-quenching device.

6.2 Broader Impact

Bacteria rarely, if ever, exist in a single-species environment outside of the lab. Bacteria on the skin, in the gut, in the mouth, in the soil and associated with most infections are comprised of several species of bacteria. And, as has been mentioned, many of these bacteria have multifaceted means of biofilm formation and toxicity; so multiple signals need to be quenched to adequately prevent biofilm formation. This research demonstrates two powerful quorum quenching enzymes are active simultaneously to provide a multifaceted approach in

preventing biofilm formation, which is an important step in using quorum quenching as a substitute for antibiotics.

By combining two quenching enzymes this could provide greater insight into biofilm formation by modifying the bacteria environment rather than modifying bacteria directly. Often, in research settings, bacteria are modified to understand how the quorum sensing enzymes (or absence thereof) effects phenotype including biofilm formation. This capability to modify the bacteria culture environment may aid in academic research to better understand the dynamic environment of single, or even multi-species cultures. In addition to academic applications this dual approach provides a more powerful way to effect changes to the multi-species environments that often compose infections. As a result this multi-faceted approach has the potential to prove a more powerful implementation of quorum quenching in preventing virulence.

Each of these quenching enzymes has been engineered for covalent binding to a biopolymer surface. This covalent binding provides the capability to not only deliver the quorum quenching enzymes to a specific location/environment, but coat surfaces with active enzymes to prevent biofilm build-up. The nature of the binding reaction makes it is possible to bind the enzymes in tubes and small spaces and rinse away the binding agent, leaving only the enzyme. By providing a means of functionalizing surfaces with enzymes it provides a new way of preventing biofilm formation without affecting the broader environment.

Additionally, there is the potential for the capsule, or a modified form, to be used as part of treatment of intestinal ailments. This capsule, in contrast to cell-based solutions, could provide a time-limited AI-2 and AI-1 depletion. This approach could reduce impacts of harmful pathogens and allow the resurgence of normal gut biome, which has been shown to require AI-2[246].

6.3 Challenges

While the amount of each enzyme bound to the surface area of the film and capsule has been calculated, determining the amount of each enzyme in a combined environment is a larger challenge for the current system. The manner by which the current films and capsules are constructed precludes a specific way to differentiate proportions of each enzyme bound. In addition, because *Sso*Pox is approximately half the size of LsrK it is possible that twice as much will bind based on size alone. However, because the two enzymes have different binding modalities, it should be possible to specify the amount of each in other systems, where surface properties can be manipulated at the molecular level.

While there is a reduction in both quorum sensing signals, neither has been demonstrated to be completely eliminated from the environment in this work. Reducing AI-2 concentration to below 5 μM was demonstrated to have lead to less biofilm formation than higher concentrations (11 μM) and therefore reducing to these low levels may be sufficient to reduce virulence caused by biofilms[32]. As mentioned previously, a minimum level of AI-2 may aid ensuring the natural biome is maintained, though additional work would need to be conducted to determine preferable levels of AI-2 in the health gut biome.

In addition low levels of AI-1 seem not to be detrimental to mammalian cells[237], however because the molecule can have antibiotic properties and is an autoinducer it would be preferable to more completely eliminate this molecule to a nanomolar level[239]. Additional reduction could be achieved with the use of additional enzymes, perhaps through delivery with smaller particles. In the case of AI-1 elimination this would particularly advantageous as the *Sso*Pox hydrolysis is significantly slower than the phosphorylation as completed by the LsrK kinase.

Although the capsules constructed here provide a degree of quenching of the 'universal' quorum-sensing signal, AI-2 and a widely recognized AI-1, with potential for quenching other AHLs based on the enzyme's previous performance, this is only a start. Bacterial infections are often a multi-faceted environment. As a result, while quenching two common quorum sensing molecules will aid in reducing biofilm formation and pathogenicity of some bacteria, other molecules need to be quenched to further reduce the toxic effects of bacteria.

Specifically, a third class of quorum sensing molecules, autoinducing peptides (AIPs), are not addressed. AIPs that bind to transmembrane receptors are used by Gram-positive bacteria [27,100,101] including *C. difficile*[91]. This addition would also be particularly valuable in addressing *S. aureus* and S*. epidermis* infections. It has been shown that genes coding for virulence, including apoptosis proteins and inflammatory peptides, are under the control AI-2 system as well as the *agr* system which recognizes AIPs in *S. aureus* and *S. epidermis* [247,248]. Of particular note in making this addition is that a lack of AI-2 has been attributed to increased

biofilm formation[249] and resistance to phagocytes by *S. aureus*[85]. As a result, providing a system that not only quenches AI-2, limiting biofilm formation and virulence of several species of bacteria, but also quenches the AIPs that cause toxicity in *S. aureus* would be highly advantageous.

6.4 Future Directions

First, it would be beneficial to understand the full capabilities of the lactonase-activated capsule. Additional testing of the modified *Sso*Pox enzyme, both bound and unbound would be required. Particularly of interest would be determining if the enzyme maintains the promiscuous lactonase and organophosphate hydrolysis activity of the original enzyme[63,229,240]. Should this be the case, there would be far broader implications of the capsules. Specifically they would have the capability to quench many more AHL molecules, such as those use by *Y. pestis*[250]. However, perhaps more profoundly, the capsules would have the capability of immobilizing an enzyme capable of neutralizing the harmful neurological effects of organophosphates[222].

Given that these capsules have the capability to impact many of the most prevalent antibacterial resistant strains, it would also be recommended to test the impact on *C. difficile* directly. This harmful bacterium flourishes in the gut when the natural biome is degraded by administered antibiotics, leading to further gut-biome degradation as *C. difficile* itself produces toxin which targets other bacteria[91]. Research suggests that *C. difficile* has a LuxS-like enzyme[3], that

[3] LuxS produces AI-2 in other bacteria

when absent, prevents the formation of biofilms[33]. While other sensing molecules have been directly related to toxin production[91], the capsules in present form may have an impact on *C. difficile* by reducing the amount of AI-2 in the environment, and may also provide greater insight into *C. difficile* biofilm formation and toxicity.

Finally, the AI-1 reporter could be modified for AI-1 quenching by inserting the *Sso*Pox gene where the sfGFP is currently. By quenching the AI-1, OdDHL, this new cell could allow additional growth of beneficial Gram-negative bacteria and reduce the impact to mammalian cells[88].

7 APPENDIX A: MODELING ATP DIFFUSION OUT OF CAPSULE

7.1 Introduction

Using data collected in capsule development and verification of quorum quenching a mathematical model can be constructed for use in future work. Modeling the quorum quenching systems designed herein requires consideration for mass transfer and reaction kinetics. For the first quenching capsule, loading of ATP in the capsule, ATP release or diffusion from the capsule should be considered. For both capsules the reaction kinetics will be considered; the phosphorylation of AI-2 by LsrK-Tyr for the first capsule and hydrolysis of OdDHL. The capsules are assumed to be a uniform spherical core with a uniform spherical shell so that diffusion is symmetrical.

Preliminary modeling was done in Matlab R2012b (Mathworks, Natick, MA).

7.2 Modeling AI-2 Quenching

Mathematical modeling of solute diffusion in a hollow capsule has been proposed by Yao et al[251], and supported experimentally by Zhang et al [252]. However Yao and Zhang's model measures the diffusion of the solute from a bulk solution into a capsule as has been done in other characterizations of calcium-alginate beads [253] and is explained by Truskey et al [254]. In this study, and other bead and capsule characterizations, the concentration inside the bead or capsule is known and diffusion into solution is measured[255,256]. Tanaka et al [257] has provided an equation for the diffusion from spherical beads as was derived by Crank[258], and,

as a result, creation of the model starts with the same mass balance equation as in Crank[258].

In preliminary tests it was noted that capsules swelled when removed from chitosan and placed in other solutions. This is assumed to be due to osmolarity differences between the capsule alginate core and the solution. Because swelling increases the radius this affects ATP diffusion and is considered in the model.

The initial conditions are as follows where C_A is the overall capsule concentration, C_{Ai} is the initial capsule concentration and C_b is the bulk solution concentration:

$C_A(r,0) = C_{Ai}$, $C_{Ai} = C_{Ci} = C_{Si}$, $0 < r < r_S$ 1

$C_b(r,0) = 0 \quad r > r_S$ 2

Where r_S is the outer diameter of the capsule, r_C is the outer diameter of the capsule core/inner diameter of the capsule shell, D_S is the diffusion coefficient of the capsule shell, and D_C is the diffusion coefficient of the capsule core, as illustrated in Figure 39A.

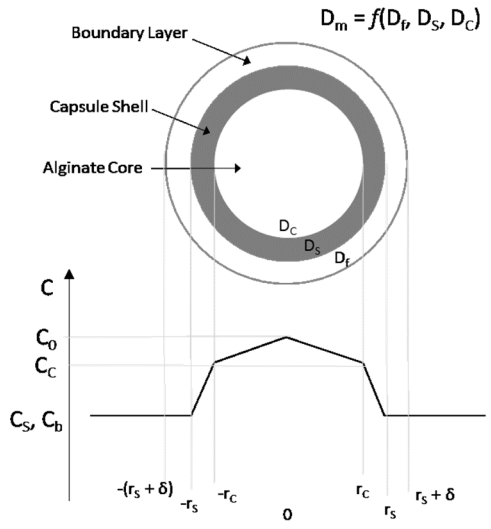

Figure 39A: Illustration of capsule
This illustration of the capsule with the boundary layer film illustrates the system being modeled by the preliminary model. The ATP concentration profile is below the capsule.

7.2.1 ATP Loading

For the AI-2 quenching system, ATP is delivered with LsrK5'-1 and diffuses out of the capsule to first bind to LsrK5'-1 and then phosphorylate AI-2[65]. The encapsulation efficiency was calculated by the equation below. Where ATP_A is the measured/actual loading and ATP_T is the theoretical loading, 222µM.

$$ATP_e(\%) = \left({ATP_A}/{ATP_T}\right) * 100 \quad 3$$

Known concentrations of ATP in LB were plotted against their measured luminescence. The plot was compared to the manufacturer's specification, and an exponential line of fit was determined with R^2 value over 0.98 to determine concentration based on luminescence for LB as plotted in Figure 40. Using the steady-state bulk concentration of 2.1 µM of LB, as can be seen in Figure 40, the initial concentration per capsule can be calculated and was found to be 120 µM[4], which is an encapsulation efficiency of 54%, similar to that found in other work[213].

The reasonably low encapsulation efficiency may be due in part to the low molecular weight of ATP, 507g/mol, as Tanaka et al showed L-trytophan, 204 g/mol, diffused into Ca-alginate beads in less than 30 min and similar results for fast initial ATP release have been seen in other work[213]. Note that in this work capsules were not measured for ATP concentration until at least 10min after formation, due to rinsing and incubation in $CaCl_2$ solution.

[4] =(0.0000021M* 0.005L)/8 capsules/10.9 µL per capsule

The characteristics of the ATP molecule is another factor that should be considered. In some studies sodium tripolyphosphate (Na-TPP) is used to crosslink chitosan membranes[259], and ATP has a similar structure, size, and charge, and therefore may also be crosslinking chitosan. In addition, ATP has been shown to stabilize the structure of alginate calcium carbonate gels[260]. Qi et al found a decrease in the UV-vis absorption peak for ATP, 558 nm, after one minute of reacting with $CaCl_2$, Na_2CO_3 and ATP, and there was a positive correlation between $CaCO_3$ absorption and ATP concentration. As a result, it is possible that ATP is being crosslinked with alginate.

7.2.2 ATP Diffusion

The diffusion of ATP through the core and the shell of the capsule must be considered when determining the overall diffusion coefficient of ATP from the capsule. This includes both the binary diffusion coefficient of ATP in the viscous alginate core and the effective diffusion coefficient of ATP across the alginate-chitosan cross-matrix shell of the capsule, both of which are assumed to maintain a spherical shape. In this preliminary model no partition coefficients are calculated or included. It is assumed that the initial ATP concentration, based on loading efficiency, is the same in both the core and the shell, C_{Ai}.

Below is the equation for substrate concentration in the bulk solution as provided by Crank and Tanaka, where r_S is the outer radius of the capsule, t is time and the liquid film or boundary layer is included in the model [257,258]

$$C_b = \frac{C_{Ai}}{1+\alpha}\left[1 - \sum_{n=1}^{\infty} \frac{6\alpha(1+\alpha)\exp(-D_{all}q_n^2\frac{t}{r_S{}^2})}{9+9\alpha+q_n^2\alpha^2}\frac{(r_s)}{(r_s+\delta)}\frac{\sin\left({}^{q_n r_s}/_{(r_s+\delta)}\right)}{\sin(q_n)}\right] \qquad 4$$

Where:

$$\alpha = \frac{V}{N\left(\frac{4}{3}\pi {r_S}^3\right)} \qquad 5$$

Where V is the volume in the bulk solution, 5ml, or 5000mm^2 and N is the number of spheres, 8, [252]. q_n are non-zero positive roots of Equation 6, for this work the first ten roots will be used:

$$\tan q_n - \frac{3q_n}{3+\alpha q_n^2} = 0 \quad 6$$

D_{all}, can be defined in terms of D_C, D_S, r_S, and r_C when applying the same conditions as in Yao et al[251]. The diffusion coefficient in the core, D_C, is assumed to be that of ATP in aqueous solution as has been found a reasonable assumption in previous work for diffusion of similarly sized and larger substances in and out of Ca-alginate and Ca-alginate-chitosan capsules[252,257]. As a result, the diffusion of ATP through the core, $D_C = D_W = 3.5x10^{-6}$ cm^2/sec [261], or $2.1x10^{-2}$ mm/min. The shell diffusion coefficient, Ds, is assumed to be 10% that of ATP in aqueous solution as was found to be the diffusion coefficient for L-tryptophan, a similarly sized molecule passing through an alginate-crosslinked shell/membrane[252].

The initial capsule weight was determined by averaging the weight of nine rinsed and dried capsules and found to be 9.8mg. Because the initial total weight of ATP in the capsule at the start of formation is 1.12 µg[5] or 0.03% of the average

[5] 1.12µg=(0.000222 M*0.000010 L)*507.18g/mol

initial capsule weight the change in capsule weight due to ATP release is considered negligible.

The capsule weight was used to calculated shell radius, r_S. The weight increase is the result of osmosis into the capsule[255,262]. Because water has a known density of 1 g/mL or 1 μg/mm^3 the shell radius at time, t, r_{St}, can be calculated by

$$r_{St} = \sqrt[3]{\frac{3}{4\pi}(V_i + (W_t - W_i))} \quad 7$$

Where V_i is the initial volume of the capsule as calculated from initial diameter, W_i is the initial weight in grams and W_t is the weight in grams at time t=t. Figure 40 shows the average weight with standard deviation for three samples, which increased steadily over time. This average weight was used to calculate the outer capsule radius, which was also plotted vs time and a line of best fit was determined such that the R^2 value greater than 0.95. This line of best fit was used to represent r_s and as input for calculation of α. We assume that only the core is swelling due to osmosis. Shell thinning is assumed to be linear according to studies conducted previously on chitosan alginate films in mixed solutions of PBS[263]. The initial and final shell thicknesses were used to find a linear function of the value of shell thickness, s_t which was used for all solutions. Using the function of shell thickness combined with the calculated shell radius, core radius, r_c can be determined using Equation 8. The initial and boundary conditions are as follows:

$$r_{Ct} = r_{St} - s_t \quad 8$$

$s_{t=0} = 0.2\text{mm}, 0 \leq x \leq s_t\,, t \leq 0\,, C = C_{Ai}\;\; s_{t=0} = 0.2mm\;\; r_{St=0} = 1.375\text{mm}\,, r_{Ct=0} = 1.275$ 9

$0 \leq x < s_t\,, t \geq 0\,, C = C_{Ai} \qquad x = s_t\,, t \geq 0\,, C = C_b$ 10

Capsules were measured and then sliced open to find initial diameter, radius and thickness of the chitosan-alginate shell was found. Given that the initial shell thickness is 0.2mm, a new equation for effective diffusion was calculated. The initial and final shell thicknesses are used to find a linear function of the value of shell thickness, s_t which will be used for all solutions.

$s_t = \frac{s_{t=f} - s_{t=0}}{t_f}\text{t} + s_{t=0}$ 11

And the overall diffusion coefficient is, where δ is the width of the boundary layer, 0.01mm, and D_F=0.001*D_W is the diffusion coefficient through this boundary layer.

$D_{all} = \frac{(A_F)(r_S+\delta)}{\left({A_F\delta}/{D_F} + {A_S(r_S-r_C)}/{D_S} + {A_C r_C}/{D_C}\right)}$ 12

Plotting this concentration profile with an initial capsule ATP concentration of 120µM yields a good representation of the initial ATP release as seen in Figure 40A, which also shows the subsequent effect on reaction kinetics. While this model doesn't reach the concentration measured in 120 minutes, it does appear to approach the same 'steady-state'.

7.2.3 LsrK-Tyr Reaction Kinetics

As was demonstrated, the modified protein LsrK-Tyr is still active and capable of phosphorylating AI-2 when bound to chitosan. Based on DNA sequence analysis and verified enzyme activity, it is assumed that the enzyme active-site has not been altered in LsrK-Tyr and that reaction kinetics found in previously work still hold[65], where, for the purposes of this study, DPD and AI-2 are equivalent.

Zhu et al, using fitting and replot analysis against Michaelis-Menten, found that the reaction kinetics of LsrK were dependent on both ATP and DPD concentration, with ATP binding occurring first[65]. Using the data from Zhu et al the concentration profile can be used to show a reaction kinetics profile with varying concentrations of DPD.

With a known concentration of either substrate Zhu et al through experimentation found values that could be used in the Michaelis-Menten equation. Here *v* is the reaction rate, [S] is the substrate concentration or ATP in bulk solution, C_b, V_{max} is the maximum rate at which the reaction can take place, which will vary dependent on DPD concentration, and $K_{m,}$ the Michaelis constant is the concentration of ATP when the reaction rate is at half its max.

$$v = \frac{V_{max}[S]}{K_m + [S]} \quad 13$$

The model uses the concentration determined by Equation 4 for the ATP concentration, [S], in the Michaelis-Menten equation. Because the initial concentration of ATP in the capsules, 222uM, is less than saturation[65] the V_{max}

and K_m values will be estimated from Zhu et al, depending on the AI-2/DPD concentrations being plotted.

$$v = \frac{(V_{max})_{[DPD]}\, C_b}{(K_m)_{[DPD]} + C_b} \qquad 14$$

Preliminary model results in Figure 40A shown that reaction velocity mirrors the concentration profile, as was expected based on the work of Zhu et al. In

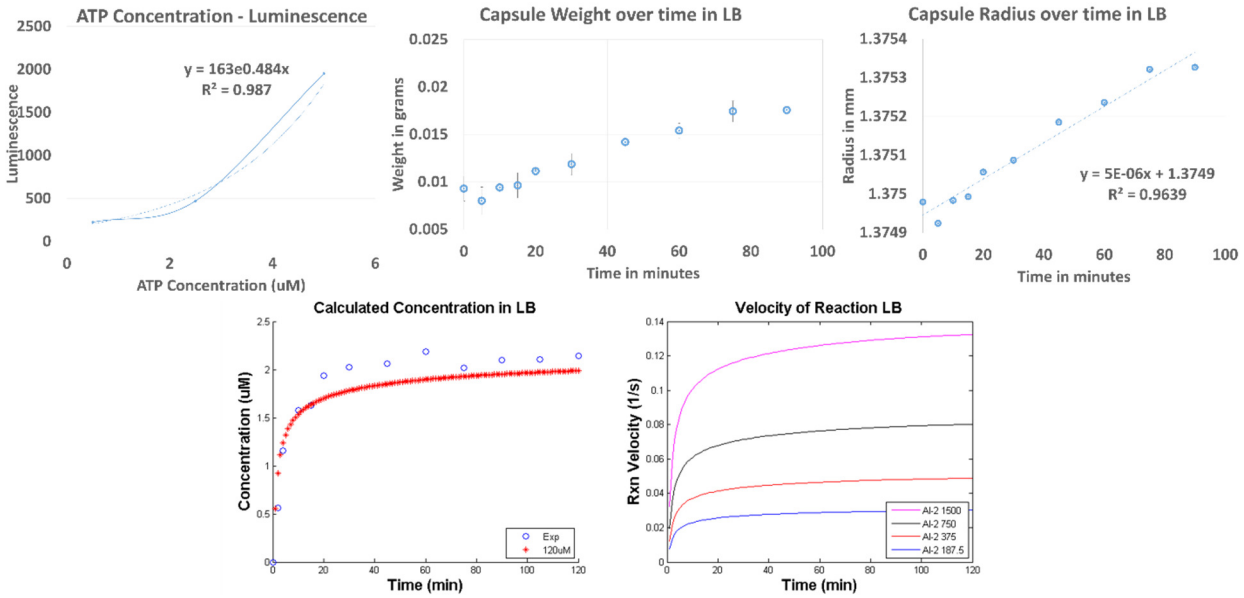

Figure 40A: Preliminary AI-2 Quorum Quenching Model
The Luminescence shown in the first graph is a plot of the measured luminescence normalized to luciferase vs known concentrations of ATP. The line of best fit on the graph is used for conversion of luminescence in measure of ATP concentration as the known values were in the sample set. The second graph are the measured weights of capsules over time. The third graph is the calculated radius as a result of the measured weight increase as a result of osmosis. The bottom two charts have been generated from the preliminary Matlab model. The first shows the measured ATP concentration as circles and the model as stars. The second shows the estimated reaction velocity at various concentrations of AI-2 based on the ATP release profile.

addition, increased reaction velocities are correlated with increasing concentrations of DPD/AI-2, which are less than those seen in the work of Zhu et al, as the ATP concentration is only approximately 2µM compared with the 500µM and both the ATP and AI-2 concentrations affect the overall reaction rate.

7.3 Modeling AHL Quenching Capsules

Because lactonases require only water as a substrate for hydrolysis of AHLs, and it can reasonably be assumed that water will not be a limiting factor, the modeling of the AHL quenching capsule is primarily reliant on the enzyme kinetics of *Sso*Pox-Gln, and the concentration of OdDHL.

Hiblot et al, determined the reaction kinetics and constants of wild-type *Sso*Pox with OdDHL, where k_{CAT} is the number of substrate molecules turned to product per second by each enzyme, K_M is the Michaelis-Menten constant, and k_{CAT}/K_M is the enzyme efficiency:

k_{cat} (1/s) = 1.01 ± 0.13

K_M (µM) = 456 ± 128

k_{cat}/K_M (1/s*M) = 2.22(±0.68)x10^{363}

Using these values and a known initial concentration of the enzyme, *Sso*Pox-Gln, $[E]_0$, in the reaction the maximum velocity of the reaction, V_{max}, can be calculated for input into the Michaelis-Menten equation to find the reaction velocity:

$V_{max} = k_{cat}*[E]_0$ 15

$$v = \frac{V_{max}[S]}{K_m+[S]}$$ 13

where [S] is the substrate concentration or OdDHL in bulk solution.

8 APPENDIX B: AI-1 REPORTER PLASMID DIAGRAMS

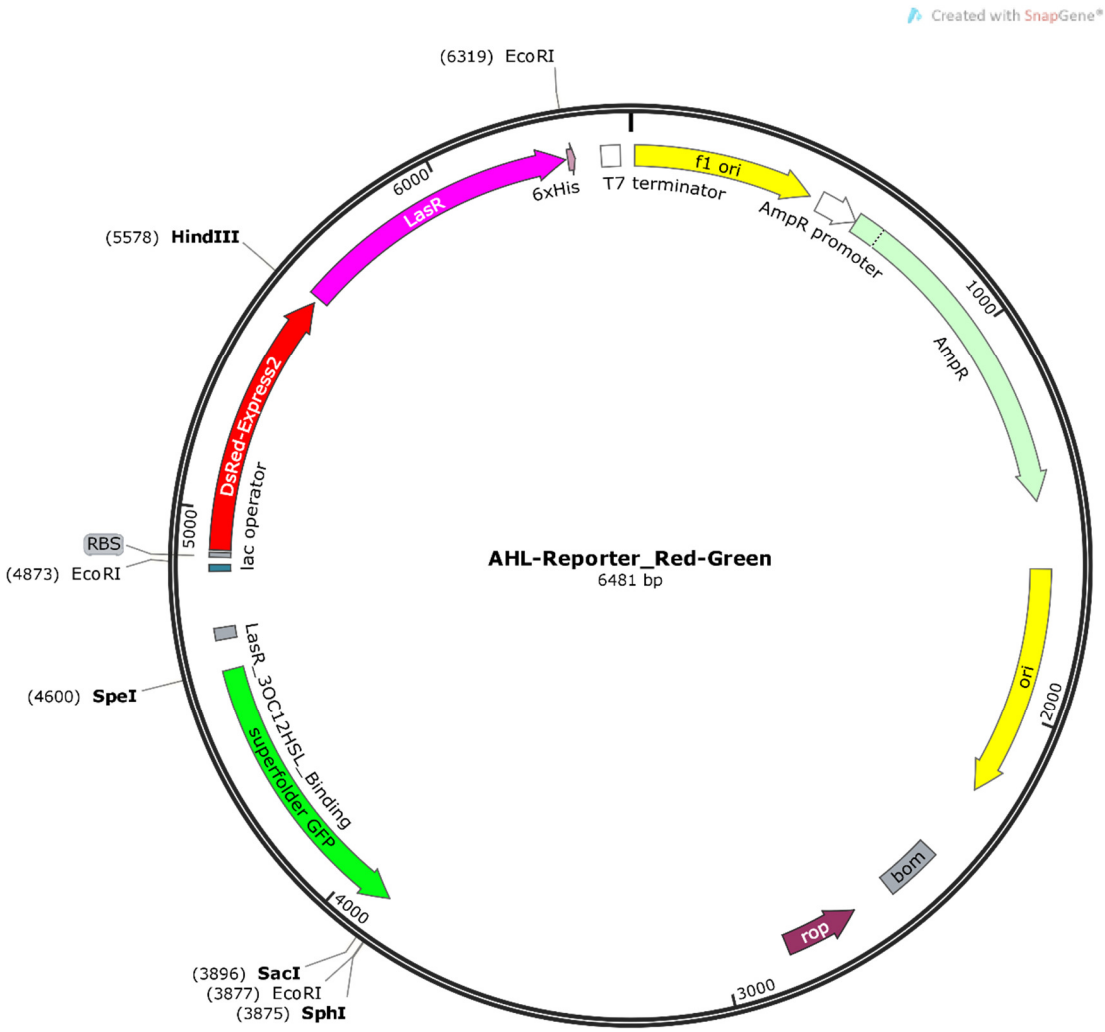

Figure 41B. Red-Green Reporter plasmid map
A map of the plasmid constructed for reporting on AI-1 concentration. The construct was placed into the p21A plasmid with ampicillin resistance. In addition the T7 promoter was removed and a T5 promoter added before the dsRed-Express2 gene. The bi-directional LasR-OdDHL binding site is the only promoter for sfGFP and could further amplify dsRed and LasR production.

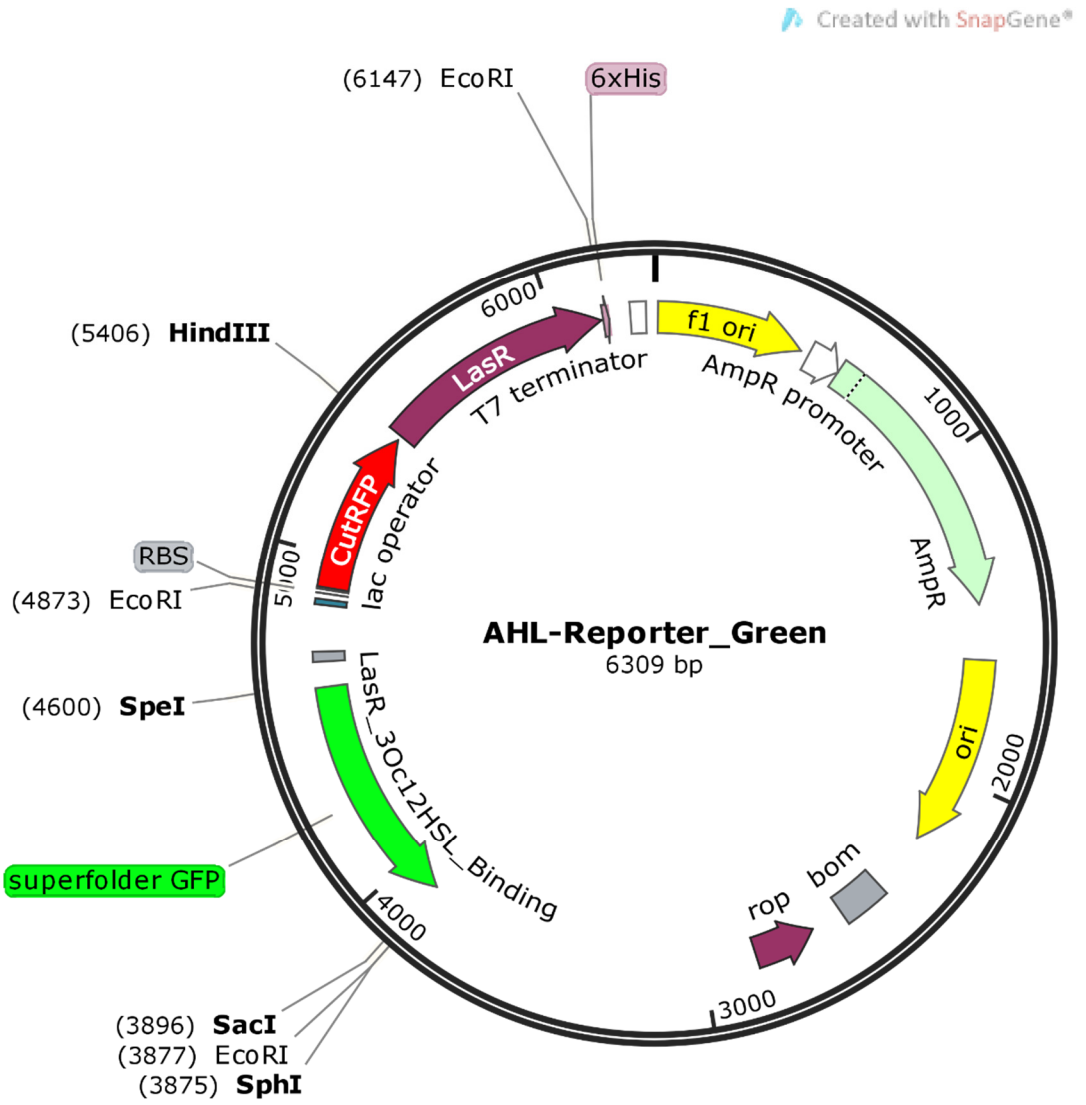

Figure 42B. Green Reporter plasmid map
A map of the plasmid constructed for reporting on AI-1 concentration with no working red gene. It is the same as the previous plasmid except that 200bps have been removed from dsRedExpress2 with the BstEII restriction enzyme.

9 BIBLIOGRAPHY

1. Zimlichman, E. et al. Health care–associated infections: a meta-analysis of costs and financial impact on the US health care system. *JAMA internal medicine* **173**, 2039-2046 (2013).
2. Klevens, R.M. et al. Estimating health care-associated infections and deaths in US hospitals, 2002. *Public health reports*, 160-166 (2007).
3. Magill , S.S. et al. Multistate Point-Prevalence Survey of Health Care–Associated Infections. *New England Journal of Medicine* **370**, 1198-1208 (2014).
4. House, T.W. National Strategy for Combating Antibiotic-Resistant Bacteria. 1-33 (2014).
5. McKenna, M. Antibiotic resistance: the last resort. *Nature* **499**, 394-6 (2013).
6. Reardon, S. Antibiotic resistance sweeping developing world. *Nature* **509**, 141-2 (2014).
7. Fuqua, C., Winans, S.C. & Greenberg, E.P. CENSUS AND CONSENSUS IN BACTERIAL ECOSYSTEMS: The LuxR-LuxI Family of Quorum-Sensing Transcriptional Regulators. *Annual Review of Microbiology* **50**, 727-751 (1996).
8. Pereira, C.S., Thompson, J.A. & Xavier, K.B. AI-2-mediated signalling in bacteria. *FEMS Microbiology Reviews* **37**, 156-181 (2013).
9. Galloway, W.R.J.D., Hodgkinson, J.T., Bowden, S.D., Welch, M. & Spring, D.R. Quorum Sensing in Gram-Negative Bacteria: Small-Molecule Modulation of AHL and AI-2 Quorum Sensing Pathways. *Chemical Reviews* **111**, 28-67 (2010).
10. Gupta, A. et al. Encapsulated fusion protein confers “sense and respond” activity to chitosan–alginate capsules to manipulate bacterial quorum sensing. *Biotechnology and Bioengineering* **110**, 552-562 (2013).
11. Chronopoulou, L. et al. Chitosan-coated PLGA nanoparticles: A sustained drug release strategy for cell cultures. *Colloids and Surfaces B: Biointerfaces* **103**, 310-317 (2013).
12. Sung, H.-W., Sonaje, K., Liao, Z.-X., Hsu, L.-W. & Chuang, E.-Y. pH-Responsive Nanoparticles Shelled with Chitosan for Oral Delivery of Insulin: From Mechanism to Therapeutic Applications. *Accounts of Chemical Research* **45**, 619-629 (2012).
13. Walter, C.J., Dumville, J.C., Sharp, C.A. & Page, T. Systematic review and meta-analysis of wound dressings in the prevention of surgical-site infections in surgical wounds healing by primary intention. *British Journal of Surgery* **99**, 1185-1194 (2012).
14. Jayakumar, R., Prabaharan, M., Sudheesh Kumar, P.T., Nair, S.V. & Tamura, H. Biomaterials based on chitin and chitosan in wound dressing applications. *Biotechnology Advances* **29**, 322-337 (2011).
15. Nolan, R., Kemmoona, M., Polyzois, I. & Claffey, N. The influence of prophylactic antibiotic administration on post-operative morbidity in dental implant surgery. A prospective double blind randomized controlled clinical trial. *Clinical oral implants research* **25**, 252-259 (2014).
16. Inacio, M. et al. The risk of surgical site infection and re-admission in obese patients undergoing total joint replacement who lose weight before surgery and keep it off post-operatively. *Bone & Joint Journal* **96**, 629-635 (2014).
17. Berger, A., Edelsberg, J., Yu, H. & Oster, G. Clinical and economic consequences of post-operative infections following major elective surgery in US hospitals. *Surgical infections* **15**, 322-327 (2014).
18. Wendler, O. & Baghai, M. Infections Post-Cardiac Surgery: New Information During Challenging Times∗. *Journal of the American College of Cardiology* **64**, 382-384 (2014).

19. Donlan, R.M. A New Approach to Mitigate Biofilm Formation on Totally Implantable Venous Access Ports. *Journal of Infectious Diseases* (2014).
20. Christoffersen, R.E. Antibiotics[mdash]an investment worth making? *Nat Biotech* **24**, 1512-1514 (2006).
21. O'Brien, S. Meeting the societal need for new antibiotics: the challenges for the pharmaceutical industry. *British journal of clinical pharmacology* **79**, 168-172 (2015).
22. Bax, R. & Green, S. Antibiotics: the changing regulatory and pharmaceutical industry paradigm. *Journal of Antimicrobial Chemotherapy* **70**, 1281-1284 (2015).
23. Marx, V. Cell communication: Stop the microbial chatter. *Nature* **511**, 493-497 (2014).
24. Dobretsov, S., Teplitski, M. & Paul, V. Mini-review: quorum sensing in the marine environment and its relationship to biofouling. *Biofouling* **25**, 413-427 (2009).
25. Hense, B.A. & Schuster, M. Core Principles of Bacterial Autoinducer Systems. *Microbiology and Molecular Biology Reviews* **79**, 153-169 (2015).
26. Vidal, J.E., Howery, K.E., Ludewick, H.P., Nava, P. & Klugman, K.P. Quorum-Sensing Systems LuxS/Autoinducer 2 and Com Regulate Streptococcus pneumoniae Biofilms in a Bioreactor with Living Cultures of Human Respiratory Cells. *Infection and Immunity* **81**, 1341-1353 (2013).
27. Brackman, G. & Coenye, T. Quorum Sensing Inhibitors as Anti-Biofilm Agents. *Current pharmaceutical design* **21**, 5-11 (2015).
28. Rampioni, G., Leoni, L. & Williams, P. The art of antibacterial warfare: Deception through interference with quorum sensing–mediated communication. *Bioorganic Chemistry* **55**, 60-68 (2014).
29. Kim, S.-R. et al. Biofouling Control with Bead-Entrapped Quorum Quenching Bacteria in Membrane Bioreactors: Physical and Biological Effects. *Environmental Science & Technology* **47**, 836-842 (2012).
30. Hammer, B.K. & Bassler, B.L. Quorum sensing controls biofilm formation in Vibrio cholerae. *Molecular Microbiology* **50**, 101-104 (2003).
31. Suntharalingam, P. & Cvitkovitch, D.G. Quorum sensing in streptococcal biofilm formation. *Trends in Microbiology* **13**, 3-6 (2005).
32. González Barrios, A.F. et al. Autoinducer 2 Controls Biofilm Formation in Escherichia coli through a Novel Motility Quorum-Sensing Regulator (MqsR, B3022). *Journal of Bacteriology* **188**, 305-316 (2006).
33. Đapa, T. et al. Multiple Factors Modulate Biofilm Formation by the Anaerobic Pathogen Clostridium difficile. *Journal of Bacteriology* **195**, 545-555 (2013).
34. Ni, N., Li, M., Wang, J. & Wang, B. Inhibitors and antagonists of bacterial quorum sensing. *Medicinal Research Reviews* **29**, 65-124 (2009).
35. Sadekuzzaman, M., Yang, S., Mizan, M.F.R. & Ha, S.D. Current and Recent Advanced Strategies for Combating Biofilms. *CRF3 Comprehensive Reviews in Food Science and Food Safety* **14**, 491-509 (2015).
36. Wu, H., Moser, C., Wang, H.-Z., Hoiby, N. & Song, Z.-J. Strategies for combating bacterial biofilm infections. *In J Oral Sci* **7**, 1-7 (2015).
37. O'Toole, G., Kaplan, H.B. & Kolter, R. Biofilm Formation as Microbial Development. *Annual Review of Microbiology* **54**, 49-79 (2000).
38. Blackwell, H.E. & Fuqua, C. Introduction to Bacterial Signals and Chemical Communication. *Chemical Reviews* **111**, 1-3 (2011).
39. LaRock, C.N., Yu, J., Horswill, A.R., Parsek, M.R. & Minion, F.C. Transcriptome Analysis of Acetyl-Homoserine Lactone-Based Quorum Sensing Regulation in <italic>Yersinia pestis</italic>. *PLoS ONE* **8**, e62337 (2013).

40. Pearson, J.P. et al. Structure of the autoinducer required for expression of Pseudomonas aeruginosa virulence genes. *Proceedings of the National Academy of Sciences* **91**, 197-201 (1994).
41. Zargar, A. et al. Bacterial Secretions of Nonpathogenic Escherichia coli Elicit Inflammatory Pathways: a Closer Investigation of Interkingdom Signaling. *mBio* **6**, e00025-15 (2015).
42. Kravchenko, V.V. et al. Modulation of gene expression via disruption of NF-κB signaling by a bacterial small molecule. *Science* **321**, 259-263 (2008).
43. Xavier, K.B. & Bassler, B.L. Regulation of uptake and processing of the quorum-sensing autoinducer AI-2 in Escherichia coli. *J Bacteriol* **187**, 238-48 (2005).
44. Wang, L., Li, J., March, J.C., Valdes, J.J. & Bentley, W.E. luxS-dependent gene regulation in Escherichia coli K-12 revealed by genomic expression profiling. *J Bacteriol* **187**, 8350-60 (2005).
45. Servinsky, M.D. et al. Directed assembly of a bacterial quorum. *The ISME journal* (2015).
46. Surette, M.G., Miller, M.B. & Bassler, B.L. Quorum sensing in Escherichia coli, Salmonella typhimurium, and Vibrio harveyi: A new family of genes responsible for autoinducer production. *Proceedings of the National Academy of Sciences* **96**, 1639-1644 (1999).
47. Cao, J.G. & Meighen, E.A. Purification and structural identification of an autoinducer for the luminescence system of Vibrio harveyi. *Journal of Biological Chemistry* **264**, 21670-21676 (1989).
48. Vendeville, A., Winzer, K., Heurlier, K., Tang, C.M. & Hardie, K.R. Making 'sense' of metabolism: autoinducer-2, LUXS and pathogenic bacteria. *Nature Reviews Microbiology* **3**, 383-396 (2005).
49. Bassler, B.L., Swem, L.R., Ulrich, S.M. & O'loughlin, C.T. Small molecule antagonists of bacterial quorum-sensing receptors. (2014).
50. Iyer, R.S., Ganguly, K. & Silks, L.A. Synthetic analogs of bacterial quorum sensors. (Google Patents, 2013).
51. Sintim, H.O. et al. Phosphorylated and Branched Dihydroxy-Pentane-Dione (DPD) analogs as quorum sensing inhibitors in bacteria. (Google Patents, 2015).
52. Roy, V. et al. Synthetic analogs tailor native AI-2 signaling across bacterial species. *Journal of the American Chemical Society* **132**, 11141-11150 (2010).
53. Gamby, S. et al. Altering the communication networks of multispecies microbial systems using a diverse toolbox of AI-2 analogues. *ACS chemical biology* **7**, 1023-1030 (2012).
54. Hong, S.H. et al. Synthetic quorum-sensing circuit to control consortial biofilm formation and dispersal in a microfluidic device. *Nat Commun* **3**, 613 (2012).
55. Zargar, A. et al. Rational design of 'controller cells' to manipulate protein and phenotype expression. *Metabolic Engineering* **30**, 61-68 (2015).
56. Gupta, S., Bram, E.E. & Weiss, R. Genetically Programmable Pathogen Sense and Destroy. *ACS Synthetic Biology* **2**, 715-723 (2013).
57. Hwang, I.Y. et al. Reprogramming microbes to be pathogen-seeking killers. *ACS synthetic biology* **3**, 228-37 (2014).
58. Oh, H.-S. et al. Control of membrane biofouling in MBR for wastewater treatment by quorum quenching bacteria encapsulated in microporous membrane. *Environmental science & technology* **46**, 4877-4884 (2012).
59. Yi-Hu, D., Lian-Hui, W., Jin-Ling, X., Hai-Bao, Z. & et al. Quenching quorum-sensing-dependent bacterial infection by an N-acyl homoserine lactonase. *Nature* **411**, 813-7 (2001).

60. Fast, W. & Tipton, P.A. The enzymes of bacterial census and censorship. *Trends in Biochemical Sciences* **37**, 7-14 (2012).
61. Kyeong, H.-H., Kim, J.-H. & Kim, H.-S. Design of N-acyl homoserine lactonase with high substrate specificity by a rational approach. *Applied Microbiology and Biotechnology* **99**, 4735-4742 (2015).
62. Del Vecchio, P. et al. Structural determinants of the high thermal stability of SsoPox from the hyperthermophilic archaeon Sulfolobus solfataricus. *Extremophiles* **13**, 461-470 (2009).
63. Hiblot, J., Gotthard, G., Elias, M. & Chabriere, E. Differential Active Site Loop Conformations Mediate Promiscuous Activities in the Lactonase SsoPox. *PLoS ONE* **8**, 1-1 (2013).
64. Hiblot, J., Gotthard, G., Chabriere, E. & Elias, M. Structural and Enzymatic characterization of the lactonase SisLac from Sulfolobus islandicus. *PLoS ONE* **7**, 1-14 (2012).
65. Zhu, J., Hixon, M.S., Globisch, D., Kaufmann, G.F. & Janda, K.D. Mechanistic Insights into the LsrK Kinase Required for Autoinducer-2 Quorum Sensing Activation. *Journal of the American Chemical Society* **135**, 7827-7830 (2013).
66. Rezzonico, F., Smits, T.H. & Duffy, B. Detection of AI-2 receptors in genomes of Enterobacteriaceae suggests a role of type-2 quorum sensing in closed ecosystems. *Sensors* **12**, 6645-6665 (2012).
67. Yu, J. et al. Analysis of Autoinducer-2 Quorum Sensing in Yersinia pestis. *Infection and Immunity* **81**, 4053-4062 (2013).
68. Li, L. et al. Screening of Actinobacillus pleuropneumoniae LuxS Inhibitors. *Current Microbiology* **67**, 564-571 (2013).
69. Kadirvel, M. et al. Inhibition of quorum sensing and biofilm formation in Vibrio harveyi by 4-fluoro-DPD; a novel potent inhibitor of AI-2 signalling. *Chem. Commun. Chemical Communications* **50**, 5000 (2014).
70. Brackman, G. et al. Synthesis and evaluation of thiazolidinedione and dioxazaborocane analogues as inhibitors of AI-2 quorum sensing in Vibrio harveyi. *Bioorganic & Medicinal Chemistry* **21**, 660-667 (2013).
71. Roy, V., Fernandes, R., Tsao, C.-Y. & Bentley, W.E. Cross Species Quorum Quenching Using a Native AI-2 Processing Enzyme. *ACS Chemical Biology* **5**, 223-232 (2009).
72. Krajewska, B. Application of chitin- and chitosan-based materials for enzyme immobilizations: a review. *Enzyme and Microbial Technology* **35**, 126-139 (2004).
73. Wiarachai, O., Thongchul, N., Kiatkamjornwong, S. & Hoven, V.P. Surface-quaternized chitosan particles as an alternative and effective organic antibacterial material. *Colloids and Surfaces B: Biointerfaces* **92**, 121-129 (2012).
74. De Temmerman, M.-L., Demeester, J., De Smedt, S.C. & Rejman, J. Tailoring layer-by-layer capsules for biomedical applications. *Nanomedicine* **7**, 771-788 (2012).
75. Li, X., Xie, H., Lin, J., Xie, W. & Ma, X. Characterization and biodegradation of chitosan–alginate polyelectrolyte complexes. *Polymer Degradation and Stability* **94**, 1-6 (2009).
76. Zhao, Q. et al. Hollow chitosan-alginate multilayer microcapsules as drug delivery vehicle: doxorubicin loading and in vitro and in vivo studies. *Nanomedicine: Nanotechnology, Biology and Medicine* **3**, 63-74 (2007).
77. George, M. & Abraham, T.E. Polyionic hydrocolloids for the intestinal delivery of protein drugs: Alginate and chitosan — a review. *Journal of Controlled Release* **114**, 1-14 (2006).
78. Muzzarelli, R.A.A. Human enzymatic activities related to the therapeutic administration of chitin derivatives. *Cellular and Molecular Life Sciences CMLS* **53**, 131-140 (1997).

79. Anal, A.K. & Stevens, W.F. Chitosan–alginate multilayer beads for controlled release of ampicillin. *International Journal of Pharmaceutics* **290**, 45-54 (2005).
80. Laxminarayan, R. et al. Antibiotic resistance—the need for global solutions. *The Lancet Infectious Diseases* **13**, 1057-1098 (2013).
81. Ping, X. et al. The effect of quorum sensing system for growth competitiveness on Shigella flexneri. *Yi chuan= Hereditas/Zhongguo yi chuan xue hui bian ji* **37**, 487-493 (2015).
82. Taga, M.E., Miller, S.T. & Bassler, B.L. Lsr-mediated transport and processing of AI-2 in Salmonella typhimurium. *Molecular Microbiology* **50**, 1411-1427 (2003).
83. Oggioni, M.R. et al. Switch from planktonic to sessile life: a major event in pneumococcal pathogenesis. *Molecular Microbiology* **61**, 1196-1210 (2006).
84. Le, K.Y. & Otto, M. Quorum-sensing regulation in staphylococci—an overview. *Frontiers in Microbiology* **6**, 1174 (2015).
85. Zhao, L., Xue, T., Shang, F., Sun, H. & Sun, B. Staphylococcus aureus AI-2 Quorum Sensing Associates with the KdpDE Two-Component System To Regulate Capsular Polysaccharide Synthesis and Virulence. *Infection and Immunity* **78**, 3506-3515 (2010).
86. O'Loughlin, C.T. et al. A quorum-sensing inhibitor blocks Pseudomonas aeruginosa virulence and biofilm formation. *Proceedings of the National Academy of Sciences of the United States of America* **110**, 17981-6 (2013).
87. Balasubramanian, D., Schneper, L., Kumari, H. & Mathee, K. A dynamic and intricate regulatory network determines Pseudomonas aeruginosa virulence. *Nucleic Acids Research* **41**, 1-20 (2013).
88. Murray, E.J. et al. Targeting Staphylococcus aureus Quorum Sensing with Nonpeptidic Small Molecule Inhibitors. *Journal of Medicinal Chemistry* **57**, 2813-2819 (2014).
89. Li, H. et al. Autoinducer-2 regulates Pseudomonas aeruginosa PAO1 biofilm formation and virulence production in a dose-dependent manner. *BMC Microbiology* **15**, 1-8 (2015).
90. Carter, G.P., Purdy, D., Williams, P. & Minton, N.P. Quorum sensing in Clostridium difficile: analysis of a luxS-type signalling system. *Journal of Medical Microbiology* **54**, 119-127 (2005).
91. Darkoh, C., DuPont, H.L., Norris, S.J. & Kaplan, H.B. Toxin Synthesis by Clostridium difficile Is Regulated through Quorum Signaling. *mBio* **6**(2015).
92. Jiang, W., Xia, S., Liang, J., Zhang, Z. & Hermanowicz, S.W. Effect of quorum quenching on the reactor performance, biofouling and biomass characteristics in membrane bioreactors. *Water Research* **47**, 187-196 (2013).
93. Kim, J.-H., Choi, D.-C., Yeon, K.-M., Kim, S.-R. & Lee, C.-H. Enzyme-Immobilized Nanofiltration Membrane To Mitigate Biofouling Based on Quorum Quenching. *Environmental Science & Technology* **45**, 1601-1607 (2011).
94. Williams, P. & Cámara, M. Quorum sensing and environmental adaptation in Pseudomonas aeruginosa: a tale of regulatory networks and multifunctional signal molecules. *Current Opinion in Microbiology* **12**, 182-191 (2009).
95. Saha, S., Thavasi, R. & Jayalakshmi, S. Phenazine Pigments from Pseudomonas aeruginosa and Their Application as Antibacterial Agent and Food Colourants. *Research J. of Microbiology Research Journal of Microbiology* **3**, 122-128 (2008).
96. Jayaseelan, S., Ramaswamy, D. & Dharmaraj, S. Pyocyanin: production, applications, challenges and new insights. *World Journal of Microbiology and Biotechnology* **30**, 1159-1168 (2014).

97. Ponnusamy, K., Kappachery, S., Thekeettle, M., Song, J. & Kweon, J. Anti-biofouling property of vanillin on Aeromonas hydrophila initial biofilm on various membrane surfaces. *World Journal of Microbiology and Biotechnology* **29**, 1695-1703 (2013).
98. Srey, S., Jahid, I.K. & Ha, S.-D. Biofilm formation in food industries: A food safety concern. *Food Control* **31**, 572-585 (2013).
99. Walters, M. & Sperandio, V. Quorum sensing in Escherichia coli and Salmonella. *International Journal of Medical Microbiology* **296**, 125-131 (2006).
100. Reading, N.C. & Sperandio, V. Quorum sensing: the many languages of bacteria. *FEMS Microbiology Letters* **254**, 1-11 (2006).
101. Novick, R.P. & Geisinger, E. Quorum Sensing in Staphylococci. *Annual Review of Genetics* **42**, 541-564 (2008).
102. Wang, D., Ding, X. & Rather, P.N. Indole Can Act as an Extracellular Signal inEscherichia coli. *Journal of Bacteriology* **183**, 4210-4216 (2001).
103. Lee, J.-H. & Lee, J. Indole as an intercellular signal in microbial communities. *FEMS microbiology reviews* **34**, 426-444 (2010).
104. Lee, J., Jayaraman, A. & Wood, T.K. Indole is an inter-species biofilm signal mediated by SdiA. *BMC microbiology* **7**, 42 (2007).
105. Bunders, C.A. et al. Intercepting Bacterial Indole Signaling with Flustramine Derivatives. *Journal of the American Chemical Society* **133**, 20160-20163 (2011).
106. Tiaden, A. & Hilbi, H. α-Hydroxyketone synthesis and sensing by Legionella and Vibrio. *Sensors* **12**, 2899-2919 (2012).
107. Kelly, R.C. et al. The Vibrio cholerae quorum-sensing autoinducer CAI-1: analysis of the biosynthetic enzyme CqsA. *Nat Chem Biol* **5**, 891-895 (2009).
108. Tiaden, A. et al. The Legionella pneumophila response regulator LqsR promotes host cell interactions as an element of the virulence regulatory network controlled by RpoS and LetA. *Cellular microbiology* **9**, 2903-2920 (2007).
109. Kessler, A. et al. The Legionella pneumophila orphan sensor kinase LqsT regulates competence and pathogen–host interactions as a component of the LAI-1 circuit. *Environmental Microbiology* **15**, 646-662 (2013).
110. Römling, U., Galperin, M.Y. & Gomelsky, M. Cyclic di-GMP: the first 25 years of a universal bacterial second messenger. *Microbiology and Molecular Biology Reviews* **77**, 1-52 (2013).
111. Römling, U. Small molecules with big effects: Cyclic di-GMP–mediated stimulation of cellulose production by the amino acid L-arginine. *Science signaling* **8**, fs12-fs12 (2015).
112. McCarter, L.L. & Gomelsky, M. Fifty Ways To Inhibit Motility via Cyclic Di-GMP: the Emerging Pseudomonas aeruginosa Swarming Story. *Journal of bacteriology* **197**, 406-409 (2015).
113. Lee, J. et al. A cell-cell communication signal integrates quorum sensing and stress response. *Nature chemical biology* **9**, 339-343 (2013).
114. Leung, V. & Lévesque, C.M. A Stress-Inducible Quorum-Sensing Peptide Mediates the Formation of Persister Cells with Noninherited Multidrug Tolerance. *Journal of Bacteriology* **194**, 2265-2274 (2012).
115. Dufour, D. & Lévesque, C.M. Cell Death of Streptococcus mutans Induced by a Quorum-Sensing Peptide Occurs via a Conserved Streptococcal Autolysin. *Journal of Bacteriology* **195**, 105-114 (2013).
116. Kumar, S. & Engelberg-Kulka, H. Quorum sensing peptides mediating interspecies bacterial cell death as a novel class of antimicrobial agents. *Current Opinion in Microbiology* **21**, 22-27 (2014).

117. Jang, Y.-J., Choi, Y.-J., Lee, S.-H., Jun, H.-K. & Choi, B.-K. Autoinducer 2 of Fusobacterium nucleatum as a target molecule to inhibit biofilm formation of periodontopathogens. *Archives of Oral Biology* **58**, 17-27 (2013).
118. Roy, V. et al. AI-2 analogs and antibiotics: a synergistic approach to reduce bacterial biofilms. *Applied Microbiology and Biotechnology* **97**, 2627-2638 (2013).
119. Case, R.J., Labbate, M. & Kjelleberg, S. AHL-driven quorum-sensing circuits: their frequency and function among the Proteobacteria. *ISME journal* **2**, 345-9 (2008).
120. Park, J., Kaufmann, G.F., Bowen, J.P., Arbiser, J.L. & Janda, K.D. Solenopsin A, a Venom Alkaloid from the Fire Ant Solenopsis invicta, Inhibits Quorum-Sensing Signaling in Pseudomonas aeruginosa. *Journal of Infectious Diseases* **198**, 1198-1201 (2008).
121. Zhu, J. et al. Disarming Pseudomonas aeruginosa Virulence Factor LasB by Leveraging a Caenorhabditis elegans Infection Model. *Chemistry & Biology* **22**, 483-491 (2015).
122. Stacy, D.M., Welsh, M.A., Rather, P.N. & Blackwell, H.E. Attenuation of quorum sensing in the pathogen Acinetobacter baumannii using non-native N-acyl homoserine lactones. *ACS chemical biology* **7**, 1719-1728 (2012).
123. Lowery, C.A. et al. Defining the mode of action of tetramic acid antibacterials derived from Pseudomonas aeruginosa quorum sensing signals. *Journal of the American Chemical Society* **131**, 14473-14479 (2009).
124. Romano, A.A. et al. The Fe(III) and Ga(III) coordination chemistry of 3-(1-hydroxymethylidene) and 3-(1-hydroxydecylidene)-5-(2-hydroxyethyl)pyrrolidine-2,4-dione: Novel tetramic acid degradation products of homoserine lactone bacterial quorum sensing molecules. *Journal of Inorganic Biochemistry* **107**, 96-103 (2012).
125. Estrela, A.B. & Abraham, W.-R. Combining Biofilm-Controlling Compounds and Antibiotics as a Promising New Way to Control Biofilm Infections. *Pharmaceuticals* **3**, 1374-1393 (2010).
126. Brackman, G., Cos, P., Maes, L., Nelis, H.J. & Coenye, T. Quorum sensing inhibitors increase the susceptibility of bacterial biofilms to antibiotics in vitro and in vivo. *Antimicrobial agents and chemotherapy* **55**, 2655-2661 (2011).
127. Karatan, E. & Michael, A.J. A wider role for polyamines in biofilm formation. *Biotechnology letters* **35**, 1715-1717 (2013).
128. Karatan, E., Duncan, T.R. & Watnick, P.I. NspS, a Predicted Polyamine Sensor, Mediates Activation of Vibrio cholerae Biofilm Formation by Norspermidine. *Journal of Bacteriology* **187**, 7434-7443 (2005).
129. Kolodkin-Gal, I. et al. A self-produced trigger for biofilm disassembly that targets exopolysaccharide. *Cell* **149**, 684-692 (2012).
130. Nesse, L.L., Berg, K. & Vestby, L.K. The effect of norspermidine and spermidine on biofilm formation by potentially pathogenic Escherichia coli and Salmonella enterica wild type strains. *Applied and Environmental Microbiology* (2015).
131. Cockerell, S.R. et al. Vibrio cholerae NspS, a homologue of ABC-type periplasmic solute binding proteins, facilitates transduction of polyamine signals independent of their transport. *Microbiology Microbiology* **160**, 832-843 (2014).
132. Minois, N. et al. Spermidine promotes stress resistance in Drosophila melanogaster through autophagy-dependent and-independent pathways. *Cell death & disease* **3**, e401 (2012).
133. Davis, R.L. Spermidine cures flies of senior moments. *Nature neuroscience* **16**, 1363-1364 (2013).
134. Mandal, S., Mandal, A., Johansson, H.E., Orjalo, A.V. & Park, M.H. Depletion of cellular polyamines, spermidine and spermine, causes a total arrest in translation and growth in

mammalian cells. *Proceedings of the National Academy of Sciences* **110**, 2169-2174 (2013).
135. Kim, S.-K., Jin, Y.-S., Choi, I.-G., Park, Y.-C. & Seo, J.-H. Enhanced tolerance of Saccharomyces cerevisiae to multiple lignocellulose-derived inhibitors through modulation of spermidine contents. *Metabolic Engineering* **29**, 46-55 (2015).
136. Tersey, S.A., Colvin, S.C., Maier, B. & Mirmira, R.G. Protective effects of polyamine depletion in mouse models of type 1 diabetes: implications for therapy. *Amino acids* **46**, 633-642 (2014).
137. Aoki, W., Kuroda, K. & Ueda, M. Next generation of antimicrobial peptides as molecular targeted medicines. *Journal of bioscience and bioengineering* **114**, 365-370 (2012).
138. Tal-Gan, Y., Ivancic, M., Cornilescu, G., Cornilescu, C.C. & Blackwell, H.E. Structural Characterization of Native Autoinducing Peptides and Abiotic Analogues Reveals Key Features Essential for Activation and Inhibition of an AgrC Quorum Sensing Receptor in Staphylococcus aureus. *Journal of the American Chemical Society* **135**, 18436-18444 (2013).
139. Desouky, S.E. et al. Cyclodepsipeptides produced by actinomycetes inhibit cyclic peptide-mediated quorum sensing in Gram-positive bacteria. *FEMS microbiology letters*, fnv109 (2015).
140. Aggarwal, C. et al. Identification of Quorum-Sensing Inhibitors Disrupting Signaling between Rgg and Short Hydrophobic Peptides in Streptococci. *mBio* **6**, e00393-15 (2015).
141. Guo, L. et al. Precision-guided antimicrobial peptide as a targeted modulator of human microbial ecology. *Proceedings of the National Academy of Sciences* **112**, 7569-7574 (2015).
142. Wynendaele, E. et al. Crosstalk between the microbiome and cancer cells by quorum sensing peptides. *Peptides* **64**, 40-48 (2015).
143. Lee, J., Attila, C., Cirillo, S.L., Cirillo, J.D. & Wood, T.K. Indole and 7-hydroxyindole diminish Pseudomonas aeruginosa virulence. *Microbial biotechnology* **2**, 75-90 (2009).
144. Lee, J., Bansal, T., Jayaraman, A., Bentley, W.E. & Wood, T.K. Enterohemorrhagic Escherichia coli Biofilms Are Inhibited by 7-Hydroxyindole and Stimulated by Isatin. *Applied and Environmental Microbiology* **73**, 4100-4109 (2007).
145. Wood, T.K., Hong, S.H. & Ma, Q. Engineering biofilm formation and dispersal. *Trends in Biotechnology* **29**, 87-94 (2011).
146. Harrison, C.F. et al. Amoebae-Based Screening Reveals a Novel Family of Compounds Restricting Intracellular Legionella pneumophila. *ACS Infectious Diseases* (2015).
147. Girennavar, B. et al. Grapefruit juice and its furocoumarins inhibits autoinducer signaling and biofilm formation in bacteria. *International Journal of Food Microbiology* **125**, 204-208 (2008).
148. Packiavathy, I.A.S.V., Priya, S., Pandian, S.K. & Ravi, A.V. Inhibition of biofilm development of uropathogens by curcumin – An anti-quorum sensing agent from Curcuma longa. *Food Chemistry* **148**, 453-460 (2014).
149. Choo, J.H., Rukayadi, Y. & Hwang, J.K. Inhibition of bacterial quorum sensing by vanilla extract. *Letters in Applied Microbiology* **42**, 637-641 (2006).
150. Tomadoni, B., Cassani, L., Moreira, M. & Ponce, A. Efficacy of vanillin and geraniol in reducing Escherichia coli O157: H7 on strawberry juice. *LWT-Food Science and Technology* (2015).

151. Pérez-Montaño, F. et al. Rice and bean AHL-mimic quorum-sensing signals specifically interfere with the capacity to form biofilms by plant-associated bacteria. *Research in microbiology* **164**, 749-760 (2013).
152. Vega, L.M. et al. Nickel and cadmium ions inhibit quorum sensing and biofilm formation without affecting viability in Burkholderia multivorans. *International Biodeterioration & Biodegradation* **91**, 82-87 (2014).
153. García-Lara, B. et al. Inhibition of quorum-sensing-dependent virulence factors and biofilm formation of clinical and environmental Pseudomonas aeruginosa strains by ZnO nanoparticles. *Letters in Applied Microbiology*, n/a-n/a (2015).
154. Vinoj, G., Vaseeharan, B., Thomas, S., Spiers, A.J. & Shanthi, S. Quorum-quenching activity of the AHL-Lactonase from Bacillus licheniformis DAHB1 inhibits Vibrio biofilm formation in vitro and reduces shrimp intestinal colonisation and mortality. *Marine Biotechnology* **16**, 707-715 (2014).
155. Takami, H. et al. Thermoadaptation trait revealed by the genome sequence of thermophilic Geobacillus kaustophilus. *Nucleic acids research* **32**, 6292-6303 (2004).
156. Chow, J.Y., Yang, Y., Tay, S.B., Chua, K.L. & Yew, W.S. Disruption of Biofilm Formation by the Human Pathogen Acinetobacter baumannii Using Engineered Quorum-Quenching Lactonases. *Antimicrobial Agents and Chemotherapy* **58**, 1802-1805 (2014).
157. Ma, F. et al. Heterologous expression of human paraoxonases in Pseudomonas aeruginosa inhibits biofilm formation and decreases antibiotic resistance. *Applied Microbiology & Biotechnology* **83**, 135-141 (2009).
158. Draganov, D.I. et al. Human paraoxonases (PON1, PON2, and PON3) are lactonases with overlapping and distinct substrate specificities. *Journal of Lipid Research* **46**, 1239-1247 (2005).
159. Xu, F., Byun, T., Dussen, H.-J. & Duke, K.R. Degradation of N-acylhomoserine lactones, the bacterial quorum-sensing molecules, by acylase. *Journal of Biotechnology* **101**, 89-96 (2003).
160. Sio, C.F. et al. Quorum quenching by an N-acyl-homoserine lactone acylase from Pseudomonas aeruginosa PAO1. *Infection and immunity* **74**, 1673-1682 (2006).
161. Koch, G. et al. Reducing virulence of the human pathogen Burkholderia by altering the substrate specificity of the quorum-quenching acylase PvdQ. *Proceedings of the National Academy of Sciences* **111**, 1568-1573 (2014).
162. Schell, U., Kessler, A. & Hilbi, H. Phosphorylation signalling through the Legionella quorum sensing histidine kinases LqsS and LqsT converges on the response regulator LqsR. *Molecular Microbiology* **92**, 1039-1055 (2014).
163. Hegde, M. et al. Chemotaxis to the Quorum-Sensing Signal AI-2 Requires the Tsr Chemoreceptor and the Periplasmic LsrB AI-2-Binding Protein. *Journal of Bacteriology* **193**, 768-773 (2011).
164. Bansal, T., Jesudhasan, P., Pillai, S., Wood, T. & Jayaraman, A. Temporal regulation of enterohemorrhagic Escherichia coli virulence mediated by autoinducer-2. *Applied Microbiology and Biotechnology* **78**, 811-819 (2008).
165. Prigent-Combaret, C., Vidal, O., Dorel, C. & Lejeune, P. Abiotic Surface Sensing and Biofilm-Dependent Regulation of Gene Expression in Escherichia coli. *Journal of Bacteriology* **181**, 5993-6002 (1999).
166. Prigent-Combaret, C. et al. Developmental pathway for biofilm formation in curli-producing Escherichia coli strains: role of flagella, curli and colanic acid. *Environmental microbiology* **2**, 450-464 (2000).

167. Pratt, L.A. & Kolter, R. Genetic analysis of Escherichia coli biofilm formation: roles of flagella, motility, chemotaxis and type I pili. *Molecular microbiology* **30**, 285-293 (1998).
168. Merritt, P.M., Danhorn, T. & Fuqua, C. Motility and chemotaxis in Agrobacterium tumefaciens surface attachment and biofilm formation. *Journal of bacteriology* **189**, 8005-8014 (2007).
169. Chorell, E. et al. Mapping pilicide anti-virulence effect in Escherichia coli, a comprehensive structure–activity study. *Bioorganic & Medicinal Chemistry* **20**, 3128-3142 (2012).
170. Greene, S.E. et al. Pilicide ec240 Disrupts Virulence Circuits in Uropathogenic Escherichia coli. *mBio* **5**(2014).
171. Chabane, Y.N. et al. Virstatin inhibits biofilm formation and motility of Acinetobacter baumannii. *BMC microbiology* **14**, 62 (2014).
172. Allen, R.C., Popat, R., Diggle, S.P. & Brown, S.P. Targeting virulence: can we make evolution-proof drugs? *Nature Reviews Microbiology* **12**, 300-308 (2014).
173. Rana, D. & Matsuura, T. Surface modifications for antifouling membranes. *Chemical reviews* **110**, 2448-2471 (2010).
174. Bazaka, K., Jacob, M., Crawford, R. & Ivanova, E. Efficient surface modification of biomaterial to prevent biofilm formation and the attachment of microorganisms. *Applied Microbiology and Biotechnology* **95**, 299-311 (2012).
175. Hickok, N.J. & Shapiro, I.M. Immobilized antibiotics to prevent orthopaedic implant infections. *Advanced Drug Delivery Reviews* **64**, 1165-1176 (2012).
176. Lee, B. et al. Effective antifouling using quorum-quenching acylase stabilized in magnetically-separable mesoporous silica. *Biomacromolecules* **15**, 1153-1159 (2014).
177. Xiong, M.-H., Bao, Y., Yang, X.-Z., Zhu, Y.-H. & Wang, J. Delivery of antibiotics with polymeric particles. *Advanced Drug Delivery Reviews* **78**, 63-76 (2014).
178. Pei, R. & Lamas-Samanamud, G.R. Inhibition of biofilm formation by T7 bacteriophages producing quorum-quenching enzymes. *Applied and environmental microbiology* **80**, 5340-5348 (2014).
179. Deakin, S.P., Ducret, V., Bioletto, S., Perron, K. & James, R.W. Modulating reconstituted high density lipoprotein functionality to target the Pseudomonas aeruginosa quorum sensing system. *Life sciences* **112**, 68-73 (2014).
180. Nissen, S.E. et al. Effect of recombinant ApoA-I Milano on coronary atherosclerosis in patients with acute coronary syndromes: a randomized controlled trial. *Jama* **290**, 2292-2300 (2003).
181. Costa, E.M., Silva, S., Pina, C., Tavaria, F.K. & Pintado, M.M. Evaluation and insights into chitosan antimicrobial activity against anaerobic oral pathogens. *Anaerobe* **18**, 305-309 (2012).
182. Stroescu, M. et al. Chitosan-vanillin composites with antimicrobial properties. *Food Hydrocolloids* **48**, 62-71 (2015).
183. Rusconi, R., Garren, M. & Stocker, R. Microfluidics Expanding the Frontiers of Microbial Ecology. *Annual review of biophysics* **43**, 65-91 (2014).
184. Hol, F.J. & Dekker, C. Zooming in to see the bigger picture: Microfluidic and nanofabrication tools to study bacteria. *Science* **346**, 1251821 (2014).
185. Terry, J. & Neethirajan, S. A novel microfluidic wound model for testing antimicrobial agents against Staphylococcus pseudintermedius biofilms. *Journal of nanobiotechnology* **12**, 1 (2014).
186. Murray, C., Adeyiga, O., Owsley, K. & Di Carlo, D. Research highlights: microfluidic analysis of antimicrobial susceptibility. *Lab on a Chip* **15**, 1226-1229 (2015).

187. Lu, H.D. et al. Modulating Vibrio cholerae Quorum-Sensing-Controlled Communication Using Autoinducer-Loaded Nanoparticles. *Nano Letters* **15**, 2235-2241 (2015).
188. Nafee, N. et al. Antibiotic-free nanotherapeutics: Ultra-small, mucus-penetrating solid lipid nanoparticles enhance the pulmonary delivery and anti-virulence efficacy of novel quorum sensing inhibitors. *Journal of Controlled Release* **192**, 131-140 (2014).
189. Chang, H.-H. et al. Origin and Proliferation of Multiple-Drug Resistance in Bacterial Pathogens. *Microbiology and Molecular Biology Reviews* **79**, 101-116 (2015).
190. Phimister, E.G., Arias, C.A. & Murray, B.E. A New Antibiotic and the Evolution of Resistance. *New England Journal of Medicine* **372**, 1168-1170 (2015).
191. Palmer, A.C. et al. Delayed commitment to evolutionary fate in antibiotic resistance fitness landscapes. *Nat Commun* **6**(2015).
192. O'Donnell, M.J., Tuttlebee, C.M., Falkiner, F.R. & Coleman, D.C. Bacterial contamination of dental chair units in a modern dental hospital caused by leakage from suction system hoses containing extensive biofilm. *The Journal of hospital infection* **59**, 348-360 (2005).
193. Metcalf, D.G. & Bowler, P.G. Biofilm delays wound healing: A review of the evidence. *Burns & Trauma* **1**, 5 (2015).
194. Jongsma, M.A., van der Mei, H.C., Atema-Smit, J., Busscher, H.J. & Ren, Y. In vivo biofilm formation on stainless steel bonded retainers during different oral health-care regimens. *In J Oral Sci* **7**, 42-48 (2015).
195. Scannapieco, F.A. & Shay, K. Oral Health Disparities in Older Adults: Oral Bacteria, Inflammation, and Aspiration Pneumonia. *Dental Clinics of North America* **58**, 771-782 (2014).
196. Desrousseaux, C., Sautou, V., Descamps, S. & Traoré, O. Modification of the surfaces of medical devices to prevent microbial adhesion and biofilm formation. *Journal of Hospital Infection* **85**, 87-93 (2013).
197. Rasmussen Tb, G.M. Quorum sensing inhibitors: a bargain of effects. *Microbiology (Reading, England)* **152**, 895-904 (2006).
198. Ivanova, K. et al. Quorum Quenching and Matrix Degrading Enzymes in Multilayer Coatings Synergistically Prevent Bacterial Biofilm Formation on Urinary Catheters. *ACS Appl Mater Interfaces* (2015).
199. Tsao, C.-Y., Hooshangi, S., Wu, H.-C., Valdes, J.J. & Bentley, W.E. Autonomous induction of recombinant proteins by minimally rewiring native quorum sensing regulon of E. coli. *Metabolic Engineering* **12**, 291-297 (2010).
200. Bassler, B.L., Wright, M., Showalter, R.E. & Silverman, M.R. Intercellular signalling in Vibrio harveyi: sequence and function of genes regulating expression of luminescence. *MMI Molecular Microbiology* **9**, 773-786 (1993).
201. Yasukawa, T. et al. Increase of solubility of foreign proteins in Escherichia coli by coproduction of the bacterial thioredoxin. *Journal of Biological Chemistry* **270**, 25328-25331 (1995).
202. Charollais, J., Dreyfus, M. & Iost, I. CsdA, a cold-shock RNA helicase from Escherichia coli, is involved in the biogenesis of 50S ribosomal subunit. *Nucleic Acids Research* **32**, 2751-2759 (2004).
203. Fernandes, R., Roy, V., Wu, H.-C. & Bentley, W.E. Engineered biological nanofactories trigger quorum sensing response in targeted bacteria. *Nat Nano* **5**, 213-217 (2010).
204. Wu, H.-C. et al. Biofabrication of antibodies and antigens via IgG-binding domain engineered with activatable pentatyrosine pro-tag. *Biotechnology and Bioengineering* **103**, 231-240 (2009).

205. González-Rodríguez, M.L., Holgado, M.A., Sánchez-Lafuente, C., Rabasco, A.M. & Fini, A. Alginate/chitosan particulate systems for sodium diclofenac release. *International Journal of Pharmaceutics* **232**, 225-234 (2002).
206. Takka, S. & Gürel, A. Evaluation of Chitosan/Alginate Beads Using Experimental Design: Formulation and In Vitro Characterization. *AAPS PharmSciTech* **11**, 460-466 (2010).
207. Richards, F.M. Areas, volumes, packing, and protein structure. *Annual review of biophysics and bioengineering* **6**, 151-176 (1977).
208. Graham, R.L., Lubachevsky, B.D., Nurmela, K.J. & Östergård, P.R. Dense packings of congruent circles in a circle. *Discrete Mathematics* **181**, 139-154 (1998).
209. McInnis, C.E. & Blackwell, H.E. Non-native N-Aroyl L-Homoserine Lactones Are Potent Modulators of the Quorum Sensing Receptor RpaR in Rhodopseudomonas palustris. *ChemBioChem* **15**, 87-93 (2014).
210. Jha, B., Kavita, K., Westphal, J., Hartmann, A. & Schmitt-Kopplin, P. Quorum Sensing Inhibition by Asparagopsis taxiformis, a Marine Macro Alga: Separation of the Compound that Interrupts Bacterial Communication. *Marine Drugs* **11**, 253-265 (2013).
211. Guan, W. et al. Amine modified graphene as reversed-dispersive solid phase extraction materials combined with liquid chromatography–tandem mass spectrometry for pesticide multi-residue analysis in oil crops. *Journal of Chromatography A* **1286**, 1-8 (2013).
212. Chen, Z. et al. Activated carbons and amine-modified materials for carbon dioxide capture—a review. *Frontiers of Environmental Science & Engineering* **7**, 326-340 (2013).
213. Du, Y.-Z. et al. Sustained release of ATP encapsulated in chitosan oligosaccharide nanoparticles. *International Journal of Pharmaceutics* **392**, 164-169 (2010).
214. Hironaka, I. et al. Glucose triggers ATP secretion from bacteria in a growth phase-dependent manner. *Applied and Environmental Microbiology* (2013).
215. Ding, Q., Quah, S. & Tan, K. Secreted adenosine triphosphate from Aggregatibacter actinomycetemcomitans triggers chemokine response. *Molecular Oral Microbiology* (2015).
216. Mempin, R. et al. Release of extracellular ATP by bacteria during growth. *BMC Microbiology* **13**, 1-25 (2013).
217. Stoppel, W.L. et al. Terminal sterilization of alginate hydrogels: efficacy and impact on mechanical properties. *Journal of Biomedical Materials Research Part B: Applied Biomaterials* **102**, 877-884 (2014).
218. San Juan, A. et al. Degradation of chitosan-based materials after different sterilization treatments. in *IOP Conference Series: Materials Science and Engineering* Vol. 31 012007 (IOP Publishing, 2012).
219. WHO. Media Centre: Fact Sheet: Antibiotic Resistance. Vol. 2016 (October 2015).
220. WHO. Exposure to Highly Hazardous Pesticides: A Major Public Health Conern. *Preventing Disease Through Healthy Environments*, 6 (2010).
221. Raushel, F.M. Bacterial detoxification of organophosphate nerve agents. *Current opinion in microbiology* **5**, 288-295 (2002).
222. López-Granero, C. et al. Comparative study on short- and long-term behavioral consequences of organophosphate exposure: Relationship to AChE mRNA expression. *NeuroToxicology* **40**, 57-64 (2014).
223. Costa, L.G. Current issues in organophosphate toxicology. *Clinica Chimica Acta* **366**, 1-13 (2006).
224. Aubert, S.D., Li, Y. & Raushel, F.M. Mechanism for the Hydrolysis of Organophosphates by the Bacterial Phosphotriesterase†. *Biochemistry* **43**, 5707-5715 (2004).

225. Afriat-Jurnou, L., Jackson, C.J. & Tawfik, D.S. Reconstructing a Missing Link in the Evolution of a Recently Diverged Phosphotriesterase by Active-Site Loop Remodeling. *Biochemistry* **51**, 6047-6055 (2012).
226. Tsai, P.-C. et al. Enzymes for the Homeland Defense: Optimizing Phosphotriesterase for the Hydrolysis of Organophosphate Nerve Agents. *Biochemistry* **51**, 6463-6475 (2012).
227. Elias, M. & Tawfik, D.S. Divergence and Convergence in Enzyme Evolution: Parallel Evolution of Paraoxonases from Quorum-quenching Lactonases. *Journal of Biological Chemistry* **287**, 11-20 (2012).
228. Del Giudice, I. et al. An efficient thermostable organophosphate hydrolase and its application in pesticide decontamination. *Biotechnology and Bioengineering*, n/a-n/a (2015).
229. Hiblot, J., Gotthard, G., Chabriere, E. & Elias, M. Characterisation of the organophosphate hydrolase catalytic activity of SsoPox. *Sci. Rep.* **2**(2012).
230. Elias, M. et al. Structural Basis for Natural Lactonase and Promiscuous Phosphotriesterase Activities. *Journal of Molecular Biology* **379**, 1017-1028 (2008).
231. Ng, F.S.W., Wright, D.M. & Seah, S.Y.K. Characterization of a Phosphotriesterase-Like Lactonase from Sulfolobus solfataricus and Its Immobilization for Disruption of Quorum Sensing. *Applied and Environmental Microbiology* **77**, 1181-1186 (2011).
232. Bhokisham, N. et al. Modular construction of multi-subunit protein complexes using engineered tags and microbial transglutaminase. *Metabolic engineering* **38**, 1-9 (2016).
233. Sarmento, B. & das Neves, J. *Chitosan-based systems for biopharmaceuticals: delivery, targeting and polymer therapeutics*, (John Wiley & Sons, 2012).
234. Studier, F.W. Protein production by auto-induction in high-density shaking cultures. *Protein Expression and Purification* **41**, 207-234 (2005).
235. Lindsay, A. & Ahmer, B.M. Effect of sdiA on biosensors of N-acylhomoserine lactones. *Journal of bacteriology* **187**, 5054-5058 (2005).
236. Bhokisham, N. et al. Modular Construction of Multi-Subunit Protein Complexes using Engineered Tags and Microbial Transglutaminase. *Metabolic Engineering*.
237. Telford, G. et al. The Pseudomonas aeruginosaQuorum-Sensing Signal MoleculeN-(3-Oxododecanoyl)-l-Homoserine Lactone Has Immunomodulatory Activity. *Infection and Immunity* **66**, 36-42 (1998).
238. Hentzer, M. & Givskov, M. Pharmacological inhibition of quorum sensing for the treatment of chronic bacterial infections. *The Journal of Clinical Investigation* **112**, 1300-1307 (2003).
239. Hentzer, M. et al. Inhibition of quorum sensing in Pseudomonas aeruginosa biofilm bacteria by a halogenated furanone compound. *Microbiology* **148**, 87-102 (2002).
240. Hraiech, S. et al. Inhaled Lactonase Reduces *Pseudomonas aeruginosa* Quorum Sensing and Mortality in Rat Pneumonia. *PLoS ONE* **9**, e107125 (2014).
241. Sirotkina, M. & Efremenko, E. Rhodococcus lactonase with organophosphate hydrolase (OPH) activity and His6-tagged OPH with lactonase activity: evolutionary proximity of the enzymes and new possibilities in their application. *Applied Microbiology and Biotechnology* **98**, 2647-2656 (2014).
242. Cequier, E., Sakhi, A.K., Marcé, R.M., Becher, G. & Thomsen, C. Human exposure pathways to organophosphate triesters — A biomonitoring study of mother–child pairs. *Environment International* **75**, 159-165 (2015).
243. Harrad, S., Brommer, S. & Mueller, J.F. Concentrations of organophosphate flame retardants in dust from cars, homes, and offices: An international comparison. *Emerging Contaminants* (2016).

244. Gao, Y., Truong, Y.B., Cacioli, P., Butler, P. & Kyratzis, I.L. Bioremediation of pesticide contaminated water using an organophosphate degrading enzyme immobilized on nonwoven polyester textiles. *Enzyme and Microbial Technology* **54**, 38-44 (2014).
245. Ong, H.B., Lee, W.S., Patterson, S., Wyllie, S. & Fairlamb, A.H. Homoserine and quorum-sensing acyl homoserine lactones as alternative sources of threonine: a potential role for homoserine kinase in insect-stage Trypanosoma brucei. *Molecular Microbiology* **95**, 143-156 (2015).
246. Sun, Z., Grimm, V. & Riedel, C.U. AI-2 to the rescue against antibiotic-induced intestinal dysbiosis? *Trends in Microbiology* **23**, 327-328 (2015).
247. Li, M., Villaruz, A.E., Vadyvaloo, V., Sturdevant, D.E. & Otto, M. AI-2-dependent gene regulation in Staphylococcus epidermidis. *BMC Microbiology* **8**, 1-9 (2008).
248. Kong, K.F., Vuong, C. & Otto, M. Staphylococcus quorum sensing in biofilm formation and infection. *Int J Med Microbiol* **296**(2006).
249. Yu, D., Zhao, L., Xue, T. & Sun, B. Staphylococcus aureus autoinducer-2 quorum sensing decreases biofilm formation in an icaR-dependent manner. *BMC Microbiology* **12**, 1-12 (2012).
250. Bobrov, A.G. et al. Functional quorum sensing systems affect biofilm formation and protein expression in Yersinia pestis. in *The Genus Yersinia* 178-191 (Springer, 2007).
251. Yao, S. & Cho, M.G. Diffusion characteristics in microcapsules. *CHINESE JOURNAL OF CHEMICAL ENGINEERING* **6**, 116-123 (1998).
252. Zhang, L.-Y., Yao, S.-J. & Guan, Y.-X. Diffusion Characteristics of Solutes with Low Molecular Weight in Sodium Alginate/Cellulose Sulfate−CaCl2/Poly(methylene-co-guanidine) Capsules. *Journal of Chemical & Engineering Data* **48**, 864-868 (2003).
253. Oyaas, J., Storrø, I., Svendsen, H. & Levine, D.W. The effective diffusion coefficient and the distribution constant for small molecules in calcium-alginate gel beads. *Biotechnology and bioengineering* **47**, 492-500 (1995).
254. Truskey, G.A., Yuan, F. & Katz, D.F. *Transport phenomena in biological systems*, (Pearson, Boston, 2010).
255. Pasparakis, G. & Bouropoulos, N. Swelling studies and in vitro release of verapamil from calcium alginate and calcium alginate–chitosan beads. *International Journal of Pharmaceutics* **323**, 34-42 (2006).
256. Chen, A.-Z. et al. Poly(L-histidine)-chitosan/alginate complex microcapsule as a novel drug delivery agent. *Journal of Applied Polymer Science* **124**, 3728-3736 (2012).
257. Tanaka, H., Matsumura, M. & Veliky, I.A. Diffusion characteristics of substrates in Ca-alginate gel beads. *Biotechnology and bioengineering* **26**, 53-8 (1984).
258. Crank, J. *The mathematics of diffusion*, (Clarendon Press, Oxford [Eng], 1975).
259. Taqieddin, E. & Amiji, M. Enzyme immobilization in novel alginate–chitosan core-shell microcapsules. *Biomaterials* **25**, 1937-1945 (2004).
260. Qi, C. et al. ATP-Stabilized Amorphous Calcium Carbonate Nanospheres and Their Application in Protein Adsorption. *Small* **10**, 2047-2056 (2014).
261. Bowen, W.J. & Martin, H.L. A study of diffusion of ATP through glycerol-treated muscle. *Archives of Biochemistry and Biophysics* **102**, 286-292 (1963).
262. Sankalia, M.G., Mashru, R.C., Sankalia, J.M. & Sutariya, V.B. Reversed chitosan–alginate polyelectrolyte complex for stability improvement of alpha-amylase: Optimization and physicochemical characterization. *European Journal of Pharmaceutics and Biopharmaceutics* **65**, 215-232 (2007).

263. Chen, T.W., Chang, S.J., Niu, G.C.-C., Hsu, Y.T. & Kuo, S.M. Alginate-coated chitosan membrane for guided tissue regeneration. *Journal of Applied Polymer Science* **102**, 4528-4534 (2006).